Portales Valley: Petrology of a metallic-melt meteorite breccia

Alex Ruzicka [1], Marvin Killgore [2], David W. Mittlefehldt [3] and Marc D. Fries [4]

Submitted to *Meteoritics & Planetary Science*

May 14, 2004

1 Address to whom correspondence should be sent: Cascadia Meteorite Laboratory, Portland State University, Department of Geology, 17 Cramer Hall, 1721 SW Broadway, PO Box 751, Portland, OR 97207. e-mail address: ruzickaa@pdx.edu

2 Southwest Meteorite Laboratory, P.O. Box 95, Payson, AZ 85547.

3 C23/Basic and Applied Research Department, Lockheed Martin SMSS Company, Houston, TX 77058.

4 Carnegie Institution of Washington, Geophysical Laboratory, 5251 Broad Branch Rd., NW, Washington, D.C. 20015

Abstract– Portales Valley is an unusual metal-veined meteorite that has been classified as an H6-chondrite. It has been regarded either as an annealed impact-melt breccia, as a primitive achondrite, or as a meteorite with affinities to silicated iron meteorites. We studied the petrology of Portales Valley (PV) using a variety of geochemical-mineralogical techniques (optical petrography, SEM, electron microprobe, XRD, Raman spectroscopy, SIMS, INAA, ICP-MS, and XRF). Our results suggest that Portales Valley is the first well-documented metallic-melt meteorite breccia. Mineral-chemical and other data suggest that the protolith to PV was an H-chondrite. The composition of FeNi-metal in PV is somewhat fractionated compared to H-chondrites and varies between coarse vein and silicate-rich portions. It is best modelled as having formed by partial melting at temperatures of ~940-1150 EC, with incomplete separation of solid from liquid metal. Solid metal concentrated in coarse vein areas, and S-bearing liquid metal concentrated in silicate-rich areas, possibly as a result of a surface energy effect. Both carbon and phosphorus must have been scavenged from large volumes and concentrated in metallic liquid. Graphite nodules formed by crystallization from this liquid, whereas phosphate formed by reaction between P-bearing metal and clinopyroxene components, depleting clinopyroxene throughout much of the meteorite and growing coarse phosphate at metal-silicate interfaces. Some phosphate probably crystallized from P-bearing liquids, but most probably formed by solid-state reaction at ~975-725 EC. Phosphate-forming and FeO-reduction reactions were widespread in PV and entailed a change in the mineralogy of the stony portion on a large scale. Portales Valley experienced protracted annealing from supersolidus to subsolidus temperatures, probably by cooling at depth within its parent body, but the main differences between PV and H-chondrites arose because maximum temperatures were higher in PV. A combination of a relatively weak shock event (shock stage S1-S2) and elevated pre-shock temperatures probably produced the vein-and-breccia texture, with endogenic heating being the main heat source for melting, and with stress waves from an impact event being an essential trigger for mobilizing metal. Portales Valley is best classified as an "H7 metallic-melt breccia" of shock stage S1. The meteorite is transitional between more primitive (chondritic) and evolved (achondrite, iron) meteorite types, and offers clues as to how differentiation could have occurred in some asteroidal bodies.

1. INTRODUCTION

The Portales Valley (PV) meteorite is classified as an H6 chondrite (Grossman, 1999) but is recognized as unusual. It is atypical in containing coarse FeNi-metal veins that exhibit Widmanstätten texture, unlike any other known ordinary chondrite, and in exhibiting a large variation in metal content in different specimens, ranging from metal-depleted to enriched (e.g., Kring et al., 1999a,b; Rubin and Ulff-Møller, 1999; Rubin et al., 2001; Ruzicka et al., 1999a,b, 2000a; Pinault et al., 1999). Even in hand specimens, these features can make it clear that PV is no typical H6 chondrite. Other unusual features include the presence of unusually coarse and abundant phosphate (Ruzicka et al., 1999a), large graphite nodules (Ruzicka et al., 2000b), and an unusually bright, red reflectance spectrum (Britt and Kring, 2001).

Another perplexing feature is that radiometric ages based on differing geochemical systems give discordant results (Chen et al., 1999, 2000; Papanastassiou et al., 2001, 2002; Garrison and Bogard, 2001), which has led to differing interpretations (Papanastassiou et al., 2002; Floss et al., 2002; Ruzicka and Killgore, 2002).

Although it is generally believed that Portales Valley originated as an H-chondrite based on mineral-chemical data, oxygen-isotope data, and the presence of relict chondrules (e.g., Kring et al., 1999b; Rubin et al., 2001), the many anomalous features of PV suggest that it was processed in unusual ways. The role of shock in the origin of the meteorite is controversial. The shock stage of PV has been reported to be S1-S3 (Grossman, 1999), and is listed in some data compilations as S3 (Koblitz, 2003), based on the inference that the main features of the meteorite were established by shock, and that subsequent annealing erased shock features (Kring et al., 1999b; Rubin and Ulff-Møller, 1999; Rubin et al., 2001). Others have attributed only a minor role to shock (Pinault et al., 1999; Scott and Pinault, 1999). An underlying point of agreement is that PV was partly melted, although the nature of this melting event has been debated. Possible origins include impact melting (Rubin et al., 2001), partial melting caused by endogenic heating (Pinault et al., 1999), collisions between differentiated and undifferentiated bodies (Ruzicka et al., 1999a; 2000a), or low-velocity collisions between already-warm, accreting bodies (Haack et al., 2000). Portales Valley has been alternately interpreted as an annealed impact-melt breccia (Kring et al., 1999b; Rubin et al., 2001; Rubin, 2004), a primitive achondrite (Pinault et al., 1999; Scott and Pinault, 1999), or a meteorite transitional between chondrites and silicated iron meteorites (Ruzicka et al., 1999a; 2000a; Scott and Pinault, 1999).

We studied Portales Valley using a variety of petrographic, mineralogic, chemical, and modelling techniques to better understand how it may have originated. Both geochemical and thermodynamic modelling were used to constrain the processes and conditions under which the meteorite formed. Our results indicate that PV is the first well-documented example of a metallic-melt breccia, and we suggest that it is transitional between chondrites and various classes of differentiated meteorites.

2. SAMPLES AND ANALYTICAL METHODS

A variety of analytical methods were used to study multiple samples of Portales Valley (Table 1). Eight polished sections of Portales Valley were studied using optical, scanning-electron-microscopy (SEM), electron microprobe (EMP), secondary-ionization-mass-spectrometry (SIMS), x-ray diffraction (XRD), and Raman techniques. These include five sections (4978-1 through -5) of a specimen (AMNH 4978) that contains thin metal veins and large phosphate grains; a fine-grained silicate-rich sample (CML 0056-3) of a different specimen; and two slices (K-2, K-5) of yet a third stone that contains coarse metal veins and a graphite nodule. The AMNH 4978 slices were removed from a specimen that formed roughly a cube ~5 cm across, with four of the sections taken from adjacent locations on one face and the fifth from a perpendicular section (J. Boesenberg, personal communication, 2000). The size of this specimen and the geometry of the cuts suggest that the sections sample a volume of ~125 cm^3 for the 4978 specimen.

Three electron microprobes were used to obtain quantitative phase data. A Cameca SX-50 was used to analyze olivine, orthopyroxene, phosphate, and FeNi-metal at the University of Tennessee (UT) using a 15 kV accelerating voltage and sample currents of 20 nA (silicate and phosphate) and 30 nA (metal). A different SX-50 was used to analyze FeNi-metal and troilite at Oregon State University (OSU) using a 15 kV accelerating voltage and 50 nA sample current. A Cameca SX-100 at the Johnson Spacecraft Center (JSC) was used to analyze olivine, orthopyroxene, clinopyroxene,

FeNi-metal, and troilite using a 20 kV accelerating voltage and a 40 nA sample current. Analyses of plagioclase were obtained at JSC using a 15 kV accelerating voltage and 20 nA sample current. For all analyses except plagioclase, the beam was focussed to ~1 Fm; for plagioclase, the beam was rastered over a 10 x 10 Fm area. Counting times for each element varied from 20 to 120 s depending on the phase being analyzed and the expected concentration of the element.

The UT microprobe was also used for electron petrography (BSE imaging) and x-ray modal mapping of all five AMNH sections. For modal mapping, x-ray energy dispersive spectra (EDS) were obtained from ~1 Fm spots in a grid pattern with analysis spacings every 5.2 Fm, using an Oxford Instruments (LINK) Model eXL II EDS and Feature Scan software. Operating conditions were a 20 kV accelerating voltage and a 3 nA sample current. Altogether, ~36 million EDS points were analyzed over an area of ~976 mm^2. Each EDS spectrum was classified into one of several phases based on x-ray line intensities (% peak area of regions of interest in the spectrum) for various elements. Once a spectrum was classified according to a particular phase, it was removed from consideration in the grid area. Test cases were run to obtain appropriate phase criteria and an appropriate phase identification sequence. The following sequence, elements, and x-ray peak intensities were used to identify phases: olivine (Si 30-50%, Mg 28-60%), orthopyroxene (Si 55-75%, Mg 18-27%, Ca 0-5%), kamacite (Fe 80-100%, Ni 0-6%), taenite (Ni 6.5-50%), troilite (S 30-100%), plagioclase (Al 10-40%, Si 55-85%), merrillite (P 25-75%, Cl 0-2%), apatite (P 25-70%, Cl 3-20%), clinopyroxene (Si 45-70%, Mg 5-18%, Ca 10-30%), chromite (Cr 15-70%), ilmenite (Ti 35-75%), Si-mineral (Si 85-100%), unclassified (none of the above). Roughly 9-16% of the points in the various sections remained unclassified; these included holes in the sections, epoxy from section edges, and grain boundaries. The precision of these modal data are difficult to quantify; we estimate precisions on the order of ~5% relative for each phase, in agreement with that of Gastineau-Lyons et al. (2002).

SIMS analyses were performed using a Cameca 3f at the Woods Hole Oceanographic Institution with the assistance of Dr. Nobo Shimizu. In situ analyses for various rare-earth-elements (REE) and Ca were performed for phosphate minerals (merrillite, Cl-apatite) and low-Ca pyroxene (orthopyroxene) in different textural settings. Five cycles of counts were obtained in each analysis, and count rates for each element were monitored between cycles to check for consistency and to evaluate whether overlap between phases could have occurred. Two standards (Durango apatite, KH-1 clinopyroxene) were analyzed in the same shift as the unknowns. Standard procedures were used to convert count rates for REE in the unknowns to concentrations, based on known REE and Ca abundances in the standards, and a Ca content in the unknowns obtained from EMP data. Uncertainties in concentrations were inferred from counting rate statistics.

X-ray diffraction and Raman analyses were obtained for a graphite nodule. XRD work was performed at the Applied Mineralogy Laboratory at Portland State University using Cu Kα radiation, 2-theta angles stepped at 0.02Eevery 0.80 seconds from 5 to 120E, and an incident beam mask width of 5 mm with an irradiated length of 2 mm. Raman spectroscopy was performed using a Dilor XY Modular Laser Raman Spectrometer at the University of Alabama with the Ar laser operating a wavelength of 514.5 nm. The spectroscopy was performed as Stokes spectroscopy of an unpolished sample at room temperature, with spectra collected through a 100x objective.

Nine additional samples, derived from five different bulk sample aliquots (A-E), were analyzed using instrumental-neutron-activation-analysis (INAA), x-ray fluorescence (XRF), and inductively-coupled-mass-spectrometry (ICP-MS) techniques. These included pieces of silicate-rich fragments (PVA, PVB, PVC, PVE, PVF, PVG, PVH, PVI) and a nearly pure coarse vein metal separate (PVD) (Table 1). Sample PVD was cut from a single coarse vein fragment; the remaining samples were powders of silicate-rich material. Powders of PVA, PVB, PVC, PVE, and PVF were prepared by crushing fragments obtained from unweathered interior portions of the meteorite in a automated ceramic crusher, whereas a powder of PVH was produced by first using a stainless steel chisel to remove a fusion crust, then hand grinding with an agate mortar and pestle, and finally by removing lumps of coarser metal by handpicking. Sample PVH contained two small metal veins before crushing; sample PVC contained a ~5 x 2 mm phosphate patch that was ground together with silicate. For comparison to Portales Valley, two bulk samples of the El Hammami (H5) chondrite were also analyzed using INAA and ICPMS techniques using the same procedures as employed for PV (Table 1). Analyses using INAA, ICP-MS, and XRF were performed at multiple institutions. Samples PVH and PVI were analyzed at JSC using standard INAA procedures after being irradiated at the University of Missouri Reactor Facility for 12 hours with a neutron flux of 5.5 x 10^{13} neutrons $cm^{-2}s^{-1}$ (see Mittlefehldt and Lindstrom, 1993, and references therein). These samples were analyzed along with some of the CM chondrites and Allende standard powders reported in Mittlefehldt (2002). Samples PVA, PVB, PVC, and PVD were analyzed at the OSU Radiation Center after 1-hour and 6-hour epithermal irradiations (neutron flux 3 x 10^{12} $cm^{-2}s^{-1}$), and sample PVG was analyzed at Portland State University after irradiation at the Reed Nuclear College Facility (neutron flux 1.7 x 10^{12} $cm^{-2}s^{-1}$). XRF analysis of sample PVF, and ICP-MS analysis of sample PVE, were performed at the Washington State University (Pullman) Geoanalytical Lab. XRF analyses were obtained using a Rigaku 3370 XRF spectrometer using the procedures described by Johnson et al. (1999). ICP-MS analyses were obtained using a Sciex Elan model 250 ICP-MS using the procedures described by Knack et al. (1994). Uncertainties in INAA concentrations were estimated for each element based on the relative standard deviation in repeated counts of the element in the appropriate standard, or based on counting statistics of the element in the unknown,

whichever was higher. Uncertainties in XRF data were estimated from the relative standard deviation in multiple determinations for a standard (GSP-1) during a single XRF run over a three week period. Uncertainties in ICP-MS concentrations were estimated from the relative standard deviation in multiple determinations of two standards (BCR-P and TED) in different experiments between 1992-1994 (BCR-P) and 1995-1999 (TED).

3. RESULTS

3.1 Petrography and mineralogy

3.1.1 Overall petrography of Portales Valley

Portales Valley has notable petrographic features, including metal-veining textures, Widmanstätten texture in coarse FeNi-metal veins (Fig. 1a-c, Fig. 2, Fig. 3a), troilite veins (Fig. 1b, c), and coarse phosphate (mainly merrillite, also Cl-apatite) that is usually in contact with metal (Fig. 1b, Fig. 3).

Metal-veining textures vary. Some areas show what appear to be cataclastic texture, with silicate clasts of various sizes defined by metal veining (Fig. 1a); in other areas, metal veins appear intergrown with silicates and evidence for cataclasis is not obvious (Fig. 1b, c, 2a, 3a). Different sizes of metal veins are present, ranging from ~1-2 mm wide (Fig. 1b, 2a, 3a) to >5 mm (even >few cm) wide (Fig. 1a, 4a). The coarsest metal veins appear to occur in areas with the best cataclastic texture (Fig. 1a), whereas thin metal veins are prevalent in more intergrown areas (Fig. 1b). The textures of intergrown areas are suggestive of metamorphic grain growth, whereas the textures of cataclastic areas are more consistent with deformation. The sharp, relatively straight contacts between silicate and coarse metal veins in cataclastic areas (Fig. 1a) suggest relative movement of metal and silicate. In some areas, metal appears to have been injected into already-formed silicate clasts forming small metal-rich pockets (region "x" in Fig. 1a). This suggests that metal was mobilized over an extended period of time.

Although most troilite in PV is intergrown with silicates away from metal veins, some veins of troilite are present that connect with and continue the trend of metal veins (Fig. 1b, c). At connection points with metal veins, troilite surrounds projections of metal and appears to have crystallized after metal (Fig. 1c).

Widmanstätten texture (oriented kamacite lamellae enclosed within Ni-rich metal) occurs in metal veins that are $1 mm wide (Fig. 2b-c), with thinner veins showing an incipient Widmanstätten texture composed of isolated kamacite lamellae within Ni-rich metal (Fig. 2a). In areas with Widmanstätten texture, swathing kamacite separates silicate from the cores of veins that contain oriented kamacite lamellae surrounded successively by zoned taenite and plessite (Fig. 2b-c). These features are absent in thinner veins, although like the coarser veins, kamacite often occurs at the contact with silicate, separating silicate from taenite in the core of the vein (Fig. 2a).

Phosphate in Portales Valley is locally coarse (up to ~few mm wide) and occasionally forms veins. The coarsest phosphate grains enclose silicate grains. One polymineralic vein dominated by merrillite is ~0.5-1 mm wide, ~6 mm long, and continues along the trend of both metal and troilite veins (Fig. 3c, 1b). Within merrillite veins, as well as in larger merrillite grains adjacent to metal, phosphate encloses euhedral or subhedral grains of olivine, low-Ca pyroxene,

and plagioclase in an apparently poikilitic texture (Fig. 3b, c). This texture probably indicates that merrillite and the enclosed silicates crystallized from a melt (phosphate last), but it also could be interpreted as a poikiloblastic texture produced by metamorphism (phosphate overgrowing silicates).

In silicate-rich areas, barely discernible relict chondrules are present (Fig. 1b). In contrast to poikilitic phosphate-rich areas, grains in silicate-rich areas have predominantly anhedral shapes with an interlocking polymineralic texture (Fig. 1d). The overall texture of silicate-rich areas suggests that appreciable metamorphism of a chondritic precursor occurred. Despite this, silicate grain sizes are fairly small (typically <100-200 μm) (Fig. 1c-e) and somewhat less than in other H6 chondrites (Rubin et al., 2001).

3.1.2 Shock stage and deformation

We infer a low shock stage (S1) for Portales Valley based on traditional application of the Stöffler et al. (1991) petrographic shock scale. Olivine mainly has uniform extinction, and generally lacks planar fractures or planar deformation features, although some planar features were reported present by Rubin et al. (2001). Our observations suggest that at most 5% of the olivine grains in Portales Valley have slight undulose extinction; the remainder show uniform extinction. Plagioclase has not been transformed to maskelynite and typically shows uniform extinction, although in most places it is too fine-grained to analyze reliably for extinction. No glassy or melt pockets or pseudotachylite veins are present. An S1 shock stage for PV agrees with the listing given by Rubin (2004).

Although Portales Valley has a low shock stage, it shows evidence for deformation. The most obvious evidence for deformation is the cataclastic texture (see above). Silicate clasts have been displaced along metal veins, as observed by previous researchers in polished sections (Kring et al., 1999b; Rubin et al., 2001) and by us in handspecimen (Fig. 1f). The latter evidence implies that silicate-rich clasts have moved by up to ~1 cm relative to each other and metal veins (Fig. 1f). In addition, ~5% of the larger olivine grains show undulose extinction, which is suggestive of shock-deformation. Other proposed shock indicators found in PV include the presence of small amounts of metallic Cu (Rubin, 1993; Rubin et al., 2001), rare chromite-plagioclase assemblages (Rubin et al., 2001; Rubin, 2003), and the presence of tiny metal and sulfide inclusions in silicates (Fig. 1d) (Kring et al., 1999b) that has lead to shock-blackening in some areas (Rubin et al., 2001; Rubin, 1992). "Sprays" of metal from smaller grains in the silicate-rich portion of PV were interpreted as having been produced by shock-mobilization of metal (Kring et al., 1999b).

Although it has been proposed that the coarse metal veins in Portales Valley formed by shock (Kring et al., 1999b; Rubin et al., 2001), the low shock stage of PV suggests that a shock origin for the veins is neither obvious nor conclusive. It has been proposed that PV may have been shocked to higher levels (to S3 or even to S6), but then annealed, so that the apparent shock stage changed to S1 (Grossman, 1999; Kring et al., 1999b; Rubin et al., 2001; Rubin, 2004). This is based largely on the presence of some apparent undulose extinction in plagioclase (Grossman, 1999;

Kring et al., 1999b) and the presence of localized shock blackening (Rubin et al., 2001; Kring et al., 1999b). However, as noted above, evidence for undulose extinction in plagioclase is largely equivocal. Moreover, shock-blackening can be produced at low shock stage by the "frictional melting" of metal (van der Bogert et al., 2003). Further evidence for shock is described in the next section, the origin of the coarse veins in PV is evaluated in Sec. 4.5, and the significance of shock in the overall origin of the meteorite is discussed at more length in Sec. 4.10. Here we emphasize that an S1 shock stage is most appropriate for Portales Valley, and that the S3 shock stage listed in some data compilations (Koblitz, 2003) is largely model-dependent.

3.1.3 Graphite nodules

An unusual attribute of Portales Valley is that it contains coarse (cm-sized) graphite nodules (Ruzicka et al., 2000b). Two separate nodules were found fully enclosed within coarse (2-4 cm across) metal areas. One of these nodules was studied in detail. This nodule was discovered after making a large cut which broke a blade as it cut through the nodule (Ruzicka et al., 2000b). Subsequently, multiple parallel cuts were made through the nodule, providing information on its true extent (Table 2). Overall, the nodule has an irregular shape, varying from roughly equant to highly elongate in different exposed surfaces (Table 2). Assuming an estimated cut loss of ~1.7 mm between the various slices, the nodule is >22.5 mm deep in the dimension perpendicular to the cuts. Together with the exposed surfaces of the nodule, this implies a volume of >2.3 cm^3 for the nodule.

One exposed face of the nodule (surface 9, Table 2; Fig. 4) was studied with reflected light microscopy. In this face the nodule is elongate (Fig. 4). The contact between the nodule and enclosing metal vein is irregular in detail (Fig. 4). Veinlets and inclusions of FeNi-alloy, largely or entirely kamacite, occur within the main graphite body (Fig. 4b). Most of the metal inclusions are <50 μm across, although they reach up to ~120 μm near the edges of the nodule. There are two types of veins. One type consists of semi-continuous necklaces of metal inclusions that are often aligned perpendicular to the main axis of the nodule (Fig. 4b). The other type of vein consists of very thin, continuous veinlets (<2 μm wide) that have an irregular shape and which form a branching pattern (Fig. 4b). The most prominent of these veinlets are oriented parallel to the long dimension of the nodule. Based on the observations of inclusions of graphite inside metal and vice-versa, as well as the gradational contact between the metal vein and main graphite body, contemporaneous formation of metal and graphite is inferred. In the coarse metal around the nodule, unusually thick kamacite lamellae (up to ~700 μm wide) bend around the nodule, which suggests that metal was strained around the graphite.

We evaluated whether diamond might be present in the graphite that was responsible for breaking the blade in the initial saw cut, by using Raman spectroscopy on one of the faces produced in this cut (surface 3, Table 2), as well as x-ray diffraction (XRD) of another surface (surface 9, Table 2; Fig. 4). Raman spectra and XRD can detect diamond or

other high pressure polymorphs, and Raman spectra of graphite are useful shock barometers (Kenkman et al, 2002; El Goresy et al., 2002; Lapke et al., 2000). Verification of diamond or other high pressure polymorphs in the graphite would provide evidence that the graphite was shocked, and possibly indicate an important role for shock in the origin of PV.

With XRD we moved x-ray beams into different locations in an attempt to locate diamond. Using a beam that illuminated only the vein enclosing the nodule, no graphite was detected and only kamacite and "FeNi-metal" (presumably a more Ni-rich metal) was detected. Using a beam that illuminated only the nodule, only graphite and kamacite was detected. No evidence for high-pressure polymorphs such as diamond, lonsdaleite, or chaoite was found.

Fig. 5 shows the Raman spectrum for the nodule. The Raman spectrum shows peaks at ~1580 cm^{-1} and ~1360 cm^{-1} attributed to graphite, and no peak at ~1331 cm^{-1} as would be expected for diamond. Raman peaks at ~1318 to 1333 cm^{-1} for apparently shock-produced diamond inside graphite nodules from Canyon Diablo were found by Miyamoto (1998), but no such peaks are evident in the PV Raman spectrum (Fig. 5), consistent with the generally low shock stage for PV (Sec. 3.1.2).

However, some disorder in PV graphite is implied by the Raman data. Crystalline graphite has a Raman "G-band" composed of merged peaks at ~1588 and 1582 cm^{-1} ; with increasing disorder, a "D-band" occurs at ~1355 cm^{-1} (e.g., Kagi et al., 1991, 1994) and the 1582 cm^{-1} peak broadens and moves to lower frequencies (Kagi et al., 1994; Lapke et al., 2000). Disordered graphite with small domain size also produces a Raman peak at ~1620 cm^{-1} which appears as a higher-frequency shoulder on the G-band (Kagi et al., 1994). The intensity ratio of the Raman G/D (1580/1360 cm^{-1}) peaks in graphitic carbon was attributed by Kagi et al. (1991) and Lapke et al. (2000) to the degree of structural ordering, ranging from amorphous (G/D ~1.3), to semi-ordered graphite (~2), to well-ordered graphite (~4), to "holo-ordered" graphite (4) (Kagi et al., 1991). The G/D band intensity ratio for PV graphite is ~5.6, which implies that PV graphite is "well-ordered" but not "holo-ordered". Additional evidence for minor disorder in PV graphite is provided by the G-band peak position (~1580 cm^{-1}) and high frequency shoulder (Fig. 5).

The XRD and Raman data for graphite allow a fairly precise estimate to be made of the shock pressure and shock stage of Portales Valley. Although disordering of PV graphite is relatively minor, shock pressures of just over ~5 GPa are implied, based on the calibration of the G/D Raman band intensity ratio provided by Lapke et al. (2000). Similarly, the failure to find diamond or other high-pressure C polymorphs in Portales Valley suggests shock pressures <10-15 GPa, based on the calibration provided by Bischoff and Stöffler (1992). Thus, PV may have been shocked to pressures of ~5-10 GPa, and (based on the Raman data) probably closer to ~5 GPa. This is somewhat above the S1-S2 transition pressure of ~4-5 GPa (Stöffler et al., 1991), but not by much. We conclude that although the graphite data are consistent with the possibility that some shock effects in PV (such as internal strain in olivine) were erased by annealing, they do not provide evidence for initial shock stages higher than S2.

3.1.4 Modal composition

Modal data for five sections of Portales Valley AMNH 4978 determined by x-ray modal mapping are given in Table 3. Data are shown normalized to 100% total in Fig. 6a, and normalized to metal- and sulfide-free abundances in Fig. 6b. The examined sections contain relatively small metal veins and appear to be representative of areas that contain neither very coarse (>1 cm wide) metal veins nor large silicate-rich regions depleted in metal, although some contain coarse merrillite and apatite (Fig. 1b, 3a).

In these sections, metal and sulfide contents range from values typical to those found in H-chondrites (in 4978-5) to 3-4x enriched (in 4978-1) (Fig. 6a). Metal contents locally as high as ~45 vol% are observed, and these are similar to those found in stony-iron meteorites. Phosphate abundances also vary dramatically, ranging from values similar to those in H-chondrites (in 4978-4) to ~4x enriched (in 4978-5) (Fig. 6a, Table 3). Although most phosphate is concentrated adjacent to metal, there is no correlation between the amount of phosphate and the amount of metal. The variations in phosphate and metal almost certainly manifest the inhomogeneous distribution of these relatively coarse phases. Large variations in the abundance of metal also result in large variations in the abundances of other major phases such as olivine, orthopyroxene, and plagioclase according to a mass balance effect (Fig. 6a). In contrast, the abundance of high-Ca pyroxene in PV is consistently depleted (by a factor of ~0.25x) compared to that typically present in H-chondrites (Fig. 6a, Table 3). Clinopyroxene is relatively fine-grained in PV, and the consistently low abundance for it in the five sections examined implies that large portions of PV are depleted in this phase.

Fig. 6b shows mineral abundances normalized on a metal- and sulfide-free basis. On this basis, the investigated sections of Portales Valley are significantly depleted in clinopyroxene, variably enriched in phosphate, and variably depleted in olivine and enriched in orthopyroxene (low olivine/pyroxene) compared to H-chondrites (Fig. 6b). To first approximation, the proportion of plagioclase in the non-metallic portion of PV is similar to that found in H-chondrites, although some sections are slightly enriched in plagioclase (Fig. 6b).

The variable and generally low values of olivine/pyroxene in PV warrant comment. If such low values are real, they indicate that the silicate portion of PV as a whole cannot be considered to be an H-chondrite. Fig. 6c shows olivine/pyroxene abundance ratio and FeNi-metal abundances for the five PV sections compared to H-chondrites, with the latter based on normative calculations using bulk-chemical data (Jarosewich, 1990). A field for acapulcoites, which are possible analogues to Portales Valley (Pinault et al., 1999; Scott and Pinault, 1999), is also shown in Fig. 6c. Fig. 6c shows a crude correlation between olivine/pyroxene ratio and FeNi-metal abundance in PV, with one section (4978-5) clearly having values typical for H-chondrites, and the other four sections having a low olivine/pyroxene ratio and high metal abundance. The apparent crude trend shown by PV differs from a correlation shown by H-chondrites, which can be extended to the acapulcoite field (Fig. 6c). An inverse relationship between olivine/pyroxene ratio and metal

abundance is suggestive of a redox trend, but the one shown by PV clearly differs from the one seen within H-chondrites, or between H-chondrites and acapulcoites (Fig. 6c).

Using the same x-ray mapping technique (with similar but not identical software and hardware parameters) and the same instrumentation as used here, Gastineau-Lyons et al. (2002) studied L and LL chondrites and found that modal olivine/pyroxene ratios inferred from mapping were systematically lower than what would be inferred from a normative calculation, for reasons that were unclear. If our data were subject to the same effect, apparently low olivine/pyroxene ratios might be an artifact of the procedures used. However, a systematic difference similar to that found by Gastineau-Lyons et al. (2002) cannot explain the H-like abundances of olivine, pyroxene and FeNi-metal in section 4978-5, unless this is pure coincidence (Fig. 6b, 6c). If our technique was underestimating olivine/pyroxene values, it should have done so consistently, and not provided an H-like ratio for the one section that also contains H-like metal abundances. Thus, we believe that the mapping technique we used provide accurate results, and that the relatively low abundances of olivine and high abundances of orthopyroxene found in other sections of PV are not artifacts. Instead, the low olivine/pyroxene ratio seen in some sections of PV could be indicative of a redox effect.

Based on x-ray mapping, it is clear that the modal composition of PV is unlike that of H-chondrites, even on a metal and sulfide-free basis. Notable features of PV include highly variable abundances of metal, troilite, and phosphate, a consistently low abundance of clinopyroxene, and variable olivine/pyroxene ratios, with the latter ranging from "normal" in areas with H-chondrite abundances of metal and troilite, to lower values in more metal-enriched areas. Implications of the modal data are discussed in Sec. 4.9.

3.2 Phase compositions

3.2.1 Microprobe data

Microprobe data for silicates and phosphate minerals are summarized in Table 4 and 5, respectively, and microprobe data for FeNi-metal and troilite are summarized in Table 6 and illustrated in Fig. 7-9. These data show that the major- and minor-element mineral chemistries of silicate, phosphate and troilite in PV are generally similar to those in H-chondrites, but that the composition of metal is somewhat unusual.

Olivine ($Fa_{19.6\pm0.5}$), low-Ca pyroxene ($Wo_{1.6\pm0.4}$ $Fs_{17.2\pm0.2}$), high-Ca pyroxene (augite, or subcalcic diopside), and plagioclase have compositions typical of that in type 4-6 H-chondrites (Table 4) (Brearley and Jones, 1998). A uniform An content (12.7 ± 0.3 mol%) in PV plagioclase is unlike that in some shocked type 4-6 ordinary chondrites (Rubin, 1992). The MgO and FeO contents in PV plagioclase are low (~0.01 and <0.5 wt%, respectively) compared to those for type 4-6 ordinary chondrites (~0.1-0.5 wt% and ~0.1-1.2 wt%, respectively) (Brearley and Jones, 1998). The higher MgO and FeO contents of the literature values could be an artifact caused by secondary fluorescence from adjacent ferromagnesian phases; we were careful to accept only high-quality analyses. Merrillite and Cl-apatite have relatively

uniform compositions that are similar for coarse phosphate adjacent metal, vein-forming merrillite, and smaller grains in silicate-rich areas (Table 5). These compositions are also similar to those in type 4-6 ordinary chondrites (Brearley and Jones, 1998), except that FeO and MgO contents in Cl-apatite from PV appear to be somewhat lower. Altogether, the major phases in Portales Valley are homogeneous, suggestive of a high degree of metamorphism.

The composition of metal in Portales Valley varies spatially. Fig. 7 shows spatial Ni and Co variations in a traverse obtained between two kamacite lamellae in a coarse vein with Widmanstätten texture (Fig. 2c). Kamacite adjacent to taenite shows a pronounced "Agrell dip" (Fig. 7, Table 6), consistent with diffusional exchange between kamacite and taenite occurring during slow cooling at low temperature (Ruzicka et al., 1999b). Ni-rich metal adjacent to kamacite is strongly zoned in Ni and Co (Fig. 7), with such "zoned taenite" being consistent with this type of diffusional exchange. Vein plessite shows large apparent variations in Ni and Co (Fig. 7), consistent with the presence of a fine-grained intergrowth of Ni-rich and Ni-poor metal.

Kamacite and taenite compositions differ depending on whether metal from coarse veins or fine-grained metal in silicate-rich areas is analyzed. For kamacite, coarse vein metal grains have Ni and Co compositions that overlap those found in H-chondrites, whereas metal grains in silicate-rich areas are often enriched in Co (Fig. 8a). Both coarse- and fine-grained kamacite grains have grain rims with low Ni content ("low-Ni tails" in Fig. 8a). Taenite grains also show chemical differences between coarse- and fine-grained metal, but in a manner opposite to that of kamacite. Namely, taenite in silicate-rich areas has Ni and Co contents which overlap those present in H-chondrites, whereas taenite in coarse veins has Ni and Co compositions that overlap those found in L-chondrites (Fig. 8b).

So far as we are aware, such Ni-Co fractionations in metal are unprecedented in a single ordinary chondrite. These fractionations can perhaps best be seen in a diagram which plots Co/Ni vs. Ni (Fig. 9). In this type of diagram, metal from H4-6 chondrites is well-distinguished from that in L4-6 chondrites. Portales Valley kamacite grains in both veins and silicate-rich areas have compositions that differ from one another but still generally resemble those found in H-chondrites (Fig. 9). Similarly, data for the bulk composition of PV vein metal suggest that it is enriched in Ni, but still similar to the bulk metal in H-chondrites (Fig. 9). However, the composition of coarse vein taenite is clearly more similar to the taenite present in L-chondrites, whereas taenite in silicate-rich areas is more similar to that present in H-chondrites (Fig. 9).

Traverse data (e.g., Fig. 7) shed some light on the nature of Ni-Co variations seen in PV metal (Fig. 8-9). For kamacite, it is clear that the low-Ni "tail" in PV coarse and fine metal is the result of low-temperature equilibration with taenite, but the offset Co contents between the coarse and fine metal (Fig. 8a) suggests equilibration in systems with two distinct compositions. For taenite, the inverse correlation between Ni and Co seen in both coarse and fine metal (Fig. 8b) is also clearly the result of low-temperature equilibration with kamacite, as suggested by the inverse correlation between Ni and Co in the zoned taenite (Fig. 7). Again, the offset trends between coarse and fine metal (Fig. 8b) suggest

equilibration in two systems of different bulk composition. Evidently, metal in coarse veins is chemically fractionated from that in silicate-rich areas. The significance of this fractionation is discussed in Sec. 4.2, 4.3, and 4.4.

3.2.2 Two-pyroxene geothermometry

High-quality analyses of low-Ca pyroxene and augite were used to estimate pyroxene equilibration temperatures based on a graphical pyroxene geothermometer (Lindsley and Andersen, 1983; Lindsley, 1983). With this geothermometer, temperature estimates to a precision of ~ ±10 EC can be made. For low-Ca pyroxene (N=40 analyses), the estimated temperature is 770 ± 60 EC (mean and standard deviation, respectively), with individual values ranging between 900-650 EC. For augite (N=13), the calculated temperature is 900 ± 35 EC, ranging between 995-870 EC. For comparison, McSween and Patchen (1989) used the same geothermometer and found temperatures for type 6 ordinary chondrites of ~800-900 EC for orthopyroxene, and ~900-960 EC for clinopyroxene. The values for Portales Valley overlap those in type 6 ordinary chondrites, but are somewhat lower. In PV, temperatures for orthopyroxene are lower than for clinopyroxene, as also found by McSween and Patchen (1989) for chondrites in general, which they attributed to unknown kinetic factors. The lack of agreement between ortho- and clinopyroxene in PV suggests that the pyroxene in the meteorite did not fully equilibrate at the temperatures implied by geothermometry (~700-950 EC). Further implications of this data are discussed in Sec. 4.8.

3.2.3 SIMS data

Trace-element SIMS data were obtained for eight rare-earth-elements (REE) in low-Ca pyroxene and in phosphate minerals in two sections of Portales Valley. These data are shown in Table 7 and Fig. 10. Low-Ca pyroxene (orthopyroxene) analyses were obtained for grains in different settings, including grains poikilitically enclosed within phosphate, a grain enclosed by metal, and a typical orthopyroxene grain in a silicate-rich area. Analyses were also obtained for both coarse Cl-apatite and merrillite associated with metal veins, and for a typical fine-grained merrillite in a silicate-rich area.

CI-normalized REE abundances in all of the orthopyroxenes are flat to slightly depleted in light REE (LREE) (Fig. 10a). There is no obvious difference between grains in different textural settings. Anomalously high Ce abundances were obtained for one of the orthopyroxenes (analysis 2-1-3) enclosed within phosphate (Fig. 10a, Table 7a). For this analysis, counts for Ce dropped after the first of 5 cycles (Table 7a), suggesting that the high Ce content is an artifact of weathering. For the orthopyroxene analyzed in a silicate-rich area (analysis 2-6-2), Eu counts increased significantly in the last 3 cycles, suggesting that the SIMS beam penetrated to a Eu-rich phase (plagioclase) (Table 7a). Altogether, the overall REE abundances in low-Ca pyroxene appear to be somewhat low in PV compared to other equilibrated ordinary chondrites (Fig. 10a). This could indicate that some of the REE normally found in orthopyroxene was partitioned into an REE sink such as phosphate or clinopyroxene.

In general, REE abundances of Cl-apatite and merrillite resemble those in ordinary chondrites (Fig. 10b). Cl-apatite has a CI-normalized LREE-enriched pattern with a positive Eu anomaly (Fig. 10b). REE concentrations in merrillite vary considerably (Table 7b), although all have similar CI-normalized abundance patterns, with a prominent negative Eu anomaly, a generally flat to heavy-REE (HREE) depleted pattern, and the highest CI-normalized abundances occurring for Nd (Fig. 10b). Again, there is no obvious difference between coarse phosphate associated with metal veins and with fine-grained phosphate in silicate-rich areas (Fig. 10b). The significance of these data are discussed in Sec. 4.7.

3.3 Bulk composition

Bulk-chemical data obtained by INAA, XRF, ICPMS, and modal reconstruction of various splits of Portales Valley are shown in Tables 8-10 and Figs. 11-12. Trace-element data were obtained of silicate-rich fragments (Fig. 11a-b) and a separate of coarse vein metal (Fig. 11c), whereas major-element data were obtained for various metal-veined samples and a metal-poor sample (Fig. 12).

Data for the silicate-rich fragments (Fig. 11a-b) document spatial variations in composition, primarily of those elements that concentrate in phosphate and in metal. This undoubtedly reflects an inhomogeneous distribution of these phases. Siderophile elements are generally depleted in these samples compared to a reference H5 chondrite, as one might expect for metal-poor areas, but abundances vary by a factor of ~3 and abundance patterns are somewhat fractionated (Fig. 11a). The significance of these fractionated compositions is discussed at more length later (Sec. 4.2, 4.3).

With regard to lithophile elements, Fig. 11a-b show that different silicate-rich samples vary in their abundances of those elements (REE, Y, and to a lesser extent Th) that normally concentrate in phosphate. Sample PVC is enriched in these elements, and samples such as PVE are depleted in them. The lack of significant variation in other incompatible trace elements such as Zr, Nb, Hf, Rb and Sr, and the uniform abundances of the semi-incompatible Sc (Fig. 11a-b), make it clear that significant chemical variations in PV are not caused by standard igneous processes, but rather by an inhomogeneous distribution of phosphate. Similarly, Fig. 12 shows large variations in the abundances of those elements that concentrate either in phosphate (Ca, P), metal (Fe, Ni) or troilite on a Si-normalized basis, indicating that these phases are the most spatially variable in PV.

Simple mixing models also support the idea that variations in phosphate abundance are responsible for the observed chemical variations in lithophile elements and quantify the abundance variations. Fig. 13 shows results of a mixing model for REE in which variable amounts of merrillite are added to or subtracted from an average H-chondrite containing 0.4 wt% merrillite, compared to the measured abundances in various splits. This model assumes that only the abundance of merrillite is varying, and that the composition of the remaining non-merrillite fraction is constant. The shapes of the predicted and observed patterns are similar, including the sizes of Eu anomalies (Fig. 13), suggesting that variations in the abundances of merrillite can largely account for the chemical variations seen in PV. Compared to an

average H-chondrite with ~0.4 wt% merrillite, sample PVC could be ~2-3x enriched, whereas the remaining samples could be $2-3x depleted (Fig. 13). The lack of detailed agreement between the calculated and observed abundances is easily explained if other phases besides merrillite have non-chondritic proportions. For example, comparatively low HREE abundances in sample PVE, PVH, and PVC compared to the models (Fig. 13) could indicate a low content of an HREE-rich phase such as clinopyroxene, which is widely depleted in PV compared to H-chondrites (Fig. 6).

Trace-element and Ni abundances of a coarse metal separate from PV are grossly similar to that of average metal in H4-6 chondrites, but different in detail (Fig. 11c). In both our sample and two samples of coarse metal analyzed by Rubin et al. (2001), Ga and Au abundances are higher than in H-chondrites. In both our sample and one analyzed by Rubin et al. (2001), Ni abundances are significantly higher than in H-chondrites. We also found As to be depleted in the coarse metal relative to H-chondrites, but the opposite was found by Rubin et al. (2001). These data suggest that coarse metal in PV has a spatially variable composition. This is not hard to imagine given the non-uniform textures and various proportions of Ni-rich and Ni-poor metal observed in metal veins (Fig. 2).

In general, the trace-element composition of coarse metal in PV also resembles that of metal from IIE irons, especially in elevated Ga content (Fig. 11c). The composition of coarse vein metal analyzed by us (sample PVD) overlaps the range found in IIE iron meteorites for all elements except Ni, with the concentration of this element in IIE irons being lower and more similar to that found in H-chondrites and in sample #1 of Rubin et al. (2001).

In summary, the bulk composition in significant volumes of PV is not “H-chondritic”, although there is an overall resemblance to H-chondrites. This is true both for the non-metallic and metallic fractions of the meteorite.

4. DISCUSSION

4.1 Protolith for Portales Valley

The classification of Portales Valley as an H6 chondrite (Grossman, 1999) belies the many unusual attributes of the meteorite but correctly points to a likely H-chondrite protolith of at least the silicate fraction of the meteorite. Evidence for an H-chondrite protolith includes the presence of relict chondrules, the H-chondrite like mineralogy and mineral-chemistry of olivine, orthopyroxene, clinopyroxene, plagioclase, and phosphate, and the H-chondrite-like bulk O-isotopic composition of the silicates (see above; and Kring et al., 1999b; Rubin et al., 2001).

The origin of the metallic portion of PV is more debatable. Possibilities include metal mobilized locally but derived entirely from an H-chondrite source (Kring et al., 1999a,b; Pinault et al., 1999; Rubin et al., 2001), or metal derived in part by collision with another object, such as that which could have produced IIE-iron (Ruzicka et al., 1999a; Ruzicka et al., 2000a; Mathew et al., 2001) or IAB-iron meteorites (Mathew et al., 2001). The metallic portion of PV is clearly unlike that found in ordinary chondrites, in terms of coarseness, vein-like structure, locally high concentration, and presence of well-developed Widmanstätten texture. The coarse metal has been found to contain cm-sized graphite

nodules, which are absent in other ordinary chondrites (Ruzicka et al., 2000b). Both the Widmanstätten texture and graphite nodules suggest a relationship to iron meteorites. As noted above, metal in PV has some unusual chemical features, including unusual Co/Ni vs Ni systematics (Fig. 8, 9); high abundance of Ga (Fig. 11c); and a difference in major- and trace-element composition between coarser vein metal and finer-grained metal associated with silicate-rich areas. All of these anomalies raise a question as to the provenance and origin of the metal in PV.

A high abundance of Ga in PV coarse metal has been found both in this study and that of Rubin et al. (2001), although different concentrations were measured (~30 and ~18 ppm, respectively) (Fig. 11c; Table 8). The values for both measurements are significantly higher than for metal typically present in H-chondrites (14±2 ppm) and are similar to that found in metal from IIE iron meteorites (25±3 ppm) (e.g., Wasson and Wang, 1986; Ebihara et al., 1997). Although this lends support to an admixture of IIE-like metal to PV, high Ga abundances in chondritic metal can be produced by a high degree of thermal metamorphism or by shock (Chou and Cohen, 1973), presumably by transfer of Ga from silicates to metal during heating. Thus, high Ga abundances in PV metal do not strongly favor a particular model, although they do imply an unusual history for the metal.

Data for N-isotopes also indicate that PV metal is distinct from that found in ordinary chondrites (Mathew et al., 2001). According to Mathew et al. (2001), the N-isotopic composition of the fine-grained metal in PV resembles that in IAB meteorites and could have formed by impact-melting, with a contribution from a IAB-like source region. The same authors suggested that the coarse metal may have been derived from a different iron meteorite source region, such as that which produced IIE irons. However, we note here that the N-isotope composition of the coarse vein metal in PV ($\delta^{15}N \sim$ -26 ‰; Mathew et al., 2001) is distinctly different than that in IIE irons ($\delta^{15}N = -2.3 \pm 1$ and -7.5 ± 1.5 ‰; Mathew et al. 2000), which implies that the coarse metal in PV does not directly represent material derived from a IIE-like source region. Instead, coarse vein metal in PV has a N-isotopic composition similar to that in one of two IVA iron meteorite subgroups (with $\delta^{15}N = -26 \pm 2$ ‰; Mathew et al., 2000). The significance of these findings are unclear, in part because spallation-corrections need to be made to determine the indigenous N-isotopic composition of PV metal more accurately (Mathew et al., 2000), and in part because the processes (shock? static heating?) that can affect N-isotopic composition in metal are uncertain. Although the compositional similarities of metal in PV to that in IAB, IVA, and IIE irons are tantalizing, they are inconclusive.

Clearly, PV metal has some compositional and textural similarities to silicated iron meteorites (IIE, IAB, IVA). A partly exogenous origin of metal (derived from a source region different from that of an H-chondrite) remains possible. However, the complementary pattern for large portions of PV to be depleted in metal and other portions to be enriched is best explained by a model in which metal is locally redistributed (Kring et al., 1999b; Pinault et al., 1999; Rubin et al., 2001). Below, we adopt the hypothesis that the protolith for PV was an H-chondrite, and that this protolith was modified in ways atypical for chondrites.

4.2 Evidence for melting and fractionation of metal

The most obvious distinction of Portales Valley are the coarse metal veins it contains and spatially variable abundances of metal over large portions of the meteorite. Metal appears to have been transported on a scale of a few to tens of centimeters and concentrated into sheet-like veins, leaving behind silicate-rich areas depleted in metal (Kring et al., 1999a,b; Pinault et al., 1999; Scott and Pinault, 1999; Rubin et al., 2001). Metal-silicate textures imply that a large portion of the metallic fraction in PV was fluidized, as if it were molten or substantially molten (Fig. 1, 2) (Pinault et al., 1999; Scott and Pinault, 1999; Ruzicka et al., 1999a; Rubin and Ulff-Møller, 1999; Rubin et al., 2001). Widmanstätten textures and Ni zoning patterns imply that coarse metal in veins consisted of large taenite parent crystals at high temperature, which exsolved at a lower temperature to form kamacite (Fig. 2, 7) (Kring et al., 1999a,b; Pinault et al., 1999; Ruzicka et al., 1999b; Reisener and Goldstein, 2003), consistent with idea that metal nucleated and grew from a liquid. Rubin et al. (2001) found evidence with high-resolution x-ray computerized tomography (HRXCT) for apparent flotation of smaller silicate clasts within coarser metal veins, implying not only that metal was significantly molten, but that movement of metal and silicate occurred over an extended time period in the presence of a non-negligible gravity field, or perhaps in a spinning body.

Besides textures, the composition of metal in PV is also anomalous and spatially variable (this study; Kring et al., 1999b; Rubin and Ulff-Møller, 1999; Rubin et al., 2001; Ruzicka and Killgore, 2002). Unusual Co/Ni vs Ni systematics for metal in PV and differences between coarse and fine metal (Fig. 8, 9) imply that metal in Portales Valley was geochemically processed and does not simply represent mobilized H-chondrite metal. Kring et al. (1999b) noted possible slight differences in the composition of kamacite between coarse veins and finer-grained metal (higher Ni content in kamacite from coarse veins, lower in kamacite from silicate-rich areas), and suggested this could be due to incipient differentiation. Rubin and Ulff-Møller (1999) and Rubin et al. (2001) noted that coarse metal in PV is moderately fractionated compared to H-chondrites, with Ir, Pt, and Re low, and Ga, As, and Au enriched.

The variation in metal abundance and composition in PV is clearly shown by variations in siderophile element abundances between different samples (Fig. 14). Data are shown in Fig. 14 for an essentially pure coarse metal vein separate (PVD) as well as for silicate-rich, metal-depleted samples (PVA, PVB, PVC, PVF, PVH, PVI). Also shown for reference is a bulk sample of the El Hammami H5 chondrite (EH1). The measured compositions are compared to a simple model in which various amounts of average H-chondrite metal are mixed with average H-chondrite non-metallic fraction (REFS). This mixing model tests whether variations in siderophile element abundances are caused by variations in metal abundance alone, assuming that metal maintains a constant H-chondrite-like composition. The model can explain the pattern observed for the reference EH1 sample if it contains just under ~20 wt% H-chondrite-like metal, which is similar to the average amount of metal (~17 wt%) in H-chondrites (Fig. 14). The model cannot explain the high Ga abundances in EH1 (Fig. 14). This may indicate that Ga is enriched in the EH1 sample relative to typical H-

chondrites. Based on Fe and Ni abundances, the mixing model also is consistent with the observed range in metal for various sections of PV4978 (~20-60 wt% in AMNH 4978, corresponding to ~8-44 vol% metal).

However, the simple metal-silicate mixing model shown in Fig. 14 does not reproduce the pattern for siderophile elements in silicate-rich samples of Portales Valley (PVA, PVB, PVC, PVI or PVH), and it also does not completely agree with the pattern observed for the coarse metal separate (PVD). The coarse metal contains more Au, Ni, and Ga than predicted for 100% H-chondrite metal. Although Ga and Fe abundances in bulk silicate-rich samples cannot be used as strict indicators of metal composition owing to their presence in phases other than metal (such as silicate and sulfide), consistently low Ir/Ni, Au/Ni, Co/Ni and As/Ni values obtained for silicate-rich areas indicate that fine-grained metal in PV has a non-chondritic composition (Fig. 14). These discrepancies indicate that both coarse-grained and fine-grained metal in PV are chemically fractionated compared to that in H-chondrites.

4.3 Melting and crystallization models for siderophile elements

Ruzicka and Killgore (2002) concluded that the composition of metal in Portales Valley was chemically fractionated and that additional study was needed to ascertain whether this was consistent with igneous differentiation. Here we test whether melting and crystallization models can explain the fractionated and spatially variable compositions of metal in PV.

All our models assume that Portales Valley was derived from an H-chondrite protolith. The proportion of S in the metallic (Fe + Ni + S) fraction of bulk H-chondrites was determined by taking the average composition of unweathered H-chondrite falls from Jarosewich (1990), and the abundance of trace elements in H-chondrite metal was averaged from literature data (Chou et al., 1973; Rambaldi, 1977; Kong et al., 1995). These data sets were merged to obtain a representative composition of the metallic fraction in H-chondrites (Table 11).

Modeled compositions of both metallic liquids and solids were compared to observed compositions of coarse vein metal and finer-grained metal in silicate-rich areas (Table 8) using Ni-normalized data, which gives a more accurate indication of the composition of the metal in impure, bulk samples. For convenience, these ratios are also normalized to the composition of the metallic fraction in H-chondrites (Table 11). Although Ni normalization permits comparison with model calculations, a significant amount of Ga and Fe in chondrites is contained in the silicate fraction. Consequently, measured Ga/Ni and Fe/Ni values for fine-grained metal in silicate-rich samples cannot be used as a constraint. These values also do not provide good constraints for the coarse metal analyzed by us (sample PVD). This is because in this sample, the Fe content was calculated by difference (Table 8), and the Ga concentrations appear too high to have been derived from an H-chondrite starting composition by solid-liquid metal partitioning alone, possibly for the reasons discussed above (Sec. 4.1). Thus, the major model constraints for both fine and coarse metal are provided by Ir/Ni, Au/Ni, Co/Ni, and As/Ni.

Abundances of siderophile elements were calculated using standard melting and crystallization equations (e.g., Rollinson, 1993) based on solid metal/liquid metal partition coefficients (D-values). Composition-dependent D-values for Ni, Co, Au, Ir, and Ga were determined using the formulations of Jones (1995), which are expressed in terms of the S content in metallic melt; D-values for As were calculated from a similar formulation by Liu and Fleet (2001). The equilibrium Fe-Ni-S ternary phase diagram of Hsieh et al. (1987) and the well-constrained equilibrium Fe-S phase diagram of Hansen and Anderko (1958) and Kubaschewski (1982) were used as guides to constrain the S content of metallic melts and the corresponding metallic melt fractions and temperatures. The S content of H-chondrite melts was calculated assuming that all sulfur partitions into whatever metallic melt is present, according to the mass balance expression:

$$X_S = 0.1412 + (1- F_L) * 0.4436,$$

where X_S = atom fraction of S in the metallic melt, and F_L = fraction of metallic liquid in the Fe + Ni + S system. This expression indicates that for a total melt ($F_L = 1$), $X_S = 0.1412$, which corresponds to an H-chondrite composition, whereas $X_S = 0.44$ for a Fe-S eutectic melt fraction at 988 EC (Hansen and Anderko, 1958; Kubaschewski, 1982) corresponding to $F_L = 0.326$. The addition of small amounts of Ni to the Fe-S system changes melting relations only slightly, yielding a Fe-Ni-S eutectic temperature at low pressure of ~943 EC (Usselman, 1975). As the abundances of all other modelled elements in the metallic system were determined, the amount of iron in solid and liquid metal was calculated by difference.

Various models were examined. These include (a) equilibrium "batch" melting; (b) batch melting followed by equilibrium crystallization of separated liquids; (c) batch melting followed by fractional crystallization; (d) equilibrium melting followed by *in situ* crystallization of the resulting liquids (Langmuir, 1989), and (e) equilibrium melting with incomplete separation of melt from solid. Example results for some of the "best-fit" cases of each of these models are shown in Table 11. These are discussed below. Of these models, equilibrium melting with incomplete separation of melt from solid can best explain the data for Portales Valley. Results for this case are illustrated in Fig.15.

Equilibrium batch melting– This model assumes partial melting of the metallic fraction to produce metallic melts that separate all at once from the residual solid in a "batch". Cases examined include melt fractions ranging from F_L = 0.9 to 0.33 (the latter being the minimum). The results of these models suggest that metal in Portales Valley cannot be a residue of a partial melting event, as predicted values of Ir/Ni, Au/Ni, Co/Ni, and As/Ni in solid metal all tend to be high (> H-chondrites), opposite to what is observed (Table 11). In particular, high Ir/Ni and Co/Ni values cannot be avoided. Melt compositions produced in this process are more reminiscent to those found in PV, but also do not provide a good match, in that calculated Ir/Ni values are far too low compared to Au/Ni, Co/Ni, and As/Ni (Table 11). Thus, equilibrium batch melting alone does not appear to be a viable process for PV.

Batch melting followed by equilibrium crystallization of the separated liquids– This model tests whether equilibrium crystallization of a separated batch liquid can account for metal in PV. Implicit is that all of the metal in PV originated as a metallic liquid that subsequently underwent equilibrium crystallization. Cases examined in this two-step model include F_L = 1 to 0.33 (i.e., 100-33% melting) in the initial melting step, and F_L = 0.9 to 0.4 (i.e., 10-60% crystallization) in the second crystallization step. In this model, whether the final liquid or solid more closely resembles the metal in PV depends on the precise degree of initial melting and final crystallization. No combination was found that results in a particularly good match to either the coarse or fine metal in PV. Table 11 shows what is probably the best case, which for the final solid gives roughly the appropriate Ir/Ni value for fine-grained metal in PV, but which has far

too much Co and As. The results suggest that PV metal cannot be considered to be either a liquid or solid produced by a two step melting and equilibrium crystallization process.

Batch melting followed by fractional crystallization of the separated liquids– This model is similar to the previous one except that fractional crystallization is assumed to occur. Cases examined include F_L = 1 to 0.4 in the initial melting step, and F_L = 0.9 to 0.33 in the second crystallization step. Final liquids in this model are unpromising analogues to PV as they tend to be enriched in Au and As except at lower melt fractions, and Ir becomes very low in these low-melt fractions. Final solids provide more reasonable matches to PV when both the degree of melting and subsequent fractional crystallization is extensive (e.g., $F_L \sim 1$ for melting, followed by $F_L \sim 0.5$-0.4 at the end of crystallization) or the degree or initial melting is somewhat less and subsequent fractional crystallization is small (e.g., $F_L \sim 0.9$ for melting, followed by $F_L \sim 0.9$). Table 11 shows one of the more promising cases produced by 100% melting and subsequent 50% fractional crystallization. The final liquid is much too low in Ir and much too high in Au and As, but the solid has Ir/Ni and Au/Ni values that resemble the fractionated compositions found in PV fine metal. Co/Ni and As/Ni are too high, however, for this model to be considered a good match to PV (Table 11). An additional problem with this model is that it does not seem possible to explain the different compositions of fine and coarse metal by simple variations in the amount of fractional crystallization.

Equilibrium melting followed by in situ crystallization of the resulting liquid– Equations for this type of crystallization were devised by Langmuir (1989) to model a situation thought to occur in magma chambers on Earth, in which crystallization occurs in a "crystal mush" zone along magma chamber boundaries and residual liquid is expelled from the mush zone as solidification proceeds. Cases examined include F_L = 1 to 0.33 in the initial equilibrium melting step, and F_L = 0.9 to 0.4 in the second *in situ* crystallization step. For this model, we assumed two values for the parameter f, where f represents the fraction of magma (0-1) allocated to the mush zone which is returned to the main magma body. We set f = 0.5 in one set of calculations, and tried reconnaissance calculations with f = 0.9 in another set, with the second set representing a situation not much different than that of fractional crystallization (f = 1). The results of this modelling suggest that melting followed by *in situ* crystallization is an unpromising way to make PV metal. For high degrees of melting coupled with low degrees of crystallization, As and Au tend to be enriched in liquids and depleted in solids, opposite to Ir and Co, and no match to PV is possible for either liquids or solids. H-normalized As/Ni and Ga/Ni abundances become high (>10 and >100, respectively) when the S content of liquids become high, which occurs for lower degrees of partial melting and lower degrees of crystallization. A representative case for equilibrium melting followed *in situ* crystallization is shown in Table 11; this provides the worst match to PV for any of the models shown.

Equilibrium melting with incomplete separation of residual metal from metallic liquids-- This is similar to the batch melting model described above except that liquids do not fully separate from solids, and so no distinct liquid "batch" is produced. Solids and liquid are always in direct contact and in equilibrium. Cases examined include partial melting with melt fractions ranging from F_L = 0.9 to 0.33 and metal + liquid mixtures containing 5-95% solid metal. With this model, the trace-element content of PV metal can be successfully explained as having formed by the production of metallic melts generated from an H-like precursor at relatively low temperatures.

Fig 15 shows results for various solid-liquid mixtures produced by equilibrium melting at F_L = 0.33, 0.40, and 0.5. At lower values of F_L, metal in both vein and silicate-rich areas can be modelled as representing a mixture of solid and liquid portions produced under the same melting condition, with a higher proportion of metallic liquid in silicate-rich areas and a higher proportion of solid metal in coarse vein areas. For example, at F_L = 0.33 (a eutectic melt), the H-normalized Ir/Ni, Au/Ni, Co/Ni, and As/Ni values calculated for a solid-liquid metal mixture containing ~20-40% solid agrees with the observed composition of fine metal in PV, and a mixture containing ~40-80% solid agrees with the composition of coarse metal in PV (Fig. 15a, Table 11).

With 40% partial melting, the agreement between the model and observations is less good than with the 33% partial melting case (Fig. 15b). Under these conditions, the fine metal fraction in PV could correspond to #5% entrained

solid based on Au/Ni, Co/Ni, and As/Ni values, and ~20-40% entrained solid based on Ir/Ni. The proportion of solid metal in the coarse veins in PV would have been higher, perhaps ~20-60%, although this is ill-constrained because of the poorer agreement between model and observations. With 50% partial melting, the model clearly fails (Fig. 15c). As the degree of melting increases, Co/Ni, As/Ni, and Au/Ni values increase and do not permit good matches to the observations. Essentially, the degree of fractionation diminishes as the degree of melting increases.

Summary of modelling results. It appears that a model involving partial melting and incomplete separation of solid and liquid metal can best account for the composition of metal observed in Portales Valley. Besides providing the best fit to the observations among all the models examined, this model is one of the simplest investigated, mainly requiring sufficiently high temperatures for partial melting to occur. Furthermore, the model has the advantage that the composition of metal in both coarse veins and in silicate-rich areas can be established by the same process, although different proportions of solid and liquid in different areas are implied. Incomplete separation of melt from solid is not unexpected in low-gravity objects, especially at low degrees of partial melting in which the high proportion of solid inhibits the ability of liquid and solid to separate. At the near-eutectic conditions inferred, most of the metal would be solid, and this would be even more true of the accompanying silicates (see below).

4.4 Implications for high-temperature history

Clearly, a melting process was responsible for producing fractionated metal compositions in Portales Valley. As discussed above (Sec. 4.3), the composition of metal differs between coarse- and fine-grained fractions because metal in the coarse veins and silicate-rich fractions incorporated different proportions of a solid metal to liquid metal component at the time the overall composition of metal was established. That taenite in silicate-rich areas has a lower Co/Ni ratio than in coarse veins (Fig. 8b, 9) is a direct consequence of the melting process. In contrast, the higher Co/Ni ratio of kamacite in silicate-rich areas compared to coarse veins (Fig. 8a, 9) is opposite to the trend shown by taenite and cannot be a direct result of the melting process. Most likely, this feature represents a secondary effect produced at subsolidus temperatures as kamacite exsolved from parent taenite crystals and is only indirectly related to the original formation conditions of the metal. One possibility is that variations in the composition of taenite that crystallized in different areas controlled the amount of Co and Ni that was available for kamacite that exsolved at a lower temperature through a mass balance effect.

According to the modelling results, silicate-rich areas that ultimately crystallized fine-grained metal should have incorporated a higher proportion of liquid metal than the coarse veins, including more sulfur (e.g., S/Ni ~ 4.7 for the fine metal fraction, ~2.7 for the coarse metal fraction; Table 11). Upon solidification, this excess S would be expected to lead to troilite formation. In agreement with this, troilite in PV is indeed concentrated in silicate-rich areas. Based on models for mixing solid and liquid with simple eutectic melting which provide good agreement to the observations, the vein

metal was ~40-80% solid at the time of last equilibration. This implies that ~60-20% of S-bearing liquid metal must have been expelled from the coarse veins, and probably moved into adjacent silicate-rich areas, before Portales Valley attained its present configuration of having nearly sulfide-free coarse veins. Textural evidence for this process includes the presence of thinner troilite and metal veins that interconnect to coarse veins (Fig. 1b,c), which probably served as conduits for metallic liquid that was pushed out of coarse vein areas. The interfaces between troilite and metal veins are also suggestive of later crystallization of troilite (Sec. 3.2.1), which is consistent with the model.

An overall movement of liquid from coarse veins to surrounding areas agrees with the conclusions of Pinault et al. (1999). According to these researchers, the silicate-rich matrix of Portales Valley "behaved effectively as a sponge", absorbing S-rich melt as large metal crystals grew within the veins. Rubin et al. (2001) proposed an analogous model, in which pores within the silicate-rich fraction of Portales Valley were filled with S-rich vapor, which reacted with Fe vapor or metal to form troilite. In both cases, the metal in silicate-rich areas completed crystallization after the coarse vein metal, in agreement with our results.

The modelling results suggest that equilibrium melting and incomplete separation of solid from liquid metal can explain the data for Portales Valley, but only if the composition of metal was established when the degree of metallic partial melting was less than 50%, and probably less than ~40% (Fig. 14). The models do not rule out the possibility of higher melting fractions; rather, they constrain the overall closure temperature for equilibrium between solid and liquid metal. For an H-chondrite composition, a metallic melt fraction of <40% constrains the temperature to ~940-1150EC (Hansen and Anderko, 1958; Usselman, 1975; Hsieh et al., 1987).

These temperatures are much lower than those inferred ($1480 EC) by Rubin et al. (2001). This inference was based on the overall composition of coarse, S-poor metal and evidence that metal was liquefied. However, if metal in the veins did not form all at once but rather grew to replace liquid, as argued here, this temperature estimate would be erroneous.

For temperatures of ~940-1150 EC, it is possible that the non-metallic fraction of Portales Valley was partly molten. Heating experiments of L-chondrite starting material at ~15 Kbar produces silicate melt at ~1100 EC, with lower melting temperatures expected at lower pressures (Takahashi, 1983). Equilibrium melting experiments at low pressure with H and LL ordinary chondrites under fO_2 values close to the IW buffer suggest that ~10-13 wt% and ~15-20 wt% of the silicate fraction will be molten at temperatures of ~1120-1170 EC and ~1200 EC, respectively (Jurewicz et al., 1995). This implies a maximum degree of silicate partial melting in PV of ~13 % at the time solid and liquid metal compositions were fixed. Plagioclase is fully molten even at the lowest temperatures investigated by Jurewicz et al. (1995), and plagioclase, phosphate, and clinopyroxene melt completely at 1200 EC within 1-10 hours in experiments with an L-chondrite (Feldstein et al., 2001). Thus, it is possible that some or all of the plagioclase, phosphate, and clinopyroxene were melted in Portales Valley.

4.5 Fluidization of metal

Removal of metal from large portions of the Portales Valley breccia and its concentration into larger sheet-like structures (veins) (Kring et al., 1999b; Pinault et al., 1999a; Rubin et al.,. 2001) implies that much of the metal in PV was originally mobile, either because it was able to flow in a ductile fashion or because it was liquefied (or some combination of both). Mobilization as a fluid is not hard to imagine. However, the models discussed above suggest that the overall compositional and textural features of metal in PV were established with most of the metallic fraction being solid. Unless temperatures were higher than inferred, it seems inescapable that metal would have had to flow into veins partly in a solid state. Solid-state flow would have to occur through what were likely constricted passageways in silicates.

It is unclear why metal would have been concentrated into coarse vein-like structures, but a role for hypervelocity impact seems likely. Partial melting experiments of chondrites and chondrite analogues under static conditions show that metallic melts tend to form isolated patches or globules, not veins, with little tendency for metallic melts to separate from silicate (Takahashi, 1983; Jurewicz et al., 1995; Rushmer et al., 2000b; Feldstein et al., 2001). Vein-like intergrowths of metal and sulfide have been reported in heating experiments of chondrites after 1-week heating at 700-1000 EC (McSween et al., 1978) and after 1-hour heating at 1200 EC (Feldstein et al., 2001), but such veins tend to be small (~1-2 Fm wide, rarely up to 100-150 Fm long) and do not approach either the coarseness or connectivity of veins in PV. In addition, veins do not persist in longer duration heating episodes at 1200 EC (Feldstein et al., 2001), suggesting that metal vein formation is not a prevalent feature of static melting. Metal may have filled cracks that were produced by impact brecciation prior to heating (Pinault et al., 1999; Scott and Pinault, 1999), but coarse veins are not produced by heating natural chondrite samples that have been weakly shocked and fractured (McSween et al., 1978; Feldstein et al., 2001). Alternatively, metal may have been melted and concentrated into narrow zones by a hypervelocity impact (e.g., Kring et al., 1999b; Rubin et al., 2001). However, although FeNi-metal veins up to 1 mm wide are present in shocked chondrites (Rubin, 1985), the shock stage of PV is low (S1) (Sec. 3.1.2) and unlike that of a shocked chondrite. Indeed, metallic veins as coarse as in PV have not been described in other chondrites (Rubin, 1985), whether shocked or not (Pinault et al., 1999).

A combination of elevated temperatures and a relatively weak shock event could have produced the PV vein and breccia texture. Experiments have shown that metal and troilite can be mobilized into small-scale (~µm-wide) metal and troilite veins by shear deformation with strain rates of 10^3 to 10^4 s^{-1} at ambient room pressures and temperatures (van de Bogart et al., 2003). Such shearing can occur without entailing an increase in shock stage (van de Bogart et al., 2003). Experiments involving heating under conditions of differential stress indicate that metal and sulfide can be mobilized into larger interconnected veins that surround silicate clasts (Rushmer et al., 2000a,b). For example, experiments performed on the Kernouvé H6 chondrite with a strain rate of 10^{-5} s^{-1} at 925-990 EC and a confining pressure of 1 GPa produced

cataclastic metal-silicate zones up to 100 Fm wide, with metal enclosing silicate clasts (Rushmer et al., 2000a). The texture produced in these experiments is similar to (albeit still not as coarse as) that in PV. Moreover, the composition of mobilized (solid + liquid) metal in these experiments show some similarities to the metal in IIE irons (Rushmer et al., 2004) and to that in PV. This suggests that the veins in PV could have formed by shear-induced mobilization of metal and sulfide at elevated temperature. In these shearing experiments, it appears that strain rates may be less critical than ambient temperature in producing coarse veins.

Even if static heating or impact were able to produce coarse veins of the sort found in Portales Valley, it is unclear why a solid metal (as opposed to liquid metal) component became concentrated there. Based on the models described above (Sec. 4.4), it appears that taenite parent crystals grew preferentially inside larger metallic vein bodies, and expelled metallic liquid into surrounding silicate-rich areas as they grew. Continuity of Widmanstätten structures across large veins implies that entire veins consist of single parent taenite crystals, suggesting either that the growth rate of taenite in veins was high relative to the number of nucleation sites, or that taenite grains in coarse veins were recrystallized into large grains before cooling to low temperatures. Preferential growth of taenite in veins could possibly have been caused by a nucleation or surface energy effect, with large silicate-free, taenite-bearing melt zones serving as favorable sites for additional growth of taenite. If the interfacial energy between solid metal and solid silicate were high compared to that between liquid metal and solid silicate, this could have caused solid metal to migrate to silicate-poor areas and S-rich metallic melt to become concentrated in silicate-rich areas, as observed in PV. Preferential growth of taenite on pre-existing taenite grains in the silicate-poor areas would have produced the coarse grains in the veins.

4.6 Origin of large graphite nodules

At least two distinct graphite nodules up to a few cm across have been identified in Portales Valley so far, both embedded within coarse vein metal (Fig. 4; Table 2). Coarse graphite in general, and nodules in particular, are absent in other ordinary chondrites, but similar nodules are found in iron meteorites. H-chondrites contain ~0.11 wt% carbon on average (Jarosewich, 1990), and to produce cm-sized graphite nodules from an H-chondrite precursor requires that C must have been scavenged from large volumes and concentrated locally.

One way to do this would be to dissolve C in metallic melt, and to mobilize this melt so that it could pass through large volumes of Portales Valley, removing C from large volumes and concentrating it in metallic liquid. According to the equilibrium Fe-C phase diagram (Massalski et al., 1986), a eutectic in the Fe-C system between taenite and graphite occurs at ~1150EC. This indicates that liquid metal could have co-crystallized graphite and taenite if temperatures reached this high. This is the upper temperature limit estimated for the equilibrium established between solid and liquid metal based on siderophile element abundances in metal (Sec. 4.4). In reality, however, graphite could have crystallized from liquid metal at a lower temperature in PV, as the addition of other components (Ni, S, P, etc.) to a

metallic melt would lower the actual eutectic temperature compared to the Fe-C system. It therefore seems likely that temperatures in PV were sufficiently high to place C in a metallic liquid, and that the graphite nodules in PV formed by crystallization of graphite from this liquid. The formation of coarse graphite, as opposed to smaller distributed grains in metal, implies there was an additional driving force favoring the formation of large grains, perhaps a minimization of surface energy, or a tendency for C-rich liquids to immiscibly separate from C-poor liquids.

Eutectic crystallization of graphite and FeNi-metal is entirely consistent with the observed textures of the nodules. The nodules are enclosed in coarse vein metal, have irregular and tapering contacts with this metal, and also have inclusions and veinlets of FeNi-metal inside them (Fig. 4). This suggests contemporaneous formation of graphite and coarse FeNi-metal (Sec. 3.2.2). Co-crystallization of metal and graphite from C-bearing liquids is probably the same process that produced graphite nodules in iron meteorites. The presence of coarse graphite nodules within coarse metal vein areas in PV can be taken as further evidence that such veins were significantly molten at one time.

4.7 Petrogenesis of coarse phosphate: igneous or metamorphic?

The textures of merrillite and Cl-apatite in Portales Valley are noteworthy (Sec 3.1.1; Ruzicka et al., 1999a). Phosphates in Portales Valley are much coarser (up to a few mm across) than typical in ordinary chondrites (<<1 mm; Fuchs, 1969), and are locally enriched, mainly along metal-silicate contacts (Fig. 3). Vein-like merrillite that terminates against troilite and FeNi veins (Fig. 3c) also suggests a close relationship to metal and sulfide. Coarse merrillite sometimes shows what appears to be poikilitic textures (Fig. 3b), suggestive of crystallization from melt. If the metallic portion of PV partly melted, as is certain, it is possible that phosphate was also molten, especially as phosphate is one of the first phases to melt in chondrites as temperature is increased (Feldstein et al., 2001).

If phosphate did melt, it appears that its composition reflects subsolidus equilibration rather than igneous processes. Phosphate in PV has major- and trace-element compositions typical to that found in equilibrated ordinary chondrites (e.g., Fig. 10b; Ruzicka et al., 1999a; Floss et al., 2002), providing no evidence for any unusual chemical processing. Fig. 16 shows the REE composition of melt that would be needed to be in equilibrium with merrillite and orthopyroxene, which were analyzed in the same samples. These do not agree, with the merrillite melt pattern showing a flat to HREE-enriched pattern at ~10-20 x CI, and the orthopyroxene melt pattern showing a strongly LREE-enriched pattern from ~3 to ~100 x CI (Fig. 16). This discrepancy implies that merrillite and orthopyroxene did not equilibrate with a single melt. This is true also for orthopyroxene poikilitically enclosed by merrillite, indicating that even in areas with apparent igneous texture, these phases are not in equilibrium with the same melt. Moreover, partial melting would be expected to produce an LREE-enriched pattern for a melt, but this is opposite to the HREE-enriched pattern shown by merrillite (Fig. 16). Evidently, the composition of merrillite does not reflect equilibration with a partial melt.

If the composition of phosphate in Portales Valley does not reflect igneous processes, perhaps it reflects

subsolidus equilibration. This possibility is consistent with the observation that both merrillite and apatite in PV have major- and trace-element compositions similar to those found in metamorphosed ordinary chondrites (Fig. 10b; Table 5). Fig. 17 compares observed REE abundances in merrillite, apatite, and orthopyroxene with two models in which REE abundances are established by subsolidus equilibration, using the approach of Curtis & Schmitt (1979) and Treiman (1996). Both models assume silicate-phosphate equilibrium between the chief non-metallic minerals found in H-chondrites and PV (merrillite, apatite, plagioclase, clinopyroxene, orthopyroxene, and olivine), and both assume that relative D-values for these phases at subsolidus conditions are identical to those found at magmatic temperatures. The models differ in that an H-chondrite mode and bulk REE abundance (~1.3 x CI) is assumed in one case, whereas a mode appropriate to that in PV 4978 and a bulk REE abundance of 2-3 x CI is assumed for the other case.

Both of the subsolidus equilibration models shown in Fig. 17 roughly agree with the overall REE abundances found in merrillite, apatite, and orthopyroxene, but both fail to precisely account for the observed phase compositions, especially for Cl-apatite and orthopyroxene. For example, the predicted Cl-apatite patterns show negative Eu anomalies and HREE-enriched patterns, whereas the observed pattern shows a positive Eu anomaly and an HREE-depleted pattern. The predicted HREE/LREE ratio for orthopyroxene is also much steeper than observed. Finally, the calculated pattern for merrillite assuming an H-chondrite mode resembles the observed composition except for having too much Yb, and the calculated pattern for the PV 4978 mode also resembles the observed composition except for having too much Eu (Fig. 17). These results are interpreted to indicate that there was an approach to subsolidus REE equilibrium in PV, but that equilibrium was not fully maintained, or that the assumed D-values are not exactly appropriate. The only significant discrepancy for merrillite assuming a model with the 4978 mode is an overestimate in Eu (Fig. 17), which could be explained if either the D_{Eu} value assumed for merrillite at low temperature is overestimated, or the D_{Eu} values for one or more other phases (e.g., plagioclase, clinopyroxene) at low temperatures are underestimated.

The close spatial association of phosphate with coarse metal suggests a genetic relationship between these phases. Most likely, phosphate formed by reaction of P-bearing metal with Ca-bearing pyroxene in the silicate fraction. This type of redox reaction is proposed to have occurred to form phosphate minerals in stony, stony-iron, and iron meteorites (Olsen and Fuchs, 1967; Murrell and Burnett, 1983; Harlow et al., 1984). Metamorphic reaction between metal and silicate can explain why phosphate is concentrated at the metal-silicate contact in PV (e.g., Fig. 3a), if phosphate formation was limited by the availability of P in metal. Subsolidus equilibration, and hence a predominantly metamorphic origin, of phosphate is also generally consistent with REE data for merrillite, as discussed above. In addition, formation of phosphate by reaction between Ca-pyroxene in the silicate fraction and P-bearing metal is consistent with the modal mineralogy of PV 4978, which is depleted in clinopyroxene compared to average H-chondrites (Fig. 6).

A phosphate-forming redox reaction of the following type is implied for Portales Valley:

$$\underset{\text{diopside}}{3CaMgSi_2O_6} + 2P + \underset{\text{metal}}{3Fe} + \underset{\text{gas}}{4O_2} \pm \underset{\text{merrillite}}{Ca_3(PO_4)_2} + \underset{\text{orthopyroxene}}{3MgSiO_3 + 3FeSiO_3} \quad [1]$$

In this reaction, P in metal is oxidized and Ca-pyroxene is removed. Reaction [1] (abbreviated DIMO, where D = diopside, I = iron, etc.) would have had to occur extensively in PV in order to account for the low abundances of clinopyroxene found in AMNH 4978 compared to H-chondrites (Fig. 6). Oxygen fugacity in PV may have been controlled by internal buffering between Fe-bearing olivine, orthopyroxene, and metal according to the following reaction:

$$\underset{\text{ferrosilite}}{FeSiO_3} + \underset{\text{metal}}{Fe} + \underset{\text{gas}}{\tfrac{1}{2} O_2} = \underset{\text{fayalite}}{Fe_2SiO_4} \quad [2]$$

Reaction [2] (FIF) has been proposed to be the principal oxygen buffer in ordinary chondrites (McSween and Labotka, 1993).

The temperature - oxygen fugacity conditions of the DIMO reaction [1] were evaluated with a thermodynamic model assuming phase compositions for olivine, low-Ca pyroxene, high-Ca pyroxene, and metal appropriate to those in Portales Valley and H-chondrites (Table 4, 6). This model is essentially equivalent to that derived by Harlow et al. (1984) for mesosiderites (their reaction T, Model 2) except that different phase compositions were used. The following thermodynamic parameters were assumed: ideal mixing of Fe in Fe-Ni taenite (Fraser and Rammensee, 1982) with X_{Fe} = 0.902; regular solution model for Fe-Mg olivine (Williams, 1971) with X_{Fa} = 0.18; regular solution model for Mg-Ca clinopyroxene (Holland et al., 1979) with X_{Di} = 0.823; regular solution model for Fe-Mg orthopyroxene (Williams, 1971) with X_{Fs} = 0.18; and pure $Ca_3(PO_4)_2$ merrillite. For P in metal, an activity coefficient of $\gamma_P = 1.17 \times 10^{-5}$ was assumed, which is consistent with the data of Komarek (1963) at 1050EC, and which is able to reproduce the experimentally-determined metal-silicate-phosphate equilibria of Friel and Goldstein (1976) for metal with 0.167 wt% P. Thermodynamic data for the FIF curve were taken from Williams (1971) (his OPI reaction).

Fig. 18 shows equilibrium T-fO_2 conditions for the DIMO and FIF reactions. Equilibria for two different P contents in metal (0.66 and 0.01 wt%) are shown for the DIMO reaction. The 0.01 wt% P curve corresponds to the amount of P currently observed in PV metal (Table 6), whereas the 0.66 wt% curve corresponds to the amount of P that could have been present in PV metal initially, if all P is put back into metal. The 0.66 wt% P value was calculated by combining the average P content in AMNH 4978 (Table 10) with the average amount of metal in this sample (Table 3). Fig. 18 is split into two regions to indicate that diopside + P-bearing metal form a stable assemblage at high temperature, and merrillite + orthopyroxene form a stable assemblage at low temperature.

If solid metal was present and the FIF buffer [2] controlled fO_2, the equilibrium temperature-fO_2 range of the phosphate-forming reaction in PV would be constrained by where the FIF equilibrium [2] intersects the DIMO

equilibrium [1] for a given P content in metal (Fig. 18). For ~0.66 wt% P in metal initially, reaction to form phosphate would occur at temperatures as high as ~975 EC (Fig. 18). For 0.01 wt% P in metal, phosphate would be formed at temperatures as high as ~725 EC. This indicates that upon cooling from the high temperatures reached in PV (Sec. 4.3, 4.4) and for the P contents inferred, solid metal would react with clinopyroxene to produce phosphate starting at ~975 EC, and continue until the temperature reached ~725 EC, at which point diffusion could have became too slow to maintain equilibrium.

For a bulk P content of 0.66 wt%, this upper temperature limit for producing merrillite (~975 EC) is close to but slightly below the Fe-S eutectic temperature of ~990 EC, and above the Fe-Ni-S eutectic temperature of ~940 EC. This suggests that most but not necessarily all of the phosphate in PV formed by reaction under metamorphic conditions, after metal, sulfide, and silicates had crystallized. However, a purely metamorphic origin for merrillite does not explain why coarse merrillite sometimes forms vein-like extensions of metal and troilite veins (Fig. 3c), which is better explained by crystallization of merrillite from P-rich liquids associated with thin veins of metallic melt. A metamorphic origin also is inconsistent with apparent poikilitic textures of coarse merrillite (Fig. 3b), although such merrillite may represent poikiloblasts that overgrew pre-existing silicates.

It is suggested that some phosphate in Portales Valley may have crystallized from P-rich metallic liquids. As noted above, the metallic Fe-Ni-S eutectic temperature appears to have been lower than that needed to initiate formation of phosphate by the DIMO reaction. Moreover, adding P to a metallic melt lowers the temperature at which metallic melt is possible (e.g., Doan and Goldstein, 1969), making it more likely that P-bearing metallic melt was present above the temperature needed to initiate formation of phosphate. At the highest temperatures reached in PV, phosphate was probably at least partly melted, and P would have resided in liquid that was interacting with metal. Thus, some P-bearing metallic melt could have been present at the same time solid metal was reacting with silicates to form phosphate, and some phosphate may have crystallized directly from liquid as the temperature dropped. Phosphate veins and poikilitic phosphate could have resulted.

The P content of metal could have been controlled either by equilibrium with silicates and phosphate (e.g., via the FIF and DIMO equilibria), or by equilibrium with phosphide (schreibersite), depending on the bulk composition, temperature, and fO_2. Fig. 19 shows the likely evolution of P content in PV metal with an initial P content of ~0.6 wt% and a final P content of ~0.01 wt%. This figure compares expressions for metal-phosphide equilibria (Moren and Goldstein, 1979) with the metal-silicate-phosphate equilibria described above. For the amount of P that was likely present in PV metal initially (~0.6 wt%), Fig. 19 suggests merrillite would form instead of schreibersite as temperature decreased. Once phosphate started to form, it would control the P content in metal until the currently observed low P content was attained and the closure temperature for the DIMO reaction was reached. Schreibersite would not form before phosphate unless the P content in metal was locally higher than ~ 1 wt%. Even if the P content was this high,

schreibersite would react to form phosphate as temperature decreased. For instance, taenite cooling from high temperature under P-rich (>1 wt%) conditions would follow the taenite-shreibersite (GUP) equilibrium (Fig. 19). When the temperature dropped to ~975 EC, merrillite would form as before, and schreibersite would become unstable.

In either case, schreibersite would not be stable as temperature fell. This scenario is consistent with the lack of coarse schreibersite in PV. However, we have observed micro-rhabdites in PV coarse metal. Such rhabdites probably formed by exsolution from metal at a temperature below the apparent closure temperature of ~725 EC for the DIMO reaction. This low-temperature exsolution could occur if P continued to diffuse in metal below the temperature needed to maintain silicate-phosphate-metal equilibrium.

In summary, it appears that phosphate in Portales Valley formed by reaction between P-bearing metal and clinopyroxene components, depleting clinopyroxene throughout much of the meteorite and growing coarse phosphate at metal-silicate interfaces. Some of the phosphate could have crystallized from P-bearing liquids to produce poikilitic and vein merrillite, but most probably formed under subsolidus conditions as the assemblage cooled between ~975-725 EC. As was the case for producing large graphite nodules (Sec. 4.6), the presence and distribution of coarse phosphate in Portales Valley can be attributed ultimately to initially high temperatures and a high concentration of a critical component (in this case, P) in the metallic phase. Metal that was mobilized at high temperatures was evidently able to scavenge P from large regions of the meteorite, and concentrate it into a smaller volume of metal. As the assemblage cooled, buffering reactions favored the production of phosphate at the expense of P-bearing metal and schreibersite, and P became localized in phosphate adjacent to metal. This resulted in a mineral assemblage similar to that which was present in the H-chondrite protolith, but which was locally enriched in phosphate and depleted in clinopyroxene. Trace-element and major-element abundances in phosphate were largely established under subsolidus conditions and reflect an approach to equilibrium by buffering reactions in the H-chondrite-like mineral assemblage.

4.8 Thermal history

Portales Valley appears to have experienced protracted subsolidus annealing. Evidence for this includes the formation of phosphate and removal of clinopyroxene to temperatures as low as ~725 EC, as implied by the P content in metal (Sec. 4.7); metallographic data which indicates slow cooling at low temperatures, and pyroxene geothermometry.

All researchers agree that PV cooled slowly under subsolidus conditions to produce Widmanstätten textures and Fe-Ni zoning in coarse veins, Fe-Ni zoning of taenite in silicate-rich areas, and the microtextures of metal (Ruzicka et al., 1999b: Kring et al., 1999b; Pinault et al., 1999; Rubin and Ulff-Møller, 1999; Haack et al., 2000; Rubin et al., 2001; Sepp et al., 2001). Metallographic cooling rate estimates converge on a value of ~few EC/Ma, despite being based on different approaches. These include minimum Ni contents at kamacite-taenite interfaces (Ruzicka et al., 1999: ~0.5-7 EC/Ma); central Ni contents in taenite (Pinault et al., 1999: ~5 EC/Ma); Ni profile matching (Haack et al., 2000: ~2 EC/Ma); and

microstructures in the cloudy zone of taenite, both in coarse and fine metal (Sepp et al., 2001: 6.5 ± 2.1 EC/Ma). These cooling rates are pertinent at the low temperatures (~350-700 EC) implied by the Fe-Ni phase diagram (e.g., Kubaschewski, 1982; Reisener and Goldstein, 2003) for PV-like metal compositions. Although slow, these cooling rates are not unusually slow compared to those inferred for chondrites and iron meteorites based on metallographic methods (Ruzicka et al., 1999b).

Two-pyroxene geothermometry for PV (Sec. 3.2.2) is also consistent with relatively slow rates of cooling at a somewhat higher temperature. As previously noted, geothermometry temperatures for PV pyroxene (770 ± 60 EC for orthopyroxene, 900 ± 35 EC for augite) fall on the low end of those found in other H6 chondrites (800-900 EC and 900-960 EC, respectively) (McSween and Patchen, 1989). One possible explanation of these data, that PV was heated to lower temperatures than other H6 chondrites, is untenable. If instead one interprets these temperatures as closure temperatures which should decrease as cooling rate decreases, PV cooled somewhat more slowly than a typical H-chondrite at temperatures of ~700-950 EC. The difference in derived temperatures for PV orthopyroxene and augite (~130 EC on average) imply that these pyroxenes were not in complete equilibrium at these temperatures, probably owing to sluggish diffusion. Kinetic barriers to diffusion also appears to have prevented PV metal from losing even the small amount of P (0.01 wt%) it still contains (Reisener and Goldstein, 2003), with redox reactions becoming kinetically inhibited below ~725 EC (Sec. 4.7).

Slow subsolidus cooling implies that Portales Valley cooled at depth within its parent body (e.g., Kring et al., 1999a,b). However, PV does not appear to have cooled any more slowly than other ordinary chondrites at low temperatures (~350-700 EC) and only slightly more slowly than typical type 6 chondrites at somewhat higher temperatures (~700-950 EC). The main differences between PV and H6 chondrites arose because temperatures were higher in PV (~940-1150 EC) (Sec. 4.4). These higher temperatures were probably sustained for a relatively long period, with sufficient time for metal to migrate throughout the breccia (Sec. 4.4, 4.5). The thermal history we infer for the meteorite is appropriate to a deep parent body setting, which experienced temperatures sufficiently high to cause partial melting of metal-sulfide and perhaps silicate, and subsequent slow cooling from supersolidus conditions to temperatures <500 EC.

4.9 Fractionation in the non-metallic portion of Portales Valley?

Incipient differentiation of metal in Portales Valley (Sec. 4.2, 4.4) raises the question of whether the non-metallic portion is chemically fractionated as well. This question can be addressed using both modal mapping (Table 3) and chemical data (Table 8, 9).

Mineral abundances in five sections of PV 4978 are not exactly the same as that of an H-chondrite, even on a metal and sulfide-free basis (Fig. 6b). Similarly, the bulk composition of PV 4978 deduced from these sections is

different than bulk H-chondrites, even when compared on a constant Si basis (Table 10). Taking modal data for average PV 4978 (Table 3) and comparing it to the normative composition of an average H-group chondrite calculated from the chemical data of Jarosewich (1990), the following reaction can be written, which expresses the change needed to convert an H-chondrite into PV on a metal- and sulfide-free basis:

$$3 \text{ clinopyroxene} + 8.41 \text{ olivine} \pm 1.90 \text{ merrillite} + 8.87 \text{ orthopyroxene} + 0.64 \text{ plagioclase} \quad [3]$$

In reaction [3], clinopyroxene ($En_{48.5}Wo_{44.8}$), olivine ($Fa_{19.6}$), merrillite, orthopyroxene ($En_{81.2}Wo_{1.6}$), and plagioclase ($An_{12.7}Or_{6.6}$) have been assigned the compositions appropriate to those in PV (Table 4, 5), and phase amounts have been normalized to a change of 3 moles clinopyroxene. Reaction [3] indicates that the non-metallic portion of PV 4978 is low in normative clinopyroxene and olivine, enriched in phosphate and orthopyroxene, and slightly enriched in plagioclase compared to H-chondrite silicate. Evidently, compared to H-chondrites, the non-metallic portion of PV4978 is enriched in P (phosphate), weakly enriched in Al (plagioclase), and depleted in Mg (olivine).

Comparison of reaction [3] with the DIMO reaction [1], which is also expressed in terms of 3 moles of clinopyroxene, shows an overall similarity, but also some differences. That large portions of PV are evidently depleted in clinopyroxene, and enriched in orthopyroxene and phosphate (as implied by reaction [3]), implies that the DIMO reaction [1] was able to occur on a large scale (~125 mm^3) in PV 4978. This reaction evidently occurred in an open-system manner, entailing a change in the bulk composition of the stony portion. It could have been driven by having excess P-bearing metal or metallic melt in AMNH 4978, which is consistent with the high proportion of metal and sulfide in most of the AMNH 4978 sections (Fig. 6). As noted above (Sec 4.7), the DIMO reaction in PV proceeded largely under metamorphic conditions but was probably initiated while melt was present. The transport of such melt may have enabled chemical changes to occur over a larger scale than would otherwise have been possible.

Compared to the DIMO reaction [1], reaction [3] indicates that Portales Valley has an *additional* excess of orthopyroxene and phosphate, a depletion in olivine, and a small excess in a plagioclase component, assuming an H-chondrite starting composition. Low olivine and excess orthopyroxene can be attributed to either (1) mechanical removal of olivine compared to orthopyroxene, or to (2) reduction and breakdown of olivine and formation of orthopyroxene.

The first possibility could arise by sequestering a partial melt residuum rich in olivine and depleting it in the PV breccia. Although this is supported somewhat by the inferred slight excess of plagioclase in PV, for this process one might expect more of an enrichment in a plagioclase component compared to orthopyroxene, as plagioclase melts at lower temperatures than low-Ca pyroxene in ordinary chondrites (Jurewicz et al., 1995; Feldstein et al., 2001) and should have been more enriched in a partial melt. The second possibility, reduction of olivine, is more likely. As previously noted (Sec. 3.1.4), a low value of modal olivine/pyroxene ratio in metal-rich samples of PV compared to H-chondrites (Fig. 6c) could be explained by a redox process. Reduction of olivine could be explained if reaction [2] was operative

and if it proceeded to the left. This can be rationalized, as the phosphate-forming DIMO reaction [1] would necessarily consume O_2, and this would tend to drive reaction [2] to the left, in the direction of increased Fe-orthopyroxene and diminished Fe-olivine. An additional reaction involving breakdown of Mg-olivine to Mg-orthopyroxene + silica would be needed to prevent Fe/Mg ratios in mafic silicates from changing, as required if equilibrium was maintained. So long as olivine was not exhausted, silica minerals would not form. Excess silica not used in the production of pyroxene could have been incorporated in a plagioclase component. As was proposed for the DIMO reaction, it is suggested that such a reduction process occurred on a large scale in PV, in an open-system manner that allowed changes in chemical composition to occur.

4.10 Preferred model for forming Portales Valley

The two leading models for the origin of Portales Valley envisage important roles for impact melting (Kring et al., 1999b; Rubin et al., 2001) and internal parent body heating (Pinault et al., 1999; Scott and Pinault, 1999). In the first case, PV could be a variant of an impact-melt breccia; in the second, it could be analogous to primitive achondrites such as acapulcoites or winonaites.

Our preferred model is a blend of these two extremes. On balance, evidence favors impact-triggered fluidization of already warm metal as the best explanation of the overall cataclastic and metal-veined texture of Portales Valley. Static heating experiments have so far failed to produce coarse-veined metal, but experiments involving shear deformation are able to make them easily. We speculate that a shock event involving shear could have mobilized metal even under S1 shock stage conditions (#4-5 GPa; Stöffler et al., 1991), when temperatures were relatively high (~900-950EC, typical for that of type 6 chondrites; McSween and Patchen, 1989) at the time of impact. Following impact-triggered fluidization, the meteorite experienced high temperatures and slow cooling from supersolidus to subsolidus temperatures, which enabled metal to separate from troilite, graphite to crystallize in large nodules, redox reactions to proceed in large portions of the meteorite, phosphate to crystallize and metamorphically grow in large grains, and Widmanstätten texture to form in metal. This protracted heating implies that PV cooled at depth within a parent body which remained intact. Portales Valley could have originated below a large impact crater on the parent body, as first suggested by Kring et al. (1999a,b). Alternatively, Portales Valley could have formed by the accretion of already-hot planetesimals involving low collisional velocities (Haack et al., 2000).

Although a role for shock is indicated as a trigger for metal-sulfide mobilization and the formation of cataclastic textures, we do not find compelling evidence that this shock involved high pressures. Non-traditional shock indicators present in PV, such as small amounts of metallic Cu and rare plagioclase-chromite intergrowths (Rubin et al., 2001; Rubin, 2004) have not been calibrated for peak pressures and consequently do not place tight constraints on shock levels. The shock-blackening found locally in Portales Valley (Rubin et al., 2001; Kring et al., 1999b) is often associated with

shocked meteorites, but can be produced by a shearing action without resulting in an increase in shock stage (van de Bogart et al., 2003). Our XRD and Raman data for PV graphite are consistent with a modest shock event involving shock pressures of ~5-10 GPa, probably closer to the lower value (Sec. 3.1.3). We note that if graphite crystallized from melt and the graphite was shocked, at least two shock events would have had to affect Portales Valley: an initial shock event during which the metallic melt was generated, and a second shock after graphite had crystallized. The latter shock could also have been bent kamacite lamellae around the graphite nodule (Sec. 3.1.3). However, in neither case did the shock event have to be stronger than shock stage S2. Although a shock stage as high as S3 (~15-20 GPa maximum; Stöffler et al., 1991; Bischoff and Stöffler, 1992) followed by annealing of shock features (Kring et al., 1999a,b; Rubin et al., 2001) has been proposed for PV, our data do not require this. We find no evidence to support the idea that PV was initially shocked to a shock stage as high as S6 (Rubin, 2004).

In our model, most of the heat necessary for mobilizing and melting metal and sulfide was provided by internal heat in the parent body, before the relatively weak shock event that triggered the formation of veins. We thus assign an important role to internal heating in the formation of Portales Valley, in agreement with the model of Pinault et al. (1999) and Scott and Pinault (1999). Temperatures implied for Portales Valley at the time solid and liquid metal last equilibrated are ~940-1150 EC, which suggest a post-shock temperature increase of ~0-250 EC, compared to a typical H-chondrite heated to ~900-950 EC. These temperature increases would correspond to shock pressures of ~0-30 GPa, or shock stages S1-S4, based on experiments performed at room temperature (Stöffler et al., 1991). To produce the current S1 shock stage from S4, significant recovery of shock defects in PV would have had to occur. However, as noted above, our data are consistent with the possibility that PV was affected by a shock event too weak (shock stage S1 or S2) to result in many shock defects, with only modest post-shock recovery needed. Additional microstructural (e.g., TEM) data might help discriminate between these possibilities.

Our model assigns important roles to both impact deformation and internal heating for the origin of Portales Valley. By so doing, it avoids shortcomings with either of the endmember models. We agree with other researchers that impact heating alone is unlikely to be viable for explaining Portales Valley (Kring et al., 1999b; Pinault et al., 1999; Scott and Pinault, 1999; Haack et al., 2000) owing to the large collisional velocity that would be needed, which would probably result in parent body disruption and fast cooling at high temperatures (Haack et al., 2000). By the same token, we agree with some researchers that the coarse veins in PV most likely were produced by shock (Kring et al., 1999b; Rubin et al., 2001). Experimental evidence (summarized in Sec. 4.5) suggests that shearing is probably needed to produce coarse metal veins, and shock deformation most likely was responsible for this shearing action, as it can explain a variety of other features in the meteorite. These include the presence of obvious cataclasis textures, localized shock blackening, the small amount of strain recorded by graphite and silicates, and possibly the presence of metallic copper and plagioclase-chromite intergrowths. An elevated abundance of gallium in the coarse vein metal (Sec. 3.3) is also

consistent with redistribution of this element during shock-heating (Chou and Cohen, 1973). This variety of features, and the difficulty in producing veins during static heating alone, suggest an important role for shock in the origin of Portales Valley.

4.11 Is chronologic data consistent with the preferred model?

According to our preferred model, Portales Valley formed as a result of a shock event that affected an already-warm target. This most likely requires that the veining and cataclasis event that affected PV was established early in the solar system when internal heating mechanisms for asteroids such as short-lived radionuclide decay or electromagnetic induction heating were active. Age data using a variety of chronometers have been obtained for Portales Valley (Chen et al., 1999, 2000; Garrison and Bogard, 2001; Papanastassiou et al., 2001, 2002) that can test whether our preferred model is viable. Both older and younger ages have been inferred. Here we briefly discuss what the chronologic data for PV imply. Table 12 summarizes the chronologic data.

Evidence for early formation (~4.4-4.6 Ga) consistent with our model is provided by U-Th-Pb, ^{40}Ar-^{39}Ar, and Rb-Sr data for bulk silicate-rich material, and for Re-Os data for coarse metal (Table 12). Precise argon plateau ages of 4.477 ± 0.016 Ga (Garrison and Bogard, 2001) presumably date the time when PV cooled to the closure temperature for Ar. This closure temperature is ~150-300 EC for a cooling rate of 10 EC/Ma (Bogard, 1995), which should be appropriate for PV as it is close to the cooling rate actually inferred for the meteorite based on a variety of metallographic techniques (~5 EC/Ma). If one makes plausible assumptions that the meteorite started to cool at ~5 EC/Ma when the temperature reached ~650 EC, cooled at this rate to an Ar closure temperature of ~250 EC, and cooled much more quickly at temperatures higher than 650 EC, an original formation time of ~4.56 Ga is consistent with the Ar age. This original formation time would agree with the ~4.57 Ga primary age inferred from the U-Th-Pb system, which could be dating the formation of phosphate, and with the #4.56 Ga age of the coarse vein metal inferred from the Re-Os system (Table 11). Thus, chronologic data are consistent with our hypothesis that PV formed early.

There are indications for one or more later disturbances, although the nature and timing of these later events are poorly understood.. These are suggested by an absence of short-lived radionuclide decay products, a secondary U-Th-Pb age of 94 Ma, scatter in Rb-Sr ages, apparently late Re/Os fractionation in fine-grained metal, and young T_{CHUR} Sm-Nd ages of 1.16-1.85 Ga (Table 11). The data we have obtained for PV shed some light on the nature of the Re-Os and Sm-Nd ages.

We suggest that the evidence for Re/Os variation in fine-grained metal might not represent a datable late event but that it is related to the melting event that produced veins. We have shown that compared to H-chondrites, fine-grained metal is more fractionated than the coarse vein metal, consistent with the results of Chen et al. (1999, 2000), and that variations in siderophile element compositions for metal in PV probably reflect various proportions of "solid" and

"liquid" metal components. This leads us to suspect that the differences in apparent Re-Os ages for fine- and coarse-grained metal (Chen et al., 1999, 2000) reflect sampling different amounts of "solid" and "liquid" metal components, and that the apparently younger ages for the fine metal may represent the effects of mixing, rather than a true age.

Various explanations can be advanced to explain the young Sm-Nd T_{CHUR} ages. One possible explanation is that they indicate a late impact heating event that formed phosphate (Papanastassiou et al., 2002; Ruzicka and Killgore, 2002). Another proposed explanation is that they are artifacts of terrestrial contamination unlike that expected for weathering (Floss et al., 2002). If the young ages date late impact events that were responsible for breccia, vein, and phosphate formation, our preferred model for forming PV in the early solar system would be invalidated. However, we believe that the Sm-Nd data can be understood in the context of the observed mineralogic fractionations in PV, that recourse to terrestrial contamination as an explanation for the Sm-Nd data is unnecessary, and that the "young ages" most likely represent the effects of mixing and do not necessarily date a significant late heating event.

Terrestrial contamination was proposed as an explanation for the young Sm-Nd ages because of the conclusion that apparently no combination of minerals in PV can explain the observed Sm/Nd and Sm abundances (Floss et al., 2002). However, two effects-- merrillite variation and clinopyroxene depletion-- appear largely capable of explaining the measured compositions. In samples we analyzed, merrillite abundance appears to have varied by a factor of ~30, from ~0.05 to ~1.5 wt% (Sec. 3.4, Fig. 13). Fig. 20 shows the effect on CI-normalized Sm abundances and Sm/Nd values of varying merrillite abundance from 0-2 wt% in an otherwise H-chondritic meteorite. This variation will result in Sm abundances and Sm/Nd values that vary by a factor of ~10 and ~1.5, respectively (Fig. 20). Both superchondritic Sm/Nd (low merrillite) and subchondritic Sm/Nd (high merrillite) values are possible (Fig. 20). In addition, clinopyroxene is widely depleted in PV (Sec. 3.1.4, 4.9), and this should have contributed to variations in REE abundances. Sequestering clinopyroxene from an otherwise chondritic mineral assemblage will tend to result in LREE enrichments in the remaining assemblage, as clinopyroxene in PV is strongly depleted in LREE and as it also contains relatively high abundances of the REE (Floss et al., 2002). Thus, one would expect various samples of PV to have variable Sm abundances and a tendency for LREE-enrichments (low Sm/Nd), as is observed (Fig. 20). Samples with high Sm abundances apparently contain a high proportion of phosphate and low proportion clinopyroxene, and samples with low Sm abundances contain a low proportion of both phosphate and clinopyroxene. It thus appears that plausible mixtures can explain the observed REE abundances in PV, with no compelling reason to believe that terrestrial contamination has occurred.

Samarium-Nd T_{CHUR} ages represent model ages that are based on analyses of bulk samples, and as such they have ambiguity as to whether they represent true ages or mixing effects. One reason to suspect a mixing effect is the variation in Sm and Nd abundances and Sm/Nd that would result from sampling differing amounts of phosphate and clinopyroxene in bulk samples of PV, as discussed above. Another is the considerable scatter (~60%) in the numeric value of T_{CHUR} ages (Table 12). We used the data given in Papanastassiou et al. (2002) to plot a standard Sm-Nd

isochron diagram to see whether a well-defined isochron could be obtained. We found a correlation line indicative of an apparent age of ~1.54 Ga (using a decay constant for ^{147}Sm of 6.54 x 10^{-12} a^{-1}), with considerable scatter (R^2 = 0.9487) for this correlation. This apparent young age is consistent with the reported T_{CHUR} ages, but the large scatter raises the question of whether this correlation line represents an isochron. A final reason to doubt the age significance of the Sm-Nd data is that no other chronometer, with the possible exception of a poorly-defined Re-Os age for fine-grained metal (Table 12), gives a similar young age.

Altogether, our interpretation of the chronologic data that have been obtained for Portales Valley suggest that an early formation age is possible, consistent with our preferred model. Complexities in the bulk Re-Os and Sm-Nd systems which could be interpreted as evidence for younger ages can also be plausibly interpreted as resulting from mixing effects.

4.12 Classification of Portales Valley and relationship to other meteorite classes

Portales Valley is currently classified as an H6 chondrite (Grossman, 1999) with a shock stage listed as S3 (Koblitz, 2003). The original classification of PV was made within months of the fall in 1998, and is largely based on mineral-chemical data, a bulk oxygen-isotope measurement (quoted in Rubin et al., 2001), the occasional presence of apparently strained plagioclase, and the presence of local shock blackening (Grossman, 1999; Kring et al., 1999b). Subsequently, additional data have been obtained for the meteorite that indicate that this H6 (S3) classification is misleading.

As discussed above (Sec. 3.1.2, 4.10), an S1 shock designation is more accurate than S3, with shock levels of S3 or higher being model-dependent. Moreover, although the mineral chemistry of silicates and phosphate is appropriate to an H-chondrite, the major- and trace-element composition of metal is somewhat anomalous (Sec. 3.2, 3.3, 4.2), large portions of the meteorite do not have an H-chondrite mineralogy or bulk composition (Sec. 3.1.4, 3.3, 4.9), no other ordinary chondrite contains coarse metal veins or well-developed Widmanstätten texture, and no other ordinary chondrite has been found with large graphite nodules. The presence in PV of coarse merrillite that locally forms poikilitic grains and veins is also exceptional. Even in most hand specimens, there is no mistaking Portales Valley for a typical H6 chondrite.

Based on our work it seems clear that the metallic-sulfide and perhaps even the silicate portion of the meteorite was partly melted (Sec. 4.2-4.4, 4.6), which suggests that the petrographic grade of PV was higher than “6". Considering this likely partial melt origin for PV, and evidence that the heat source was mainly endogenic to the parent body (Sec. 4.5, 4.10), Portales Valley can be properly considered to be a primitive achondrite related to H-chondrites-- in other words, it is an “H7" achondrite. As there is clear evidence for fluidization and partial melting of metal (Sec. 4.2, 4.5), and for brecciation and cataclasis (Sec. 3.1.1), we also conclude that PV is the first, well-documented example of a

metallic-melt breccia. Future work may reveal other meteorites that have coarse metallic melt veins, or a similar inferred history. In this event, Portales Valley and such meteorites could be classified as "Portalesites", with Portales Valley as the type example. Given that only one example of this potential new class of meteorites is now recognized, it may be premature to assign this group name to PV. In the meantime, we suggest that Portales Valley is more accurately classified either as an "H7 (S1) metallic-melt breccia".

The main importance of Portales Valley ultimately may lie in what the meteorite has to tell us about the formation of other meteorite classes. Clearly, the silicate protolith of PV was an H-chondrite. It is also clear that PV was partly melted, possibly analogous to the melting processes that affected achondrites and iron meteorites. Previous workers have noted that the textures of silicates and the distribution of metal and sulfide in PV are similar to those in acapulcoites, winonaites, and silicated IAB irons (Scott and Pinault, 1999; Pinault et al., 1999). Indeed, we have observed that in silicated IAB irons, troilite is usually concentrated in silicate-rich areas between coarse metal areas, similar to that in PV. Similar N-isotopic compositions for metal in IAB irons and in metal from silicate-rich areas in PV (Mathew et al., 2001) also suggest a link between PV and IAB iron meteorites. In addition, PV has chemical-isotopic-textural links to other groups of silicated irons, such as IIE irons (Scott and Pinault, 1999; Ruzicka et al., 1999a; Ruzicka et al., 2000a; Rubin and Ulff-Møller, 1999). The vein-and-breccia texture of PV is remarkably similar to the silicated IIE iron meteorite Netschäevo (Ruzicka et al., 1999a; Rubin et al., 2001), and the trace-element composition of metal in PV and in IIE irons is similar (Sec. 3.3., 4.1; Rushmer et al., 2004). In Sec. 4.1, we also noted the similarity in N-isotopic composition between metal in silicate-rich areas of PV and the metal in silicated IVA iron meteorites. Finally, the Widmanstätten texture and coarse graphite nodules of PV also generally resemble those found in iron meteorites.

These similarities suggest that the processes which formed PV may have also operated to produce other achondrites and iron meteorites, especially primitive achondrites and silicated iron meteorites. More work is needed to establish the extent to which the overall origin inferred for PV-- partial melting caused by simultaneous endogenic heating and impact-induced mobilization of metal-- can be applied to these other differentiated meteorites.

5. CONCLUSIONS

We used a variety of geochemical, mineralogical, and modelling techniques to study the petrology of the unusual Portales Valley meteorite. Our data suggest that the meteorite is the first well-documented example of a metallic melt breccia. We agree with some previous researchers that a shock event was responsible for mobilizing metal into veins, and agree with others that endogenic heating was probably the main heat source for melting. Thus, the meteorite probably formed as a result of a shock-triggered event during internal heating of the parent body early in the history of the solar system. We suggest that indications of possibly younger ages for the meteorite based on Sm-Nd and Re-Os data most likely reflect mixing processes and not crystallization ages. Portales Valley probably formed and subsequently

cooled at depth within its parent body, beneath an impact crater. The shock event, which could have been weak, added a small amount of heat, and also resulted in shearing that enabled metal to mobilize into vein-like structures. The composition of metal in PV is somewhat unusual compared to that found in H-chondrites, and varies between coarse veins and silicate-rich areas. It is best explained by a model involving equilibrium partial melting, and incomplete separation of solid and liquid metal, at temperatures not far above the metal-sulfide eutectic (~940-1150 EC). Under these conditions, most C and P were probably incorporated into metallic liquid, and some of the plagioclase, phosphate, and clinopyroxene in the meteorite could have been melted. Graphite nodules probably formed by crystallization from this metallic liquid, and phosphate formed by reaction between P-bearing metal and clinopyroxene components, depleting clinopyroxene throughout much of the meteorite and growing coarse phosphate at metal-silicate interfaces. Some of the phosphate could have crystallized from P-bearing liquids to produce poikilitic and vein merrillite, but most probably formed under subsolidus conditions as the assemblage cooled between ~975-725 EC. Trace-element and major-element abundances in phosphate were largely established under subsolidus conditions and reflect an approach to equilibrium by buffering reactions in the H-chondrite-like mineral assemblage. Phosphate-forming and FeO-reduction reactions were widespread in PV and entailed a change in the mineralogy and even bulk composition of the stony portion on a large scale ($125 mm^3). Portales Valley is best classified as an H7 (S1) metallic-melt breccia and can be considered to be a primitive achondrite, but one in which shock played a crucial role. Various textural, mineralogic, chemical, and isotopic features of Portales Valley are reminiscent to those in silicated iron meteorites. Thus, Portales Valley is somewhat transitional between more primitive (chondritic) and evolved (achondrite, iron) meteorite types, and could be providing clues as to how differentiation in some asteroidal bodies occurred.

Acknowledgments– The authors wish to thank Dr. Georg Grathoff for assistance and use of x-ray diffraction equipment at Portland State University; Allan Patchen and Dr. Roger Nielsen for assistance in operating electron microprobes at the University of Tennessee and Oregon State University, respectively; Joe Boesenberg for discussion regarding Portales Valley samples at the American Museum of Natural History; and Dr. John McHone for helping to arrange Raman spectroscopy studies of the graphite nodule. The first author also wishes to thank Dr. Martin Prinz (deceased) for stimulating an interest in research on Portales Valley.

REFERENCES

Affiatalab F., and Wasson J.T. (1980) Composition of the metal phases in ordinary chondrites: implications regarding classification and metamorphism. *Geochimica et Cosmochimica* Acta 44: 431-446.

Allen R.O., and Mason B. (1973) Minor and trace elements in some meteoritic minerals. *Geochimica et Cosmochimica Acta* 37: 1435-1456.

Anders E. and Grevesse N. (1989) Abundances of the elements: Meteoritic and solar. *Geochimica et Cosmochimica Acta* 53: 197-214.

Bogard D.D. (1995) Impact ages of meteorites: A synthesis. *Meteoritics* 30: 244-268.

Brearley A., and Jones R.H. (1998) Chondritic Meteorites. In *Planetary Materials* (ed. J.J. Papike), Reviews in Mineralogy, vol. 36, Ch. 3. Mineralogical Society of America: Washington, D.C.

Britt D.T. and Kring D.A. (2001) Portales Valley: The bidirectional spectrum of a unique H5 breccia (abstract #1475). 32nd Lunar and Planetary Science Conference.

Bischoff A. and Stöffler D. (1992) Shock metamorphism as a fundamental process in the evolution of planetary bodies: Information from meteorites. *European Journal of Mineralogy* 4: 707-755.

Chen J.H., Papanastassiou D.A., and Wasserburg G.J. (1999) Re-Os and Pd-Ag systematics in the metal-rich chondrite Portales Valley (abstract #1472). 30th Lunar and Planetary Science Conference.

Chen J.H., Papanastassiou D.A., and Wasserburg G.J. (2000) Comparative FeNi and silicate chronology in Portales Valley (abstract #1507). 31st Lunar and Planetary Science Conference.

Chou C.-L. and Cohen A.J. (1973) Gallium and germanium in the metal and silicates of L- and LL-chondrites. *Geochimica et Cosmochimica Acta* 37: 315-327.

Chou C.-L., Baedecker A.A., and Wasson J.T. (1973) Distribution of Ni, Ga, Ge and Ir between metal and silicate portions of H-group chondrites. *Geochimica et Cosmochimica Acta* 37: 2159-2171.

Crozaz G., Pellas P., Bourot-Denise M., de Chazal S.M., Fiéne C., Lundberg L.L., and Zinner E. (1989) Plutonium, uranium and rare earths in the phosphates of ordinary chondrites– the quest for a chronometer. *Earth and Planetary Science Letters* 93: 157-169.

Curtis D.B. and Schmitt R.A. (1979) The petrogenesis of L-6 chondrites: insights from the chemistry of minerals. *Geochimica et Cosmochimica Acta* 43: 1091-1103.

Doan A.S. and Goldstein J.I. (1969) The formation of phosphides in iron meteorites. In *Meteorite Research* (ed. P.M. Millman). D. Reidel, Dordrech-Holland, pp. 763-779.

Drake M. J. and Weill D.F. (1975) Partition of Sr, Ba, Ca, Y, Eu2+, Eu3+, and other REE between plagioclase feldspar and magmatic liquid: an experimental study. *Geochimica et Cosmochimica Acta* 39: 689-712.

Ebihara M., Ikeda, Y. and Prinz M. (1997) Petrology and chemistry of the Miles IIE iron. II: Chemical characteristics of the Miles silicate inclusions. *Antarctic Meteorite Research* 10: 373-388.

El Goresy A., Gillet Ph., Mostefaoui S., Chen M., and Masaitas V.L. (2002) A transparent, very hard, dense and unusually disordered form of carbon in heavily shocked gneisses from Popigai, Russia: Petrographic settings and comparison with a similar phase in shocked gneisses from the Ries (abstract #1031). 33rd Lunar and Planetary Science Conference.

Feldstein S.N, Jones R.H., and Papike J.J. (2001) Disequilibrium partial melting experiments on the Leedey L6 chondrite: Textural controls on melting processes. *Meteoritics and Planetary Science* 36: 1421-1441.

Friel J.J. and Goldstein J.I. (1976) An experimental study of phosphate reduction and phosphorus-bearing lunar metal particles. *Proceedings of the 7th Lunar Science Conference*: 791-806.

Floss C., Crozaz G., Liu M., and Scott E.R.D. (2002) Piecing together the Portales Valley chronology puzzle: clues to the origin of unusually young Sm-Nd ages (abstract #1084). 33rd Lunar and Planetary Science Conference.

Fraser D.G. and Rammensee W. (1982) Activity measurements by Knudsen cell mass spectrometry– the system Fe-Co-Ni and implications for condensation processes in the solar nebula. *Geochimica et Cosmochimica Acta* 46: 549-556.

Fuchs L.H. (1969) The phosphate mineralogy of meteorites. In *Meteorite Research* (ed. P.M. Millman), pp. 683-695. D. Reidel: Dordrecht-Holland.

Gaines R.V., Skinner H.C.W., Foord E.E., Mason B., Rosenzweig A., King, V.T., and Dowty E. (1997) *Dana's New Mineralogy*. John Wiley and Sons: New York.

Garrison D.H. and Bogard D.D. (2001) ^{39}Ar-^{40}Ar and space exposure ages of the unique Portales Valley H-chondrite (abstract #1137). 32nd Lunar and Planetary Science Conference.

Gastineau-Lyons H.K., McSween H.Y., Jr., and Gaffey M.J. (2002) A critical evaluation of oxidation versus reduction during metamorphism of L and LL group chondrites, and implications for asteroid spectroscopy. *Meteoritics and Planetary Science* 37: 75-89.

Grossman J.N. (1999) The Meteoritical Bulletin, No. 83, 1999 July. *Meteoritics and Planetary Science* 34 (Supplement): A169-A186.

Haack H., Pedersen T.P., and Rasmussen K.L. (2000) Portales Valley: Thermal history of a unique meteorite. *Meteoritics and Planetary Science* 35: A67-A68.

Hansen M. and Anderko K. (1958) *Constitution of binary alloys*. McGraw-Hill: New York.

Harlow G.E., Delaney J.S., Nehru C.E., and Prinz M. (1984) Metamorphic reactions in mesosiderites: Origin of abundant phosphate and silica. *Geochimica et Cosmochima Acta* 46: 339-348.

Holland T.J.B., Navrotsky A., and Newton R.C. (1979) Thermodynamic parameters of $CaMgSi_2O_6$ - $Mg_2Si_2O_6$ pyroxenes based on regular solution and cooperative disordering models. *Contributions in Mineral and Petrology* 69: 377-344.

Hsieh K.-C., Vlacxh K.C., and Chang Y.A. (1987) The Fe-Ni-S system, I. A thermodynamic analysis of the phase

equilibria and calculation of the phase diagram from 1173 to 1623 K. *High Temperature Science* 23: 17-38.

Jarosewich E. (1990) Chemical analyses of meteorites: A compilation of stony and iron meteorite analyses. *Meteoritics* 25: 323-337.

Joliff B.L., Haskin L.A., Colson R.O., and Wadwha M. (1993) Partitioning in REE-saturating minerals: heory, experiment, and modelling of whitlockite, apatite, and evolution of lunar residual magmas. *Geochimica et Cosmochimica Acta* 57: 4069-4094.

Johnson D.M., P.R. Hooper, and Conrey R.M. (1999) XRF analysis of rocks and minerals for major and trace elements on a single low dilution Li-tetraborate fused bead. *Advances in X-ray Analysis* 41: 843-867.

Jones J.H. (1995) Experimental Trace Element partitioning. In Rock Physics and Phase Relations– A Handbook of Physical Constants, AGU Reference Shelf 3, pp. 73-104. American Geophysical Union: Washington, D.C.

Jurewicz A.J.G., Mittlefehldt D.W., and Jones J.H. (1995) Experimental partial melting of the St. Severin (LL) and Lost City (H) chondrites. *Geochimica et Cosmochimica Acta* 59: 391-408.

Kagi H., Takahshi K., Shimuzu H., Kitajima F., and Masuda A. (1991) In-situ micro Raman studies on graphitic carbon in some antarctic ureilites. *Proceedings of the NIPR Symposium on Antarctic Meteorites* 4: 371-383.

Kagi H., Takahashi K., and Masuda A. (1994) Raman frequencies of graphitic carbon in antarctic ureilites. *Proceedings of the NIPR Symposium on Antarctic Meteorites* 7: 252-261.

Kenkman T., Hornemann U., and Stöffler D. (2002) Transformation of graphite to diamond in shock experiments: A Raman study (abstract #1052). 31st Lunar and Planetary Science Conference.

Koblitz J. (2003) MetBase– Meteorite Data Retrieval Software. MetBase Version 6.0 for Windows. CD-ROM.

Komarek K.L. (1963) Direct reduction of iron ores containing phosphorus. *Transactions of the Metallagurgical Society of AIME* 227: 136-145.

Kong P., and Ebihara M. (1996) Metal phases of L chondrites: Their formation and evolution in the nebula and in the parent body. *Geochimica et Cosmochimica Acta* 60: 2667-2680.

Kong P., Ebihara M., Nakahara H., and Endo K. (1995) Chemical characteristics of metal phases of the Richardton H5 chondrite. *Earth and Planetary Science Letters* 136: 407-419.

Knack C., S. Cornelius, and P. Hooper (1994) Trace element analyses of rocks and minerals by ICPMS. Department of Geology, Washington State University. URL: http://www.wsu.edu/%7Egeology/Pages/Services/ICP.html

Kring D.A., Hill D.H., and Gleason J.D. (1999a) Portales Valley meteorite: The brecciated and metal-veined floor of a >20 km diameter crater on an H-chondrite asteroid (abstract #1618). 30th Lunar and Planetary Science Conference.

Kring D.A., Hill D.H., Gleason J.D., Britt D.T., Consolmagno G.J., Farmer M., Wilson S., and Haag R. (1999b) Portales Valley: A meteoritic sample of the brecciated and metal-veined floor of an impact crater on an H-chondrite asteroid. *Meteoritics and Planetary Science* 34: 663-669.

Kubaschewski O. (1982) *Iron-Binary phase diagrams.* Springer-Verlag: Berlin. 185 pp.

Lapke C., Schmitt R.T., Kenkmann T., and Stöffler D. (2002) Raman microspectrometry of shocked graphite and impact diamonds from the Ries crater, Germany (abstract #1040). 31st Lunar and Planetary Science Conference.

Langmuir C.H. (1989) Geochemical consequences of *in situ* crystallization. *Nature* 340: 199-205

Lindsley D.H. (1983) Pyroxene thermometry. *American Mineralogist* 68: 477-493.

Lindsley and Anderson (1983) A two-pyroxene thermometer. *Proceedings of the 13th Lunar and Planetary Science Conference*, Journal of Geophysical Research, Suppl., 88: A887-A906.

Liu M. and Fleet M.E. (2001) Partitioning of siderophile elements (W, Mo, As, Ag, Ge, Ga and Sn) and Si in the Fe-S system and their fractionation in iron meteorites. *Geochimica et Cosmochimica Acta* 65: 671-682.

Massalski T.B, Murray J.L., Bennett L.H., and Baker, H. (1986) Fe-C Phase Diagram. In *Binary Alloy Phase Diagrams*, Vol. 1, pp. 562-566. American Society for Metals: Metals Park, Ohio.

Mathew K.J., Palma R.L, Marti, K., and Lavielle B. (2000) Isotopic signatures and origin of nitrogen in IIE and IVA iron meteorites. *Geochimica et Cosmochimica Acta* 64: 545-557.

Mathew K.J., Marti K., Lavielle B., and Ruzicka A. (2001) Nitrogen isotopic signatures in the Portales Valley meteorite. *Meteoritics and Planetary Science* 36: A126-A127.

McCoy T.J., Keil K., Clayton R.N., Mayeda T.K., Bogard D.D., Garrison D.H., Huss G.R., Hutcheon I.D., and Wieler R. (1996) A petrologic, chemical, and isotopic study of Monument Draw and comparison with other acapulcoites: Evidence for formation by incipient partial melting. *Geochimica et Cosmochimica Acta* 60: 2681-2708.

Moren A.E. and J.I. Goldstein (1979) Cooling rates of Group IVA iron meteorites determined from a ternary Fe-Ni-P model. *Earth and Planetary Science Letters* 43: 182-196.

McKay G.A. (1986) Crystal/liquid partitioning of REE in basaltic systems: Extreme fractionation of REE in olivine. *Geochimica et Comsochimica Acta* 50: 69-79.

McKay G., Wagstaff J. and Yang S.-R. (1986) Clinopyroxene REE distribution coefficients for shergottites: The REE content of the Shergotty melt. *Geochimica et Cosmochimica Acta* 50: 927-937.

McSween H.Y., Jr. and Patchen A.D. (1989) Pyroxene thermobarometry in LL-group chondrites and implications for parent body metamorphism. *Meteoritics* 24: 219-226.

McSween H.Y. Jr and Labotka T.C. (1993) Oxidation during metamorphism of the ordinary chondrites. *Geochimica et Cosmochimica Acta* 57: 1105-1114.

McSween H.Y. Jr., Taylor L.A., and Lipschutz M.E. (1978) Metamorphic effects in experimentally heated Krymka (L3) chondrite. *Proceedings of the 9th Lunar and Planetary Science Conference*: 1437-1447.

Mittlefehldt D.W. (2002) Geochemistry of the ungrouped carbonaceous chondrite Tagish Lake, the anomalous CM chondrite Bells, and comparison with CI and CM chondrites. *Meteoritics and Planetary Science* 37: 703-712.

Mittlefehldt D.W. and Lindstrom M.M. (1993) Geochemistry and petrology of a suite of ten Yamato HED meteorites.

Proceedings of the NIPR Symposium on Antarctic Meteorites 6: 268-292.

Miyamoto M. (1998) Micro Raman spectroscopy of diamonds in the Canyon Diablo iron meteorite: implications for the shock origin. *Antarctic Meteorite Research* 11: 171-177.

Murrell M.T. and Burnett D.S. (1983) The behavior of actinides, phosphorus, and rare earth elements during chondrite metamorphism. *Geochimica et Cosmochimica Acta* 47: 1999-2014.

Olsen E. and Fuchs L.H. (1967) The state of oxidation of some iron meteorites. *Icarus* 6: 242-253.

Papanastassiou D.A., Chen J.H., and Wasserburg G.J. (2001) Chronology and composition puzzles in Portales Valley (abstract #1476). 32nd Lunar and Planetary Science Conference.

Papanastassiou D.A., Chen J.H., and Wasserburg G.J. (2002) What whole rock samples of Portales Valley can and cannot tell us (abstract #1826). 33rd Lunar and Planetary Science Conference.

Pinault L.J.. Scott E.R.D., Bogard D.D., and Keil K. (1999) Extraordinary properties of the metal-veined, H6 Portales Valley chondrite: Evidence for internal heating versus shock-melting origins (abstract #2048). 30th Lunar and Planetary Science Conference.

Rambaldi E. (1976) Trace element content of metals from L-group chondrites. *Earth and Planetary Science Letters* 31: 224-238.

Rambaldi E.R. (1977) Trace element content of metals from H- and LL-group chondrites. *Earth and Planetary Science Letters* 36: 347-358.

Reisener R.J. and Goldstein J.I. (2003) Ordinary chondrite metallography: Part 2. Formation of zoned and unzoned metal particles in relatively unshocked H, L, and LL chondrites. *Meteoritics and Planetary Science* 38: 1679-1696.

Rollinson H. (1993) *Using geochemical data: Evaluation, presentation, interpretation.* Prentice Hall. 352 pp.

Rubin A.E. (1985) Impact melt products of chondritic material. *Reviews of Geophysics* 23: 277-300.

Rubin A.E. (1990) Kamacite and olivine in ordinary chondrites: Intergroup and intragroup relationships. *Geochimica et Cosmochimica Acta* 54: 1217-1232.

Rubin A.E. (1992) A shock-metamorphic model for silicate darkening and compositionally variable plagioclase in CK and ordinary chondrites. *Geochimica et Cosmochimica Acta* 56: 1705-1714.

Rubin A.E. (1993) Metallic copper in ordinary chondrites. *Meteoritics* 29: 93-98.

Rubin A.E. (2003) Chromite-Plagioclase assemblages as a new shock indicator; implications for the shock and thermal histories of ordinary chondrites. *Geochimica et Cosmochimica Acta* 67: 2695-2709.

Rubin A.E. (2004) Postshock annealing and postannealing shock in equilibrated ordinary chondrites: Implications for the thermal and shock histories of chondritic asteroids. *Geochimica et Cosmochimica Acta* 68: 673-689.

Rubin A.E. and Ulff-Møller F. (1999) The Portales Valley meteorite breccia: Evidence for impact-induced metamorphism of an ordinary chondrite (abstract #1125). 30th Lunar and Planetary Science Conference.

Rubin A.E., Ulff-Møller F., Wasson J.T., and Carlson W.D. (2001) The Portales Valley meteorite breccia: Evidence for

impact-induced melting and metamorphism of an ordinary chondrite. *Geochimica et Cosmochimica Acta*: 66, 323-342.

Rushmer T., Gaetani G., and Jones J.H. (2000a) Chondrites under stress: what can they tell us about core formation processes? (abstract #1673). 31st Lunar and Planetary Science Conference.

Rushmer T., Minarik W.G., and Taylor G.J. (2000b) Physical processes of core formation. In *Origin of the Earth and Moon* (ed. R.M. Canup, K. Righter), pp. 227-243. University of Arizona Press: Tucson.

Rushmer T., Humayan M, and Campbell A.J. (2004) Siderophile element abundances in Fe-S-Ni-O melts segregated from partially molten ordinary chondrite under dynamic conditions (abstract #1850). 35th Lunar and Planetary Science Conference.

Ruzicka A., Snyder G.A., Prinz M., and Taylor L.A. (1999a) Portales Valley: A new metal-phosphate-rich meteorite with affinities to Netschaevo and H-group chondrites (abstract #1645). 30th Lunar and Planetary Science Conference.

Ruzicka A., Bennett M.E. III, Patchen A.D., Snyder G.A., and Taylor L.A. (1999b) Widmannstätten texture in the Portales Valley meteorite: slow (but not unusually slow) cooling at low temperatures (abstract #1616). 30th Lunar and Planetary Science Conference.

Ruzicka A., Killgore M., Boesenberg J., and Prinz M. (2000a) Portales Valley: Not just another "ordinary" chondrite. *Meteoritics and Planetary Science* 35: A139-A140.

Ruzicka A., McHone J.F., and Killgore M. (2000b) Portales Valley: Discovery of a large graphite nodule. *Meteoritics and Planetary Science* 35: A140.

Ruzicka A. and Killgore M. (2002) Trace-element abundances in the Portales Valley meteorite: evidence for geochemical fractionations (abstract #1918). 33rd Lunar and Planetary Science Conference.

Scott E.R.D. and Pinault L.J. (1999) Partial melting and incipient segregation of troilite and metal in winonaites, acapulcoites, IAB and IIE irons, and fine-grained H6 chondrites (abstract #1507). 30th Lunar and Planetary Science Conference.

Schwandt C.S. and McKay G.A. (1996) REE partition coefficients from synthetic diogenite-like enstatite and the implications of petrogenetic modelling. In *Workshop on the evolution of igneous asteroids: Focus on Vesta and the HED meteorites.* LPI Technical report Number 96-02, Part 1, pp. 25-27.

Sepp B., Bischoff A., and Bosbach D. (2001) Low-temperature phase decomposition in iron-nickel metal of the Portales Valley meteorite. *Meteoritics and Planetary Science* 36: 587-595.

Stöffler D., Keil K., and Scott E.R.D. (1991) Shock metamorphism of ordinary chondrites. *Geochimica et Cosmochimica Acta* 55: 3845-3867.

Takahashi E. (1983) Melting of a Tamato L3 chondrite (Y-74191) up to 30 Kbar. *Proceedings of the 8th Symposium on Antarctic Meteorites* No. 30: 168-180.

Treiman A.H. (1996) The perils of partition: Difficulties in retrieving magma compositions from chemically equilibrated

basaltic meteorites. *Geochimica et Cosmochimica Acta* 60: 147-155.

Usselman T. M. (1975) Experimental approach to the state of the core: Part I. The liquidus relations of the Fe-Ni-S system from 30 to 100 Kb. *American Journal of Science* 275: 278-290.

Van de Bogert C.H., Schultz P.H., and Spray J.G. (2003) Impact-induced frictional melting in ordinary chondrites: A mechanism for deformation, darkening, and vein formation. *Meteoritics and Planetary Science* 38: 1521-1531.

Van Schmus W.R. and Ribbe P.H. (1969) Composition of phosphate minerals in ordinary chondrites. *Geochimica et Cosmochimica Acta* 33: 637-640.

Wasson J.T. (1985) *Meteorites– Their Record of Early Solar System History.* W.H. Freeman and Company: New York.

Wasson J.T. and Wang J. (1986) A nonmagmatic origin of group-IIE iron meteorites. *Geochimica et Cosmochimica Acta* 50: 725-732.

Wasson J.T. and Kallemeyn G.W. (1988) Compositions of chondrites. *Philosophical Transactions of the Royal Society of London A* 325: 535-544.

Watson E.B. and Green T.H. (1981) Apatite/liquid partition coefficients for the rare earth elements and strontium. *Earth and Planetary Science Letters* 56: 405-421.

Weill D.F. and McKay G.A. (1975) The partitioning of Mg, Fe, Sr, Ce, Sm, Eu and Yb in lunar igneous systems and a possible origin of KREEP by equilibrium partial melting. *Proceedings of the 6th Lunar Science Conference*: 1143-1158.

Williams R.J. (1971) Reaction constants in the system Fe-MgO-SiO2-O2 at 1 atm between 900E and 1300EC: Experimental results. *American Journal of Science* 270: 334-360.

Yugami K., Takeda H., Kojima H., and Miyamoto M. (1998). Modal mineral abundances and the differentiation trends in primitive achondrites. *Antarctic Meteorite Research* 11: 49-70.

FIGURE CAPTIONS

Fig. 1: Images illustrating overall textures and large-scale features in Portales Valley. **(a)** Typical breccia or cataclastic texture seen with reflected light in polished slab (sample K-5), showing silicate-rich clasts enclosed by FeNi-metal. Most clasts have sharp, straight boundaries; region X shows rounded metal-rich embayment inside a clast that appears to post-date clast formation. **(b)** Texture typical of veined sample (AMNH 4978-5), consisting of veins of FeNi-metal (FeNi) and troilite (FeS) that cross-cut silicate-rich areas. Coarse merrillite (merr) and Cl-apatite (apat) are found near the veins. Boundaries of veins are irregular, and clastic texture is not so evident (view of polished slab in reflected light). **(c)** Image obtained with backscattered electrons (BSE) of sample (AMNH 4978-4) showing silicate-rich grains (grey) embayed by a FeNi-metal vein (FeNi) that grades into troilite veins (FeS). Note that metallic areas fill interstices of silicate grains (mainly low-Ca pyroxene), and that metal is convex-outward against troilite. **(d)** BSE image of silicate-rich sample (CML0056-3) showing anhedral grains of olivine, low-Ca pyroxene (Opx), plagioclase (Plag), kamacite (Kam), taenite (Tae), troilite (Troi) and phosphate (Phos). Region X is an area of Opx that contains many fine-grained metal and troilite inclusions which could be locally "shock-blackened". **(e)** Plane-polarized transmitted light view of silicate-rich sample (CML0056-3) showing three relict chondrules (X, Y, Z). Black phases = opaque minerals (mainly metal and troilite); lighter areas = silicates. **(f)** View of hand specimen containing a large silicate-rich clast that appears to have been microfaulted (arrows). Fusion crust covers the microfault at left and occurs on the surface of the microfault at right, indicating that microfaulting was pre-terrestrial. Another microfault is implied at the edge of the silicate clast, along the metal vein which appears at nearly right angles to the viewing direction.

Fig. 2: BSE images illustrating internal textures of metal veins in Portales Valley. Black = silicates; white to grey = FeNi-metal. **(a)** Relatively thin, irregular vein that consists of kamacite and taenite (Ni-rich metal) intergrowths, including a small lamella of kamacite (sample AMNH 4978-3). **(b)** and **(c)** Coarser metal veins showing development of internal Widmanstätten texture and swathing kamacite borders at the vein edges. With increasing distance from kamacite, metal is zoned from higher to lower Ni (white to grey, "zoned taenite") and finally to fine intergrowths of Ni-poor and Ni-rich metal ("plessite"). Nickel and Co contents along profile A-B in (c) are shown in Fig. 7 (samples AMNH 4978-3 and -5).

Fig. 3: Images illustrating the distribution and texture of phosphate grains in Portlales Valley. **(a)** Plane-polarized, transmitted light view of AMNH 4978-2 showing preferred concentration of phosphate grains (located by white boxes) close to metal veins (black) that cross-cut silicate-rich areas. **(b)** BSE image of the coarsest phosphate region in AMNH 4978-2 (indicated by arrow in (a)) showing merrillite which encloses euhedral-subhedral silicates of all types (ol = olivine; opx = low-Ca pyroxene; plag = plagioclase) with an apparent poikilitic texture. **(c)** BSE image which

shows coarse vein-forming merrillite (light grey) extending from the termini of FeNi-metal and troilite (FeS) veins (sample AMNH 4978-5).

Fig. 4: Images of a large graphite nodule obtained in reflected light (sample K-5). **(a)** Overview image, showing enclosure of the elongated graphite nodule within an especially coarse region of Fe-Ni-metal (FeNi). **(b)** Higher magnification view of nodule showing irregular nodule edge (bottom left) and two types of internal features, including irregular Fe-Ni-metal veinlets that have a preferred orientation parallel to the maximum dimension of the nodule (upper left to lower right), and necklaces of FeNi-metal inclusions that have a preferred orientation perpendicular to the long dimension of the inclusion (lower left to upper right). Straight lines oriented from lower right to upper left are polishing scratches.

Fig. 5: Raman spectrum of graphite nodule in sample K-2 showing two peaks, a large peak at ~1580 cm^{-1} and a smaller peak at ~1360 cm^{-1}. No peak is apparent at the expected location for diamond at ~1331 cm^{-1}.

Fig. 6: Graphs illustrating modal abundances in various sections of AMNH 4978. Data are compared to normative abundances for H-chondrites based on data given in Jarosewich (1990), and to the general field for acapulcoites based on various sources (e.g., McCoy et al., 1996; Yugami et al., 1998). In (a) and (b), plotted H-chondrite values show means (points) and standard deviations (bars) of normative compositions. In (c), a linear regression is shown for H-chondrite data, and a second-order regression is shown for PV data. Compared to H-chondrites, most samples of PV have low abundances of olivine and clinopyroxene (high-Ca px), and high abundances of low-Ca pyroxene (low-Ca px) and phosphate (phos). Compared to acapulcoites, PV samples tend to be metal-enriched and have a higher olivine/pyroxene ratio.

Fig. 7: Spatial variations in Ni and Co contents within a coarse metal vein, determined by electron microprobe analysis. The location of the traverse is indicated in Fig. 2c. Large variations in Ni content within plessite are caused by fine-scale intergrowths of Ni-rich and Ni-poor metal. Compositional gradients in kamacite and taenite, including the depletion of Ni in kamacite adjacent to taenite (the Agrell Effect), are indicative of low-temperature diffusion of Ni and Co during cooling.

Fig. 8: Nickel and Co abundances within **(a)** kamacite and **(b)** taenite in Portales Valley compared to average compositions in H4-6 and L4-6 chondrites. Metal compositions within Portales Valley differ systematically between coarse vein and silicate-rich areas. For a given Ni content, taenite in coarse veins is enriched in Co compared to taenite in silicate-rich areas, while kamacite in coarse veins is depleted in Co compared to kamacite in silicate-rich areas. H4-6 and

L4-6 data sources: Rubin (1990), Affiatalab and Wasson (1980), Kong and Ebihara (1996), Kong et al. (1995).

Fig. 9: Co/Ni vs. Ni abundance plot for metal in Portales Valley compared to metal in H4-6 and L4-6 chondrites. Values for kamacite, taenite, and bulk metal are shown. Regression lines are drawn through kamacite and taenite compositions in H4-6 and L4-6 chondrites to indicate the systematic offset in Co/Ni and Ni values between H and L chondrite metal. These regression lines pass through the bulk metal compositions for the respective meteorites. For Portales Valley, kamacite and bulk vein metal have compositions that lie close to the regression line for H-chondrites, but taenite has compositions intermediate to the regression lines for H- and L-chondrites. H4-6 and L4-6 data sources: same as for Fig. 8, and Rambaldi (1976, 1977).

Fig. 10: CI-normalized abundances of some REE in **(a)** orthopyroxene and **(b)** phosphate in Portales Valley, based on SIMS analyses. For comparison, ranges show measured compositions in equilibrated ordinary chondrites (EOC orthopyroxene-- Curtis & Schmitt (1979), Allen & Mason (1973); EOC phosphate– Curtis & Schmitt (1979), Crozaz et al. (1989)). REE abundances in merrillite and Cl-apatite in Portales Valley overlap those in metamorphosed H-chondrites; REE abundances in orthopyroxene from Portales Valley appear somewhat low compared to the abundances reported from H-chondrites. The CI-chondrite abundances of Anders and Grevesse (1989) were used for normalization.

Fig. 11: CI-normalized abundances of various splits of Portales Valley. **(a)** Lithophile and siderophile/chalcophile element abundances in silicate-rich samples of Portales Valley (PV samples) compared to the El Hammami H5 chondrite (EH1 & EH2 samples), with elements arranged according to decreasing 50% condensation temperatures (Wasson, 1985). Data are from Tables 8 & 9. **(b)** Same as (a), but for an expanded number of incompatible lithophile elements, with elements arranged according to atomic number. **(c)** Siderophile element abundances arranged according to decreasing 50% condensation temperatures in coarse metal sample PVD (Table 8) compared to two analyses of coarse metal by Rubin et al. (2001) (#1 and #2), average metal in H4-6 chondrites (Chou et al. (1973), Rambaldi (1977), Kong et al. (1995)), and average metal in IIE irons (e.g., Wasson and Wang, 1986; Ebihara et al., 1997). The CI-chondrite abundances of Anders and Grevesse (1989) were used for normalization. See Text for discussion.

Fig. 12: Abundances of major elements normalized to Si and to average H-chondrites in metal-poor sample PVF and for various sections of metal-veined samples from AMNH 4978. Portales Valley data are from Table 10; data for H-chondrites are from Jarosewich (1990). Si-normalized abundance ratios for some elements (e.g., Ca, P, Fe, Ni, S) in some samples depart greatly from average H-chondrite values, whereas those for some elements (e.g., Mg, Mn, Al) in all samples resemble those in H-chondrites.

Fig. 13: CI-normalized abundances for REE in various splits of Portales Valley (PV) (Table 8, 9) are compared to a model in which merrillite is mixed in various proportions in an otherwise chondritic assemblage. The model assumes that merrillite with a composition identical to the average found in this study (Table 7a) is added to or subtracted from an H-chondrite assemblage that originally has unfractionated REE abundances of 1.33 x CI-chondrites and 0.4 wt% merrillite.

Fig. 14: CI-normalized abundances for siderophile elements in various splits of Portales Valley (PV) and in El Hammami H5 chondrite (EH1) are compared to a model in which metal of average H-chondrite composition is mixed in variable proportions in an otherwise chondritic assemblage. Measured compositions for PV and EH1 are taken from Tables 8 and 9. The model assumes that metal of average composition in H4-6 chondrites (see Fig. 11 caption) is added to or subtracted from an H-chondrite assemblage with 17 wt% metal and the average composition found in H-chondrites (Wasson and Kallemeyn, 1988).

Fig. 15: Ni-normalized and H-chondrite-normalized siderophile element abundances in Portales Valley are compared to a model in which solids and melt produced by equilibrium melting are incompletely separated. PV data are from Table 8; average H-chondrite metal compositions are from the same sources as given in Fig. 11. Error bars for the coarse vein metal (PVD) represent analytical uncertainty; errors bars for fine-grained metal in silicate-rich samples reflect the standard deviation of the mean composition. **(a)** 33% equilibrium melting (eutectic conditions) in the Fe + Ni + S system, corresponding to T ~ 940-990 EC. **(b)** 40% equilibrium melting, T~1150 EC. **(c)** 50% equilibrium melting, T ~ 1300 EC. The observed compositions are matched for mixtures produced at eutectic or near-eutectic melting conditions (~33% to as much as 40% melting), with higher proportions of solid in the coarse veins than in silicate-rich areas. See Text.

Fig. 16: Measured average REE abundances in merrillite and orthopyroxene (Table 7) are compared to the composition of melt that would be in equilibrium with these phases. The calculated parent melt composition for merrillite (~10-20 x CI) is slightly enriched in heavy REE (HREE), in contrast to the calculated composition for orthopyroxene, which is strongly HREE-depleted. Not only do the two patterns disagree, but neither corresponds to the moderately HREE-depleted pattern that would be expected for a partial melt. The model assumes mineral/melt partition coefficients (D-values) as follows: for orthopyroxene, the median D-values of Schwandt and McKay (1996) were assumed, with Gd interpolated; for merrillite, the D-values of Joliff et al. (1993) (low REE-concentration case) were assumed. The CI-chondrite abundances of Anders and Grevesse (1989) were used for normalization.

Fig. 17: Measured REE abundances for merrillite, Cl-apatite, and orthopyroxene (points, Table 7) are compared

to models in which these phases equilibrated under subsolidus conditions, assuming either a mode identical to that of average PV 4978 (Table 3) with total REE abundances of 2-3 x CI-chondrites, or a mode corresponding to average normative H-chondrite (Jarosewich, 1990) with total REE abundances of 1.34 x CI-chondrites. Generally good agreement between measured and modelled abundances are observed. The model assumes partition coefficients identical to those given at magmatic temperatures as follows: orthopyroxene and merrillite-- same as in Fig. 16; olivine-- McKay (1986), with Eu, Dy, and Er interpolated; clinopyroxene-- McKay et al. (1986), Wo_{40} augite, with Dy and Er interpolated, and a Eu anomaly (calculated from Sm/Eu) identical to that of orthopyroxene; plagioclase (all REE except Eu)-- Drake and Weill (1975), with Yb assumed to be the same as Er; plagioclase (Eu)-- Weill and McKay (1975). The CI-chondrite abundances of Anders and Grevesse (1989) were used for normalization.

Fig. 18: Temperature - oxygen fugacity conditions for reactions relevant to the petrogenesis of phosphate in Portales Valley. The FIF buffer probably controls fO_2 in ordinary chondrite-like assemblages (McSween and Labotka, 1993), whereas merrillite is believed to have formed by the DIMO reaction (given by reaction [1] in the Text.). The intersection of these equilibria will control the P content in metal and the formation of phosphate. This analysis implies that metal with an initial P content of 0.66 wt% (appropriate to that for PV) will begin to react to form phosphate as temperature drops below ~975 EC. Reaction will continue until a temperature of ~725 EC is reached, which corresponds to the observed P content in metal.

Fig. 19: Modelled evolution of P content in the metal of Portales Valley as a function of temperature. In principle, the P content in metal under subsolidus conditions could be controlled either by metal-silicate-phosphate (FIF & DIMO) equilibria or metal-phosphide equilibria (GUP or AUP), but our analysis suggests that for the range of P contents likely present in PV metal (P # 0.6 wt%), equilibria with silicates and the formation of phosphate likely controlled the evolution of P content in metal. See Text.

Fig. 20: Illustration of the effect of variable merrillite and clinopyroxene content on the expected Sm abundances and Sm/Nd ratio in bulk samples. Observed data for PV from Papanastassiou et al. (2002) and this study are shown for comparison. For all samples in this study analyzed except for PVE, Nd abundances were determined by interpolation between Sm and La. Most of our data and that of Papanastassiou et al. (2002) can be explained by a model assuming variable merrillite abundance coupled with a low abundance of clinopyroxene, in agreement with the modal data for PV. Very low Sm/Nd and high Sm abundances observed in some samples of Papanastassiou et al. (2002) would require samples more enriched in merrillite and depleted in clinopyroxene than we analyzed.

Ruzicka et al.

Fig. 1a-d

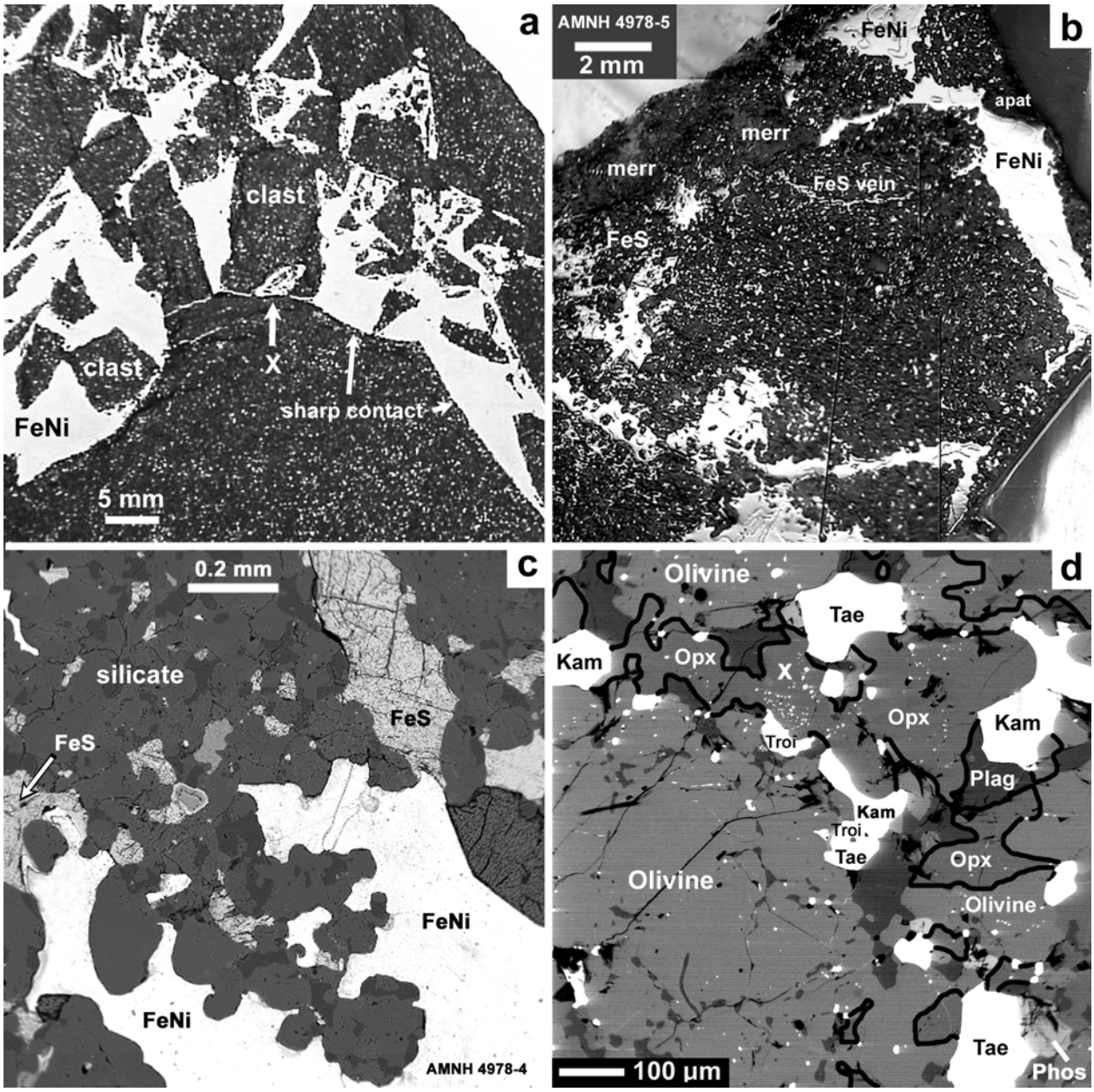

Ruzicka et al.

Fig. 1e-f

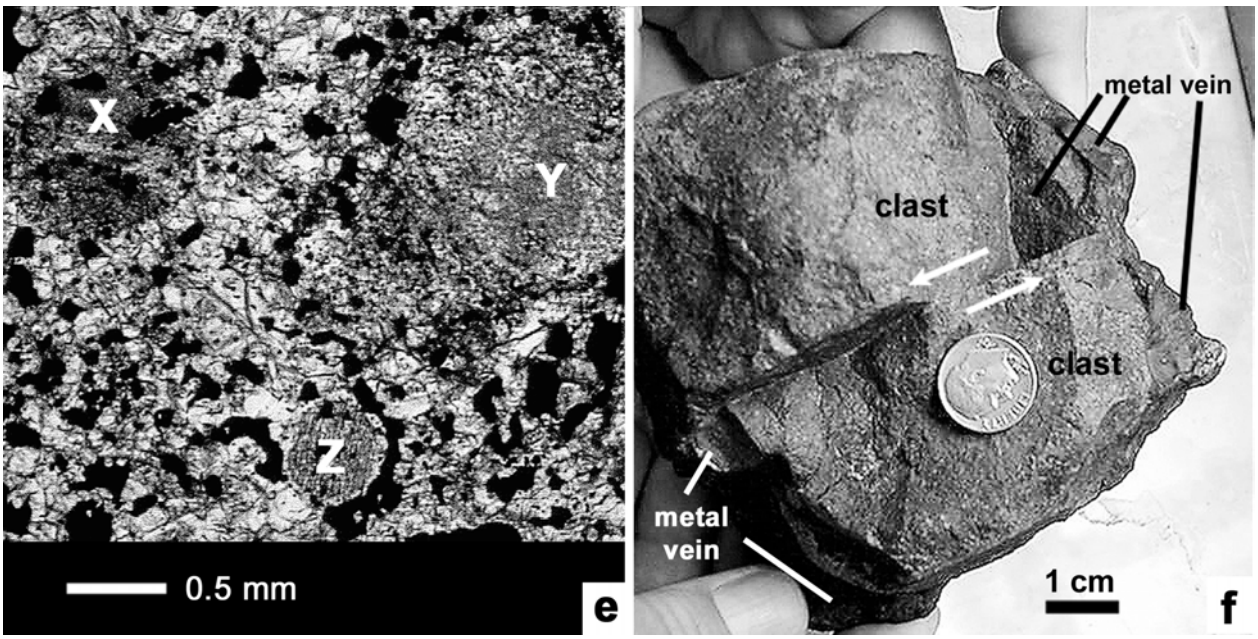

Ruzicka et al.

Fig. 2a-c

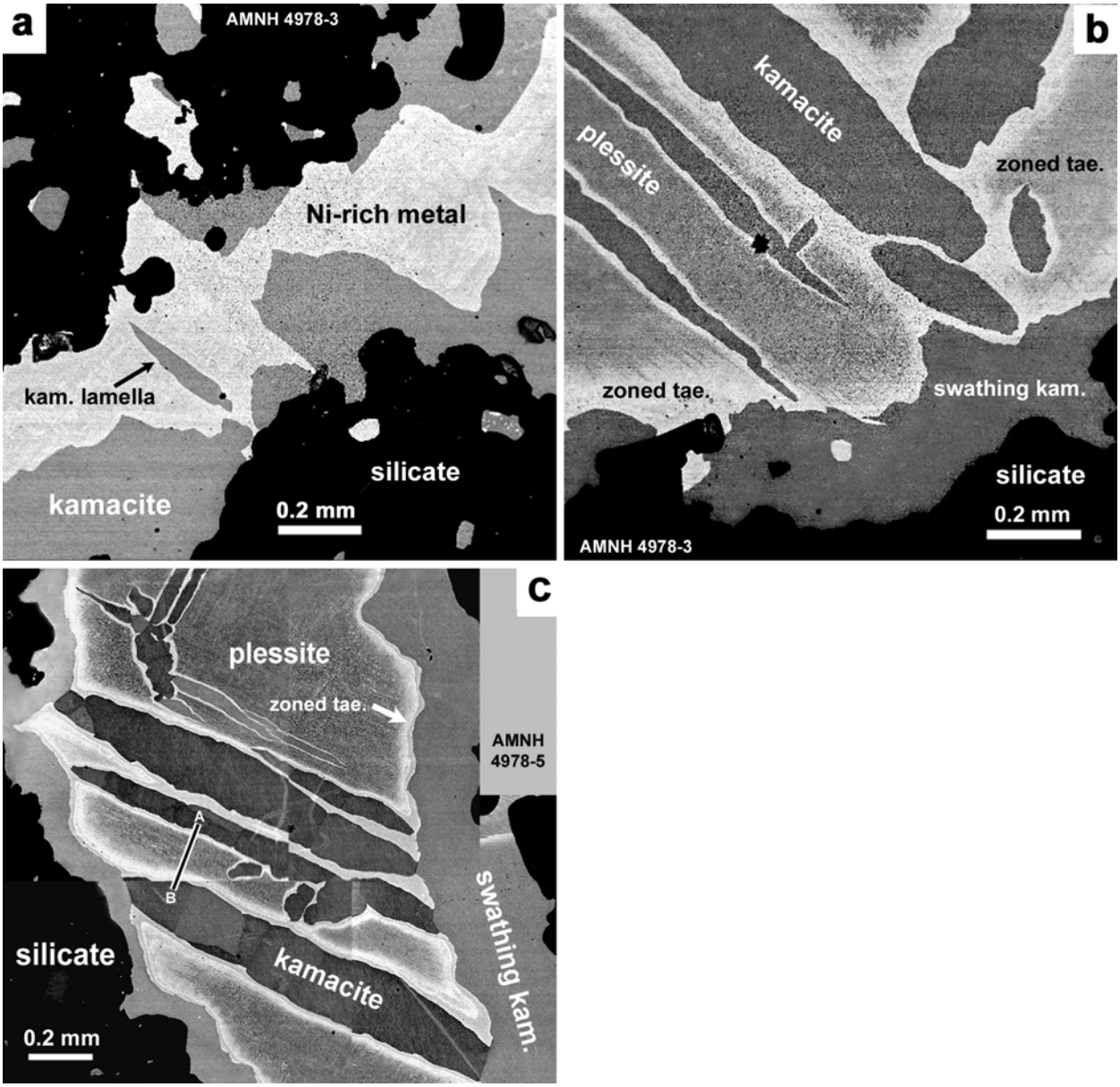

Ruzicka et al.

Fig. 3a-c

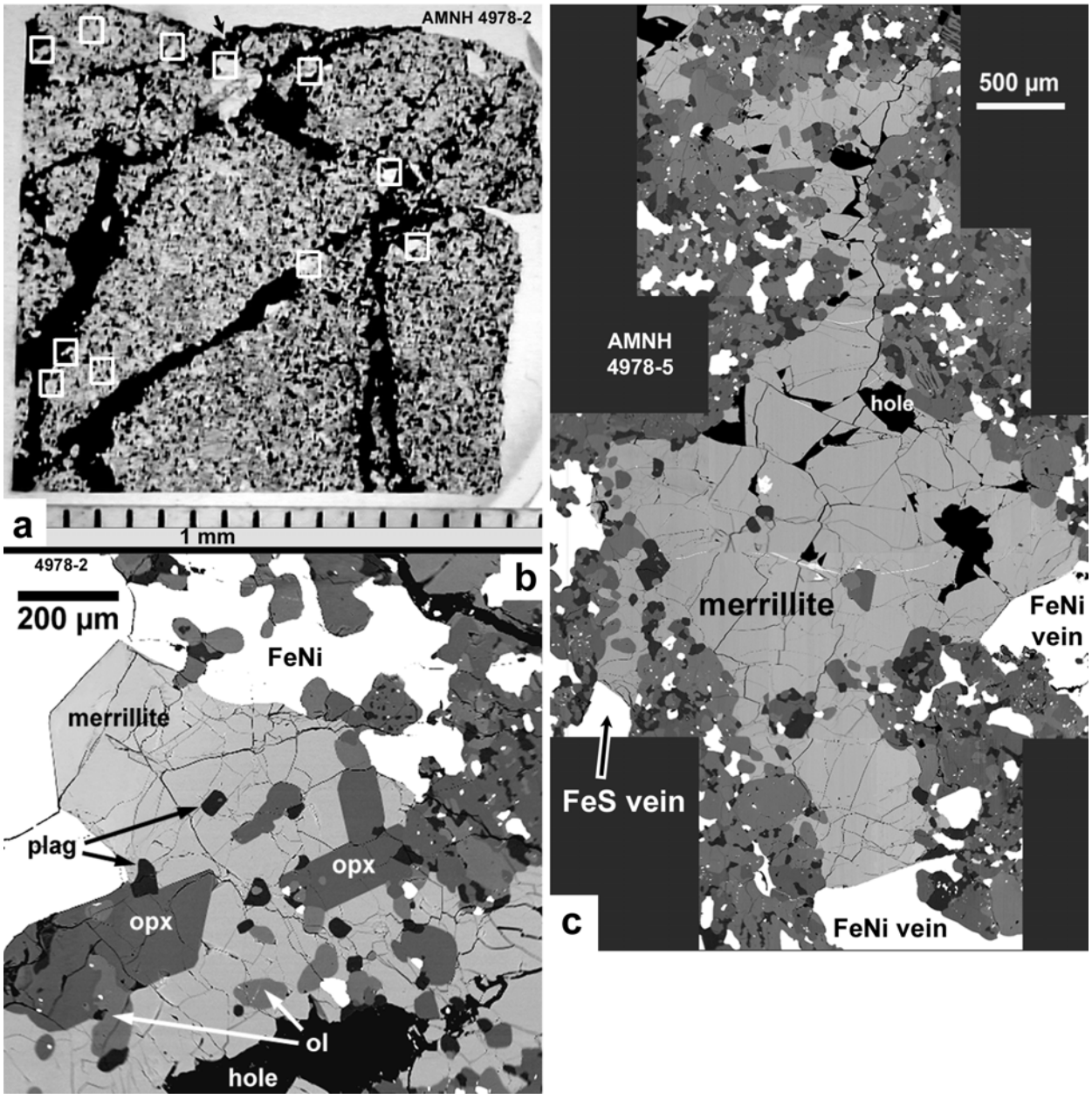

Ruzicka et al.

Fig. 4a-b

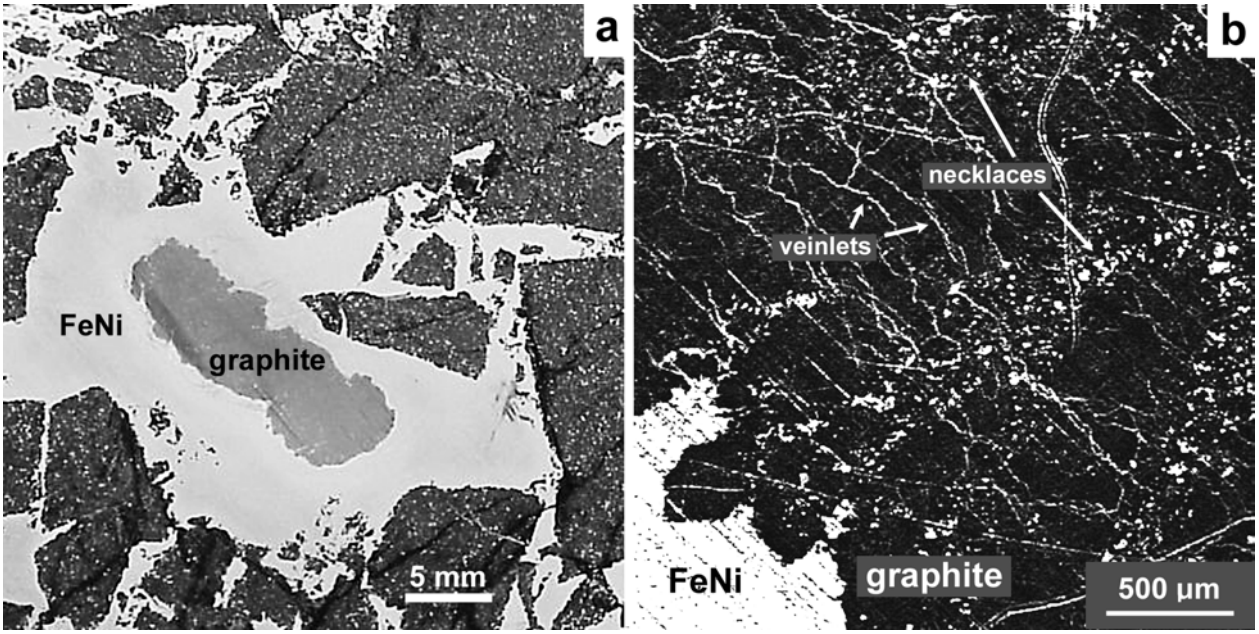

Ruzicka et al.

Fig. 5

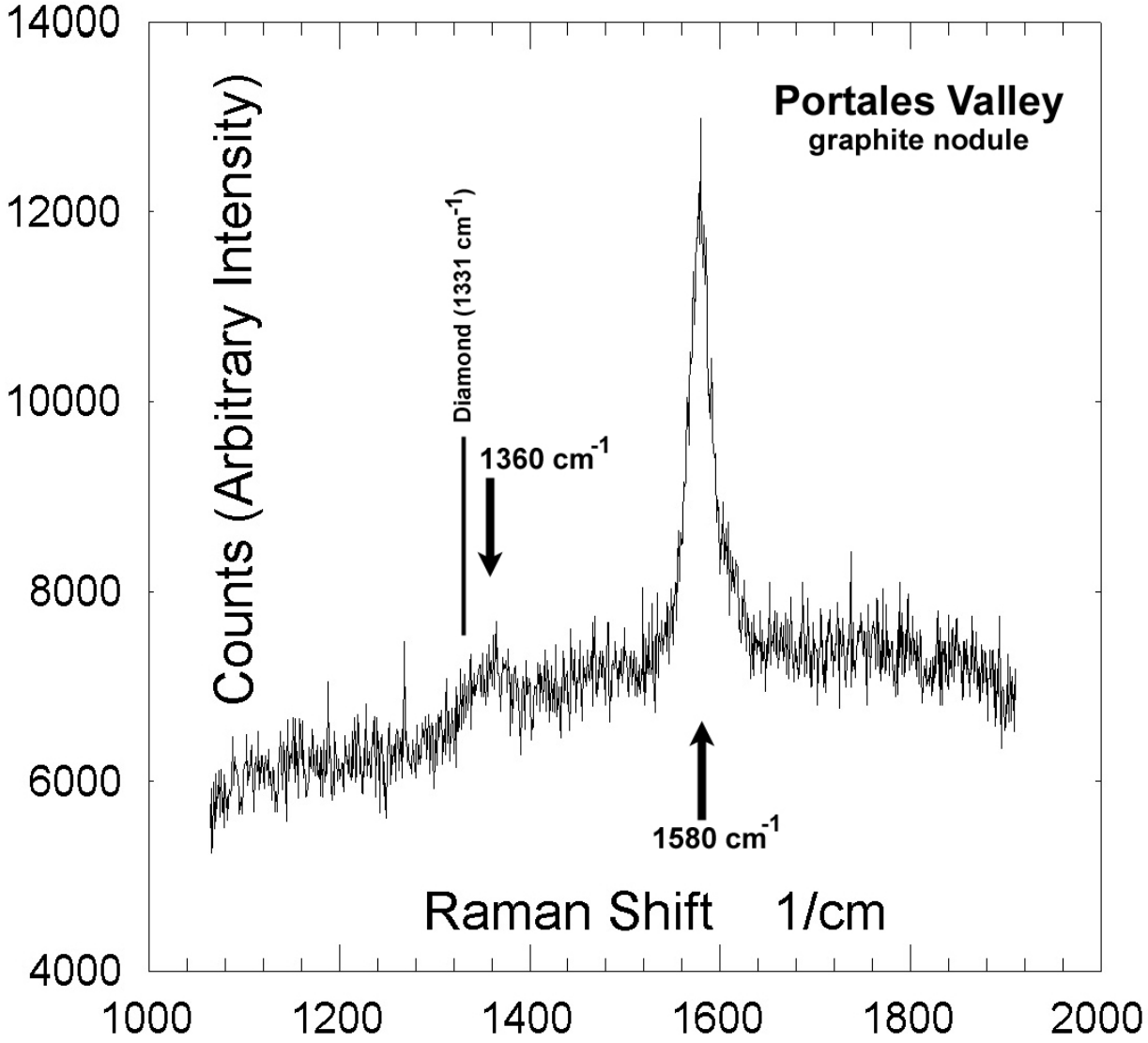

Ruzicka et al.

Fig. 6a-b

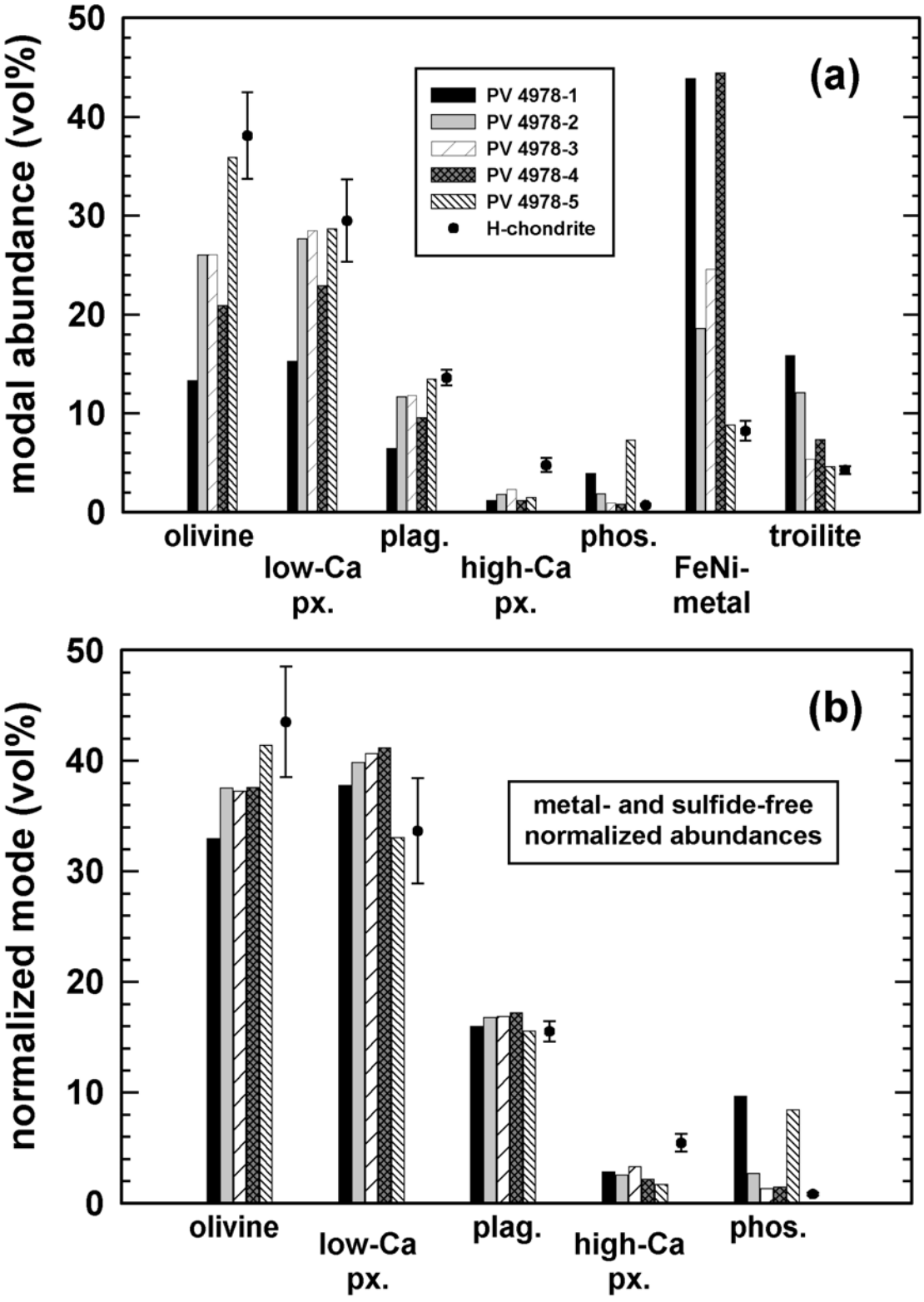

Ruzicka et al.

Fig . 6c

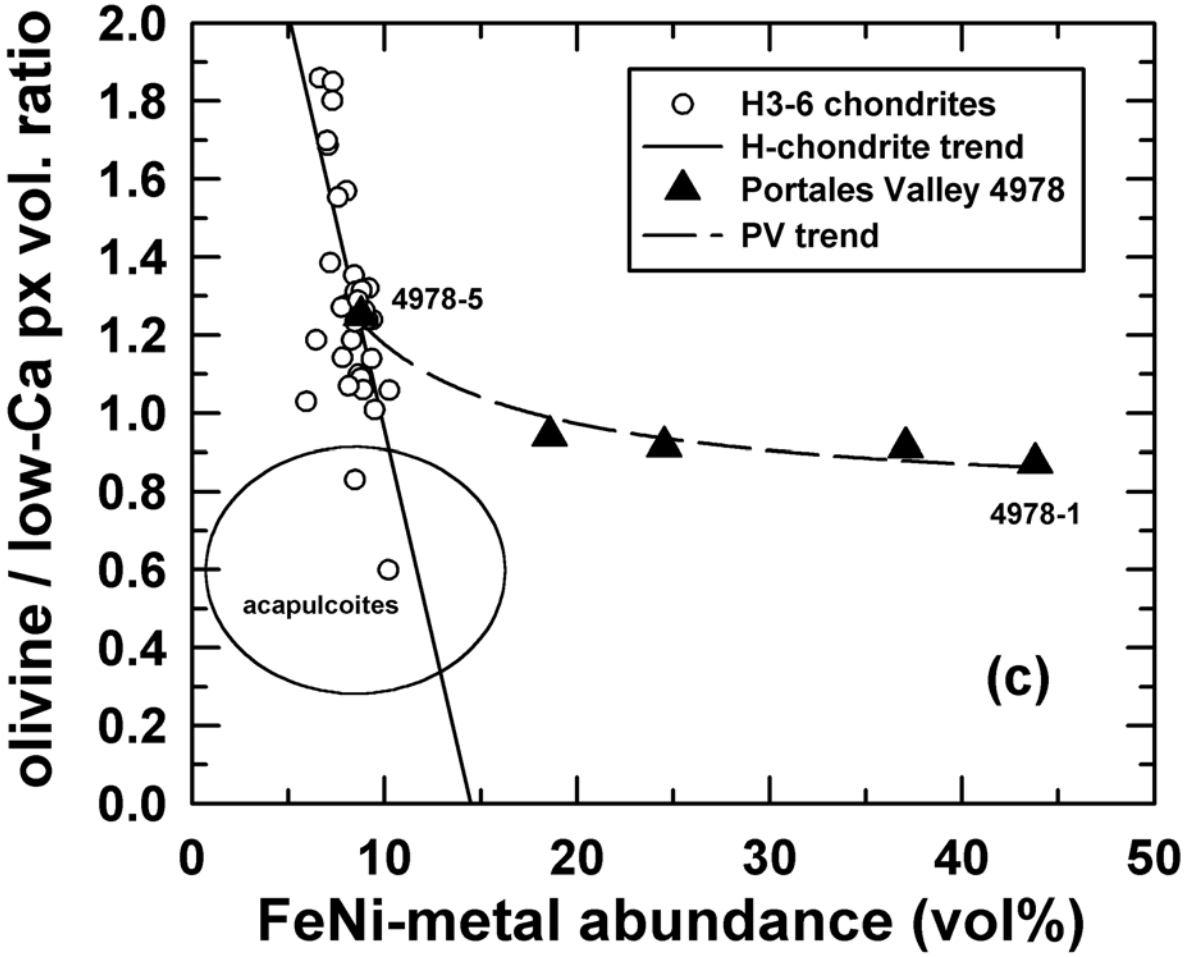

Ruzicka et al.

Fig. 7

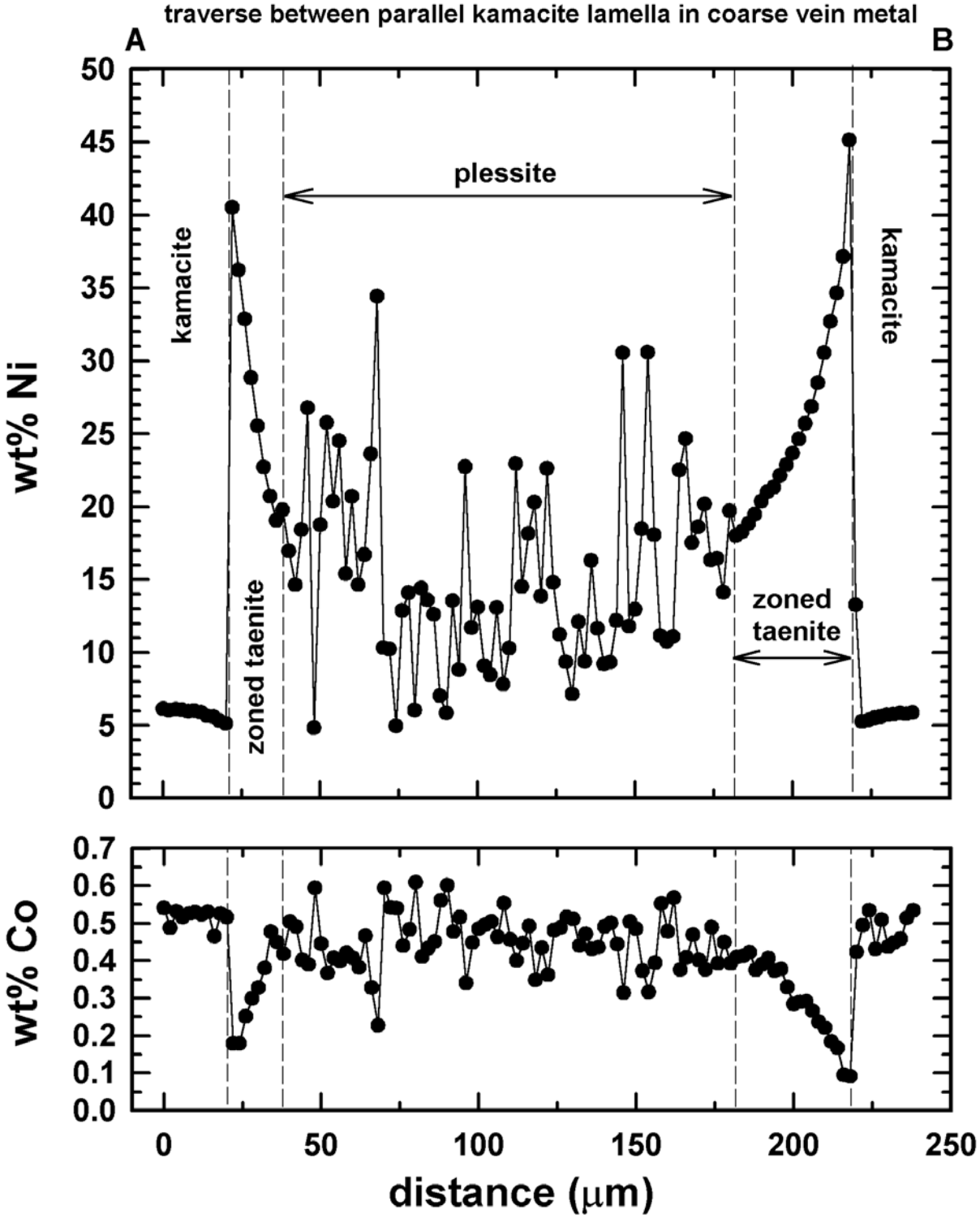

Ruzicka et al.

Fig. 8

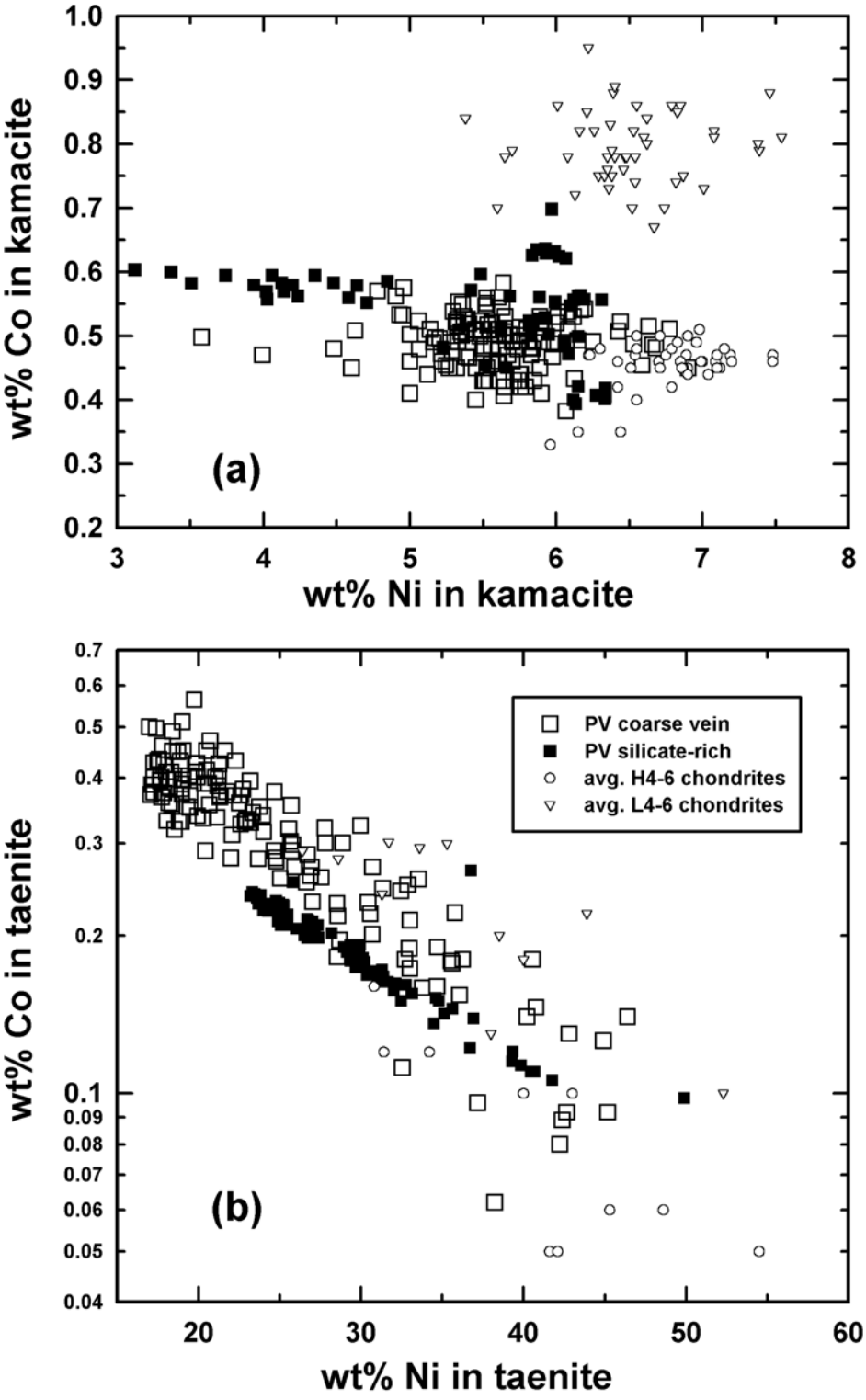

Ruzicka et al.

Fig. 9

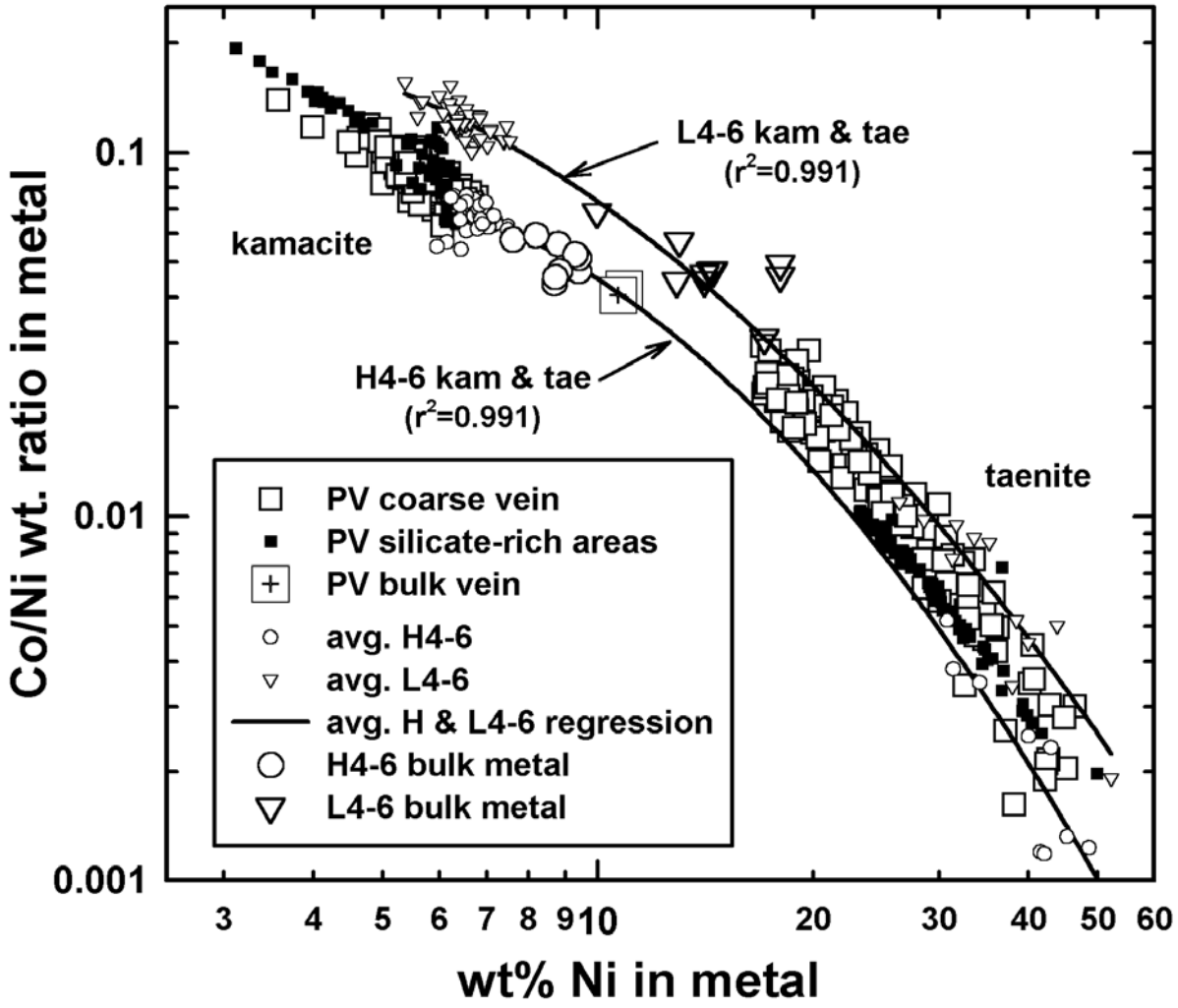

Ruzicka et al.

Fig . 10a-b

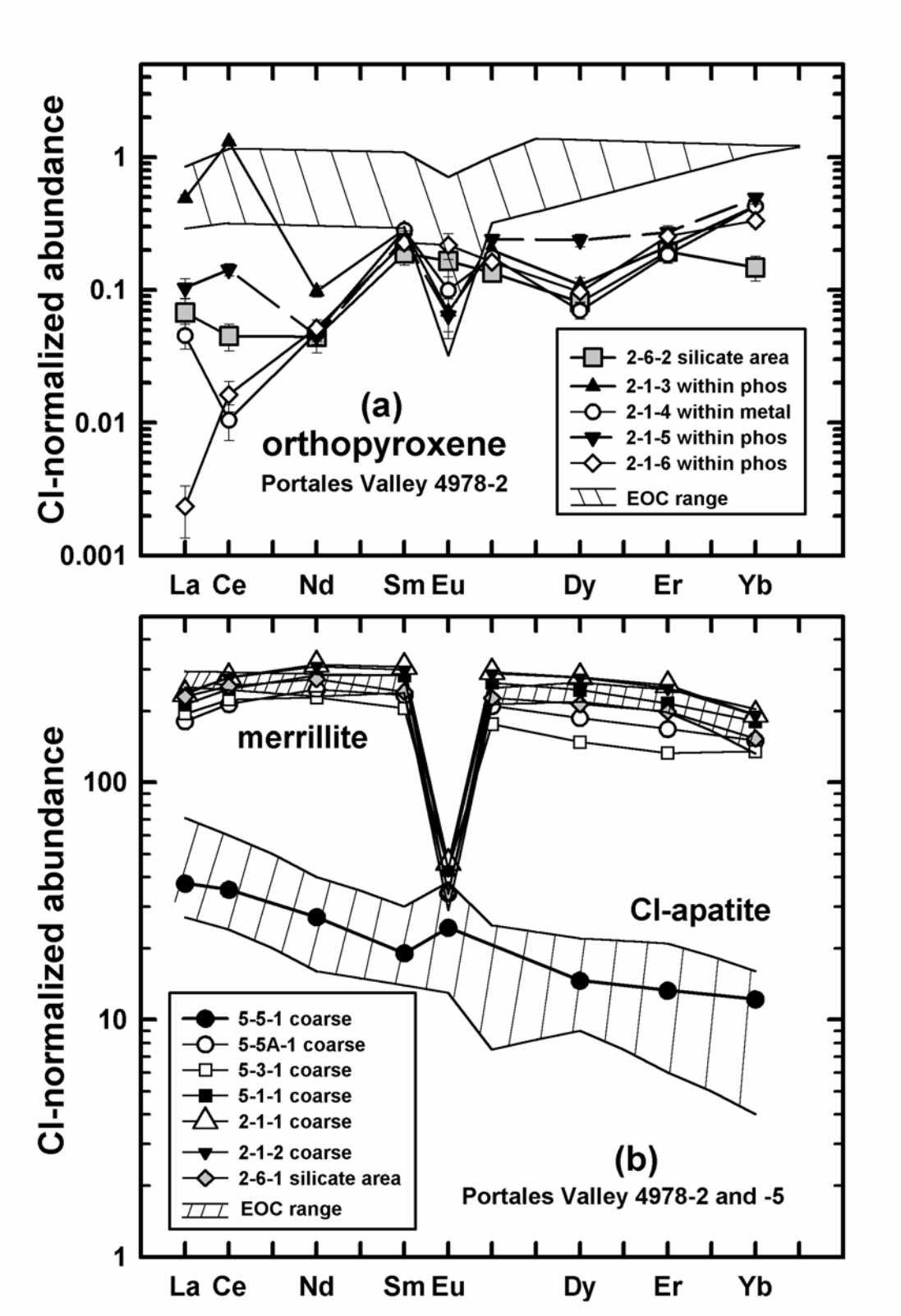

Ruzicka et al.

Fig. 11a

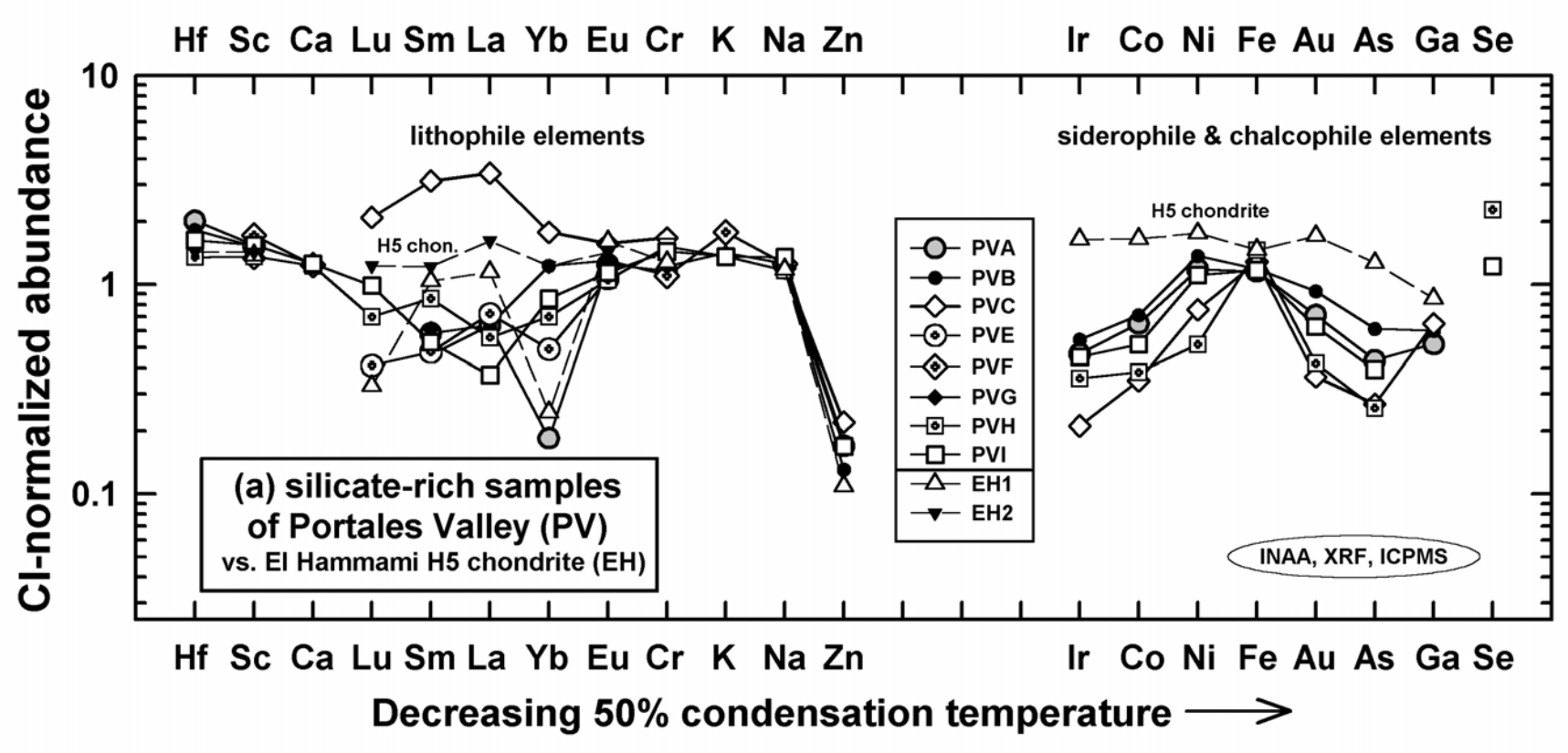

Ruzicka et al.

Fig. 11b

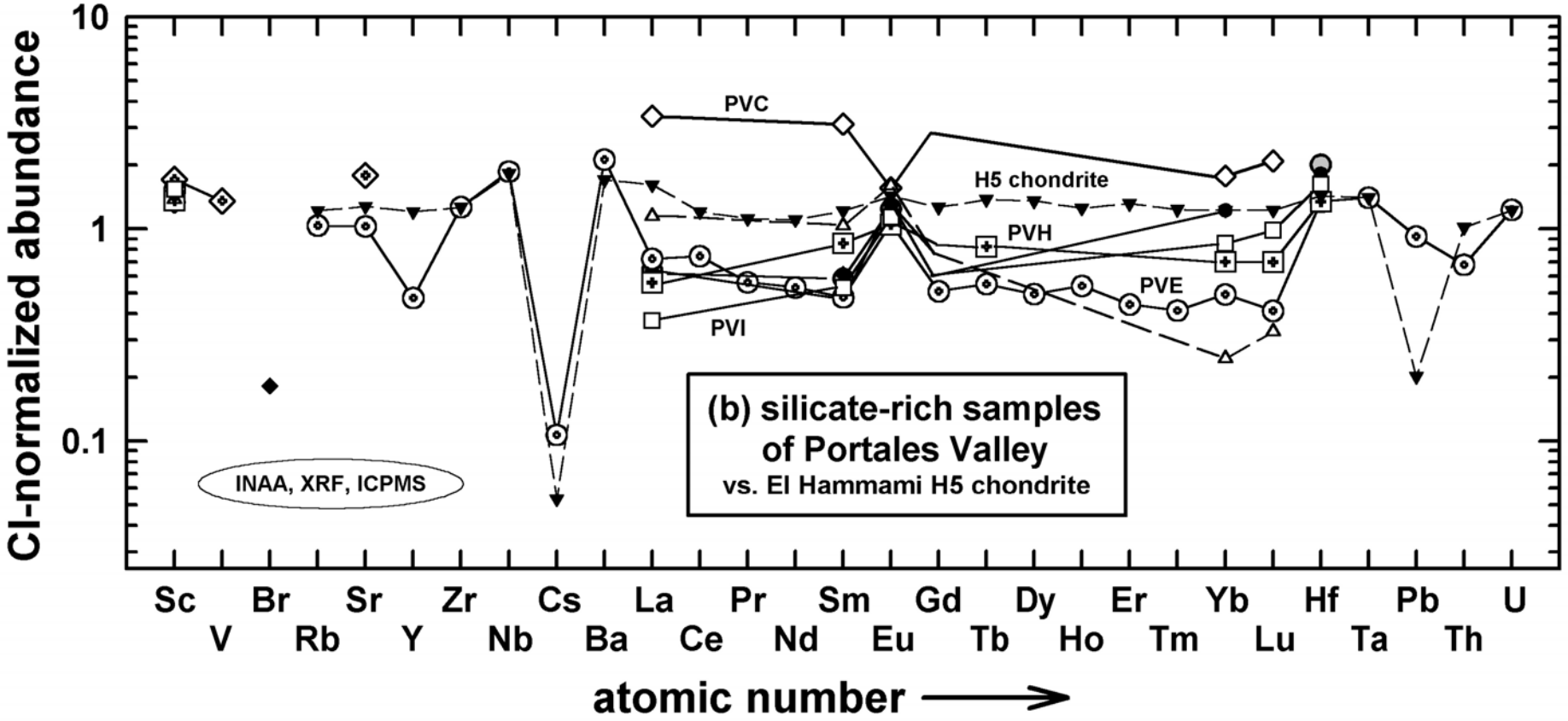

Ruzicka et al.

Fig. 11c

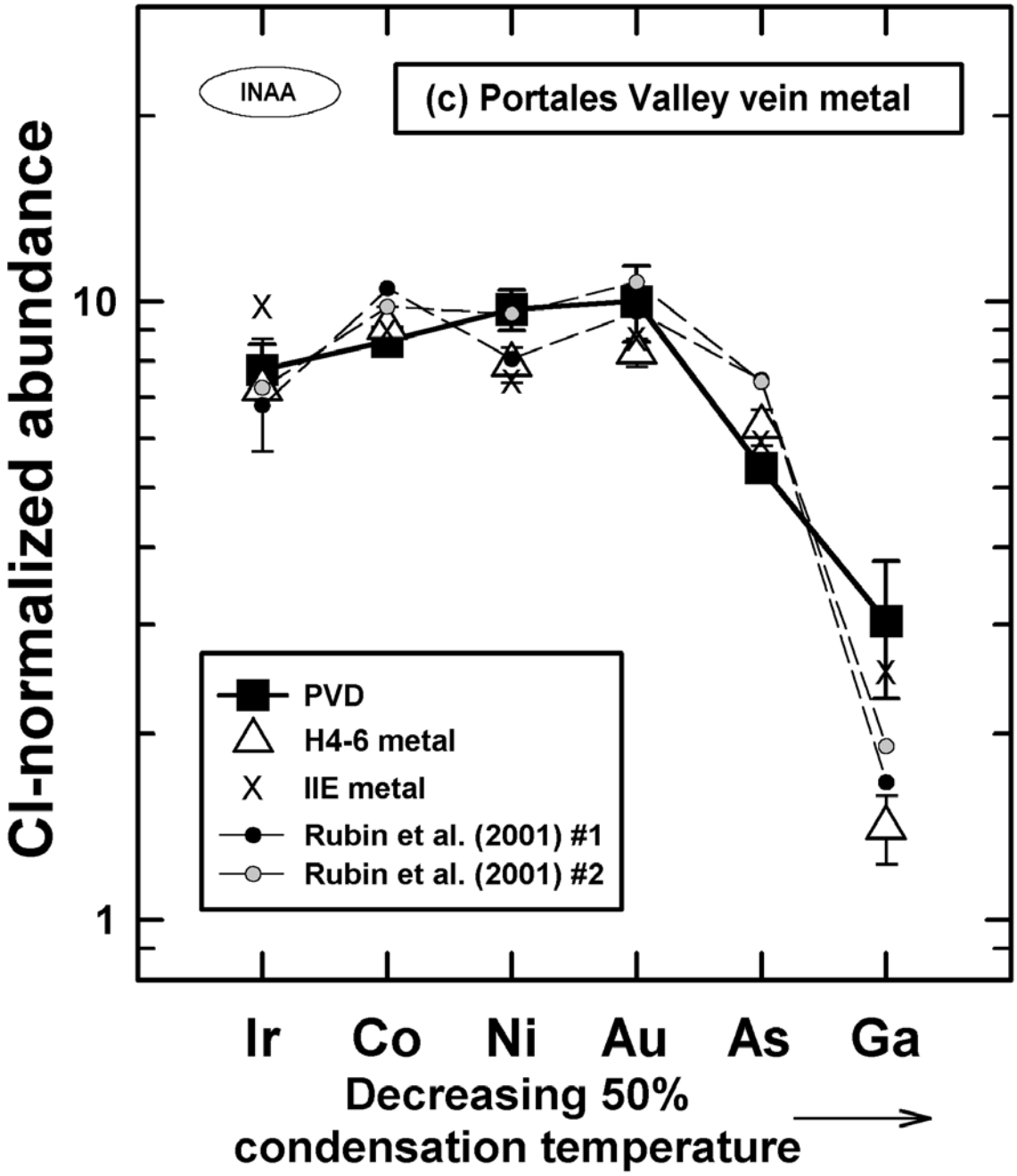

Ruzicka et al.

Fig. 12

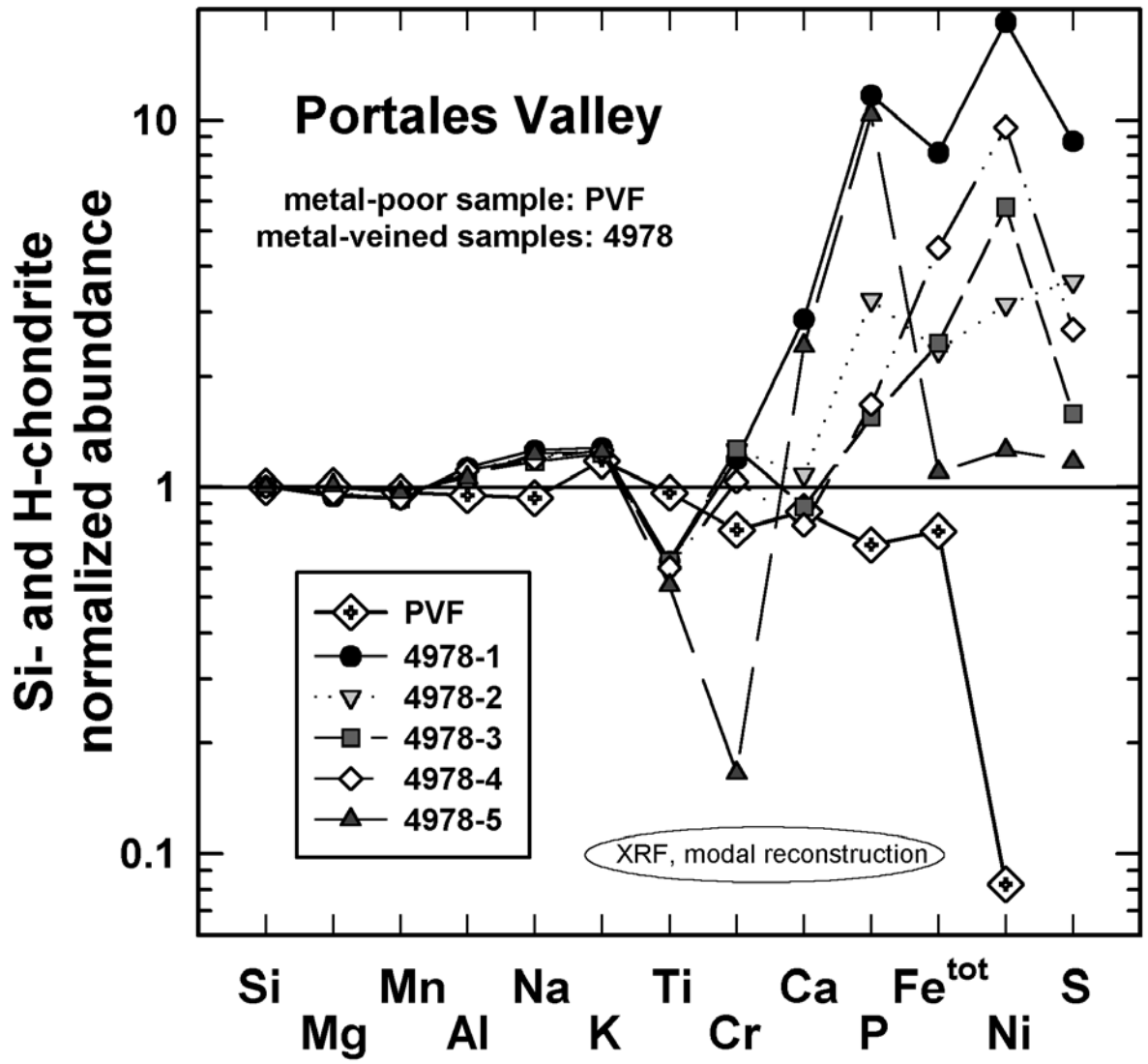

Ruzicka et al.

Fig. 13

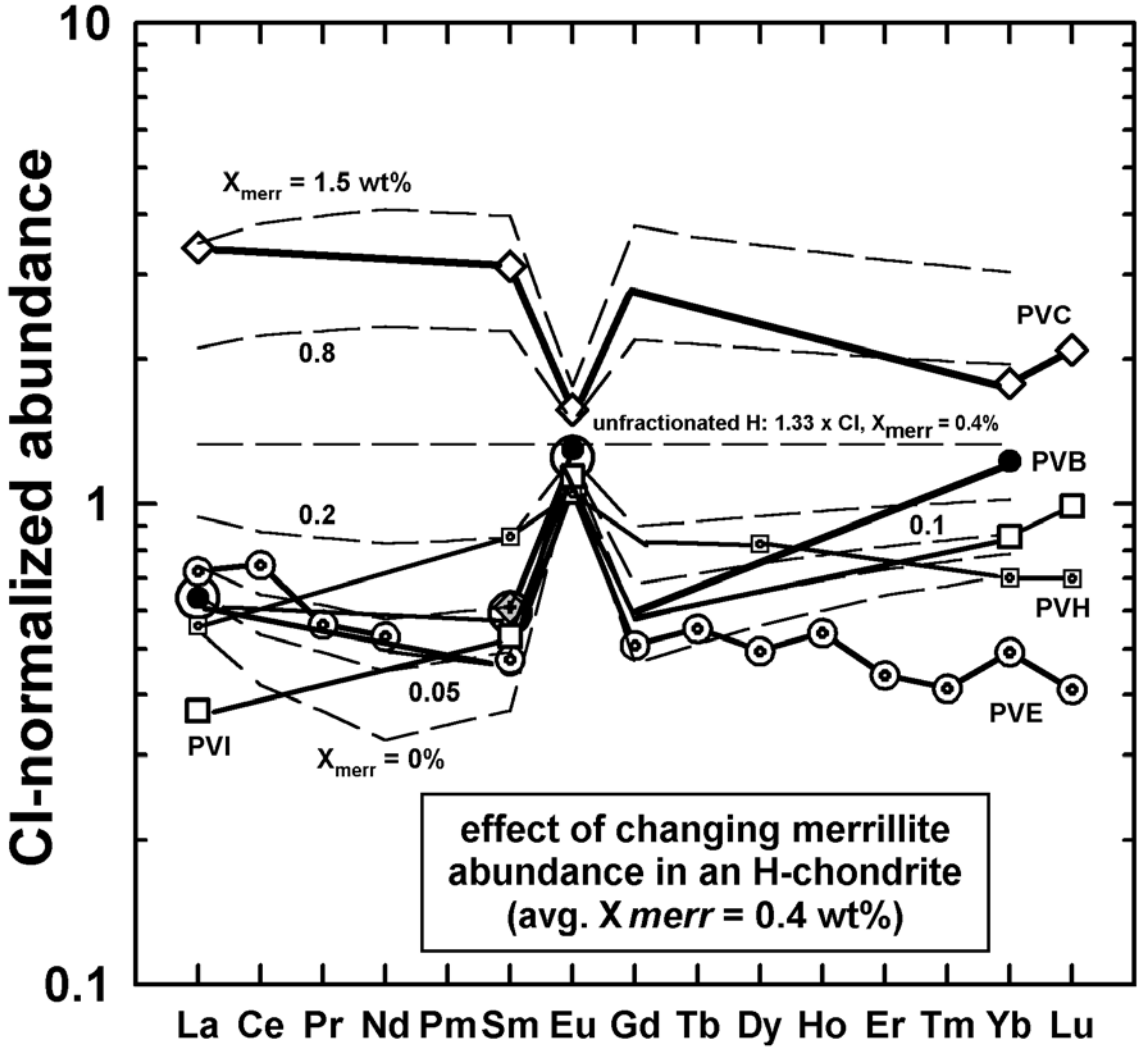

Ruzicka et al.

Fig. 14

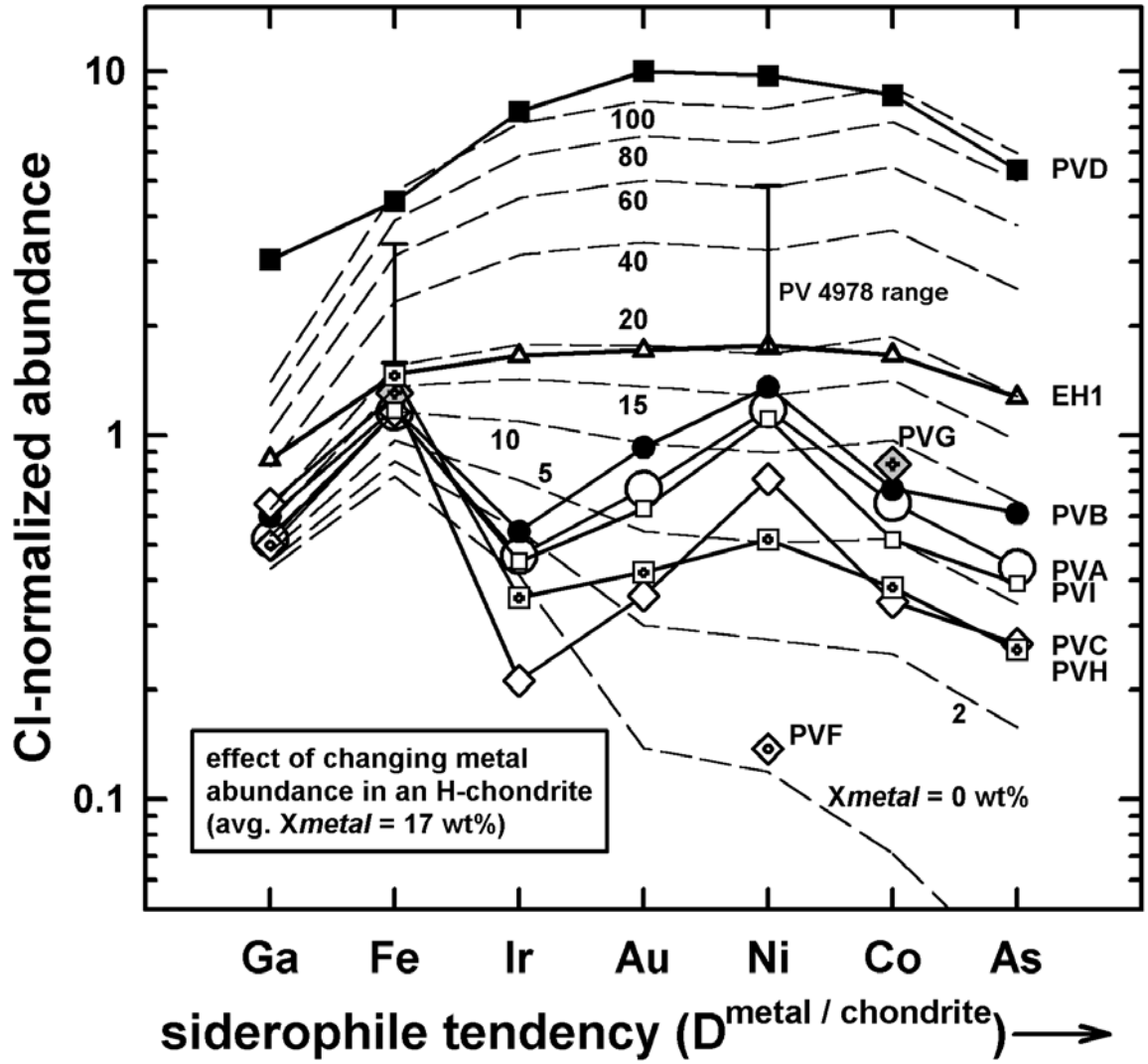

Ruzicka et al.

Fig . 15a-b

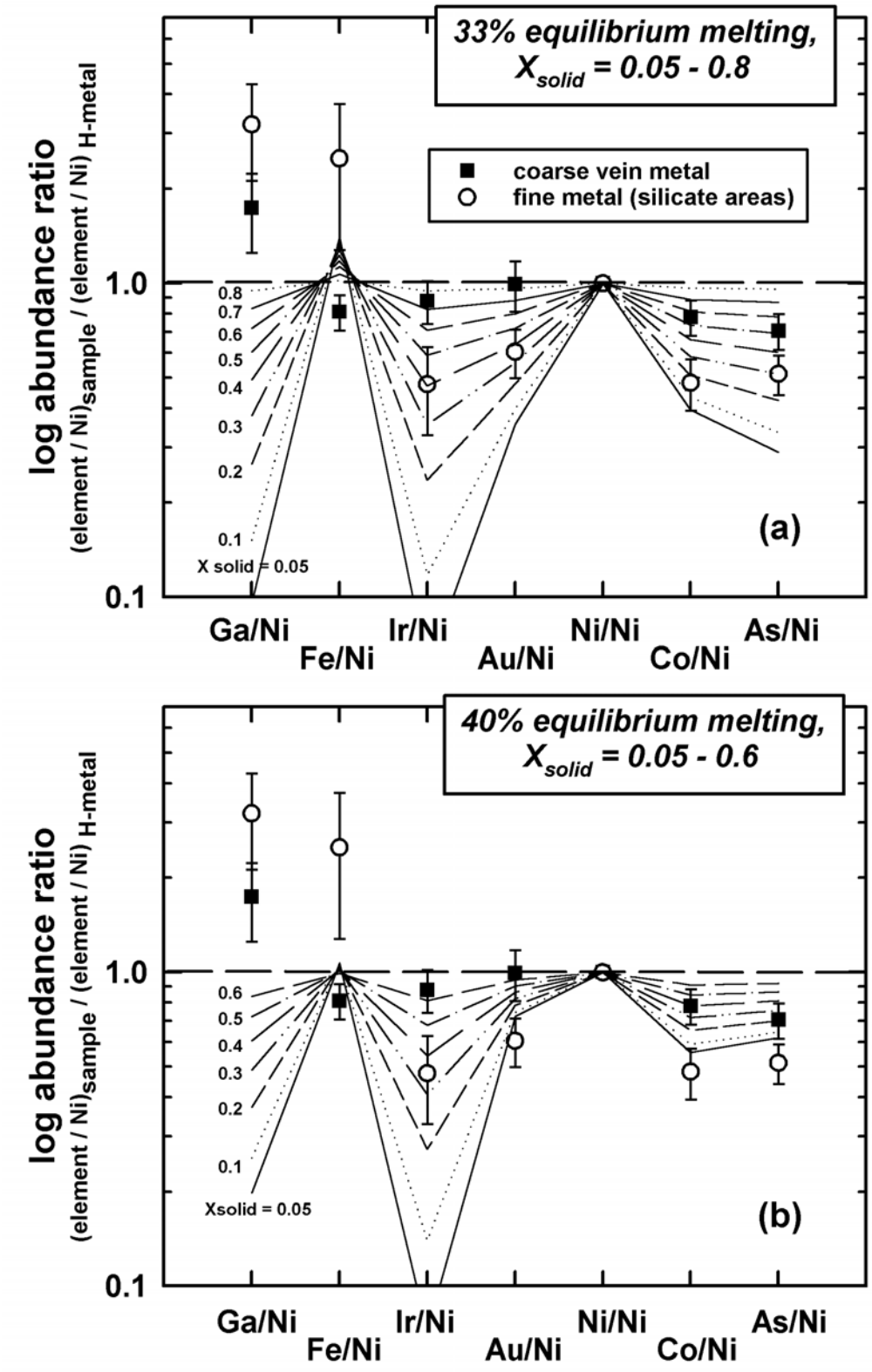

Ruzicka et al.

Fig. 15c

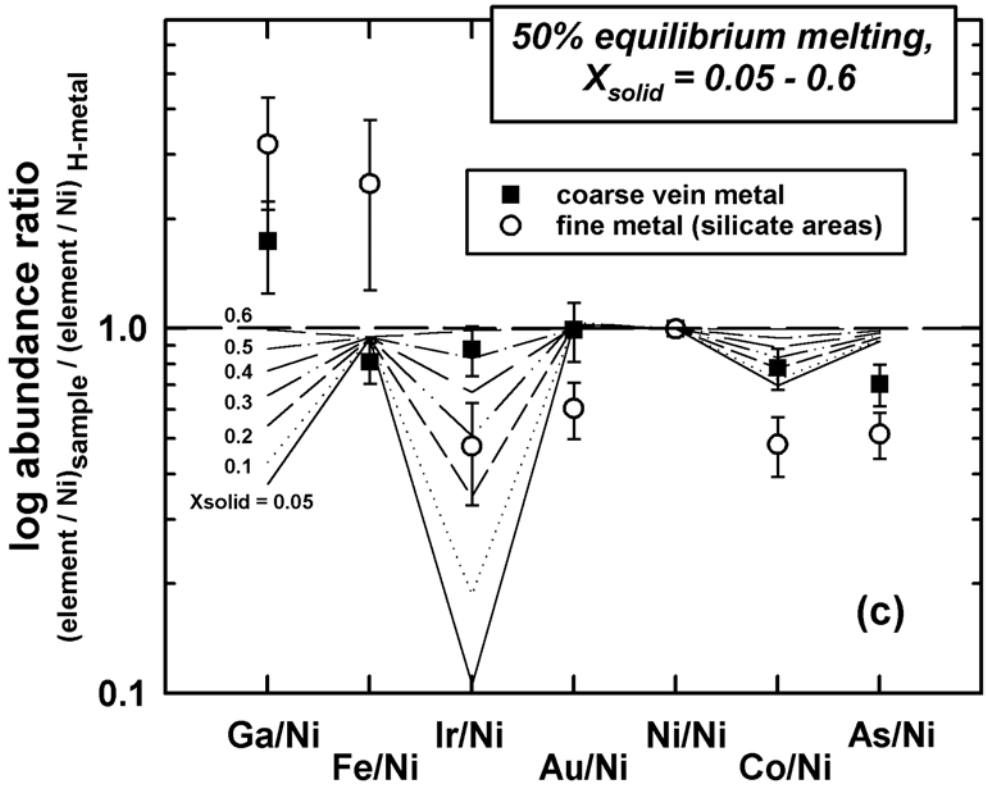

Ruzicka et al.

Fig. 16

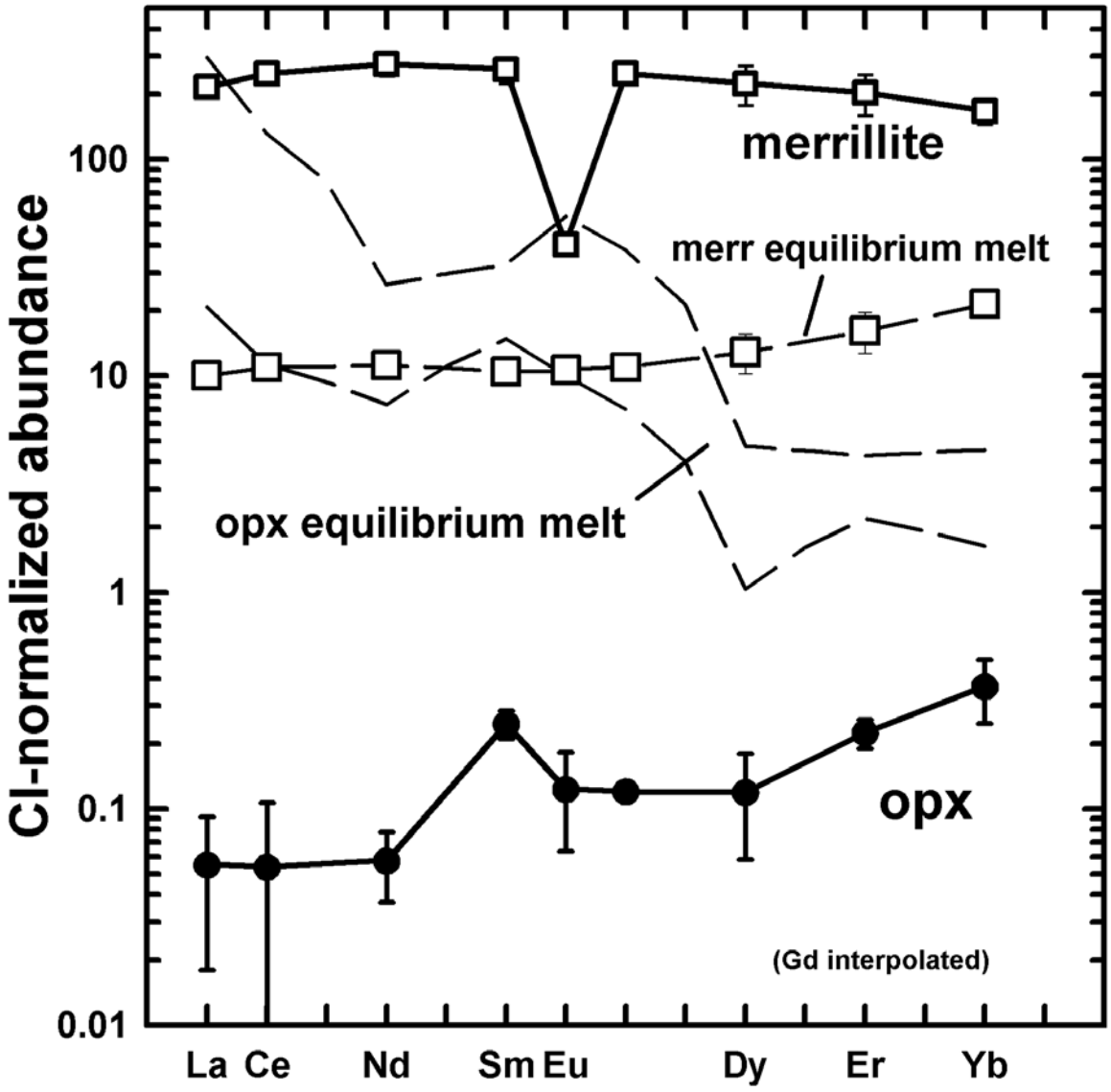

Ruzicka et al.

Fig. 17

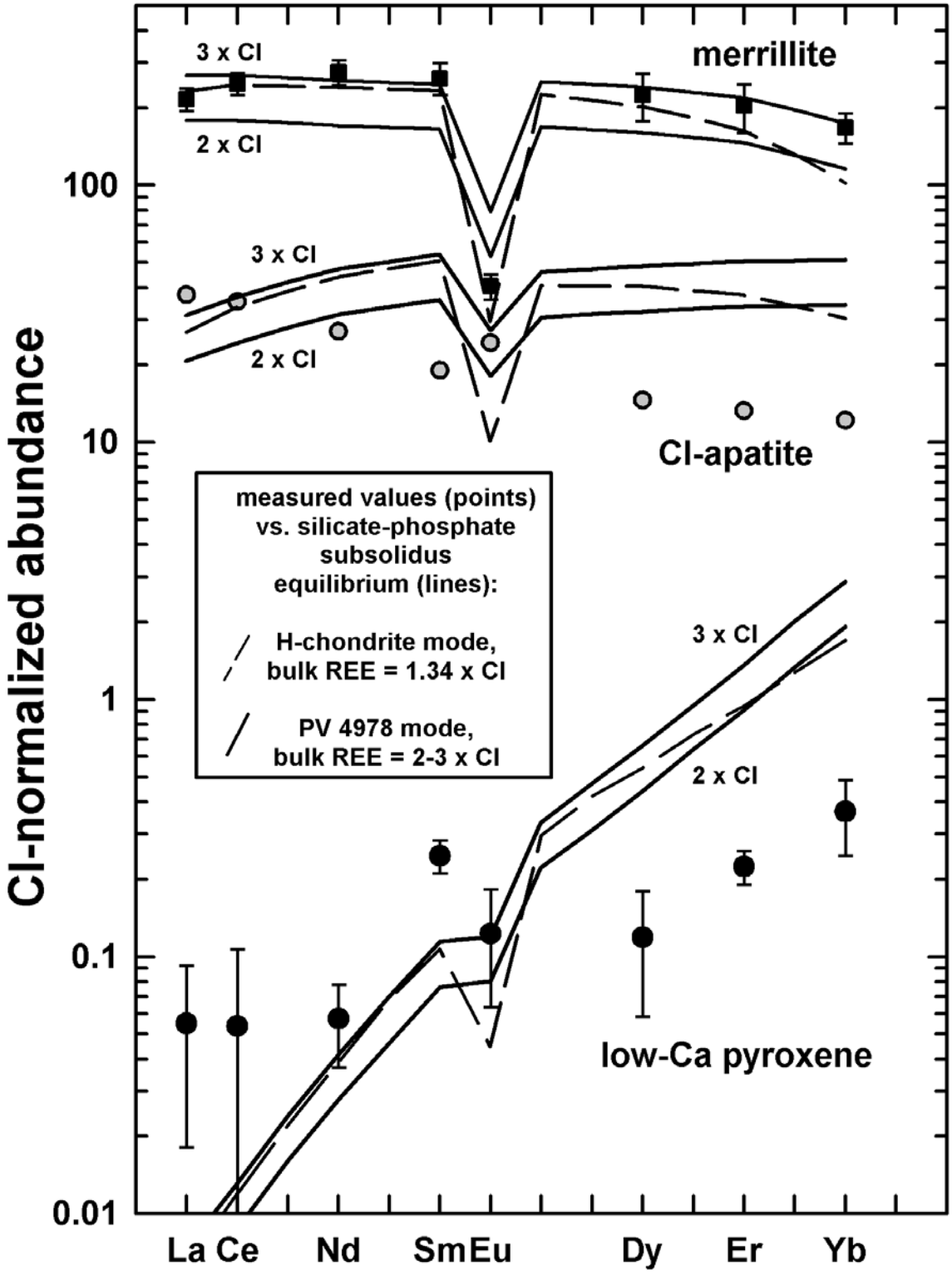

Ruzicka et al.

Fig. 18

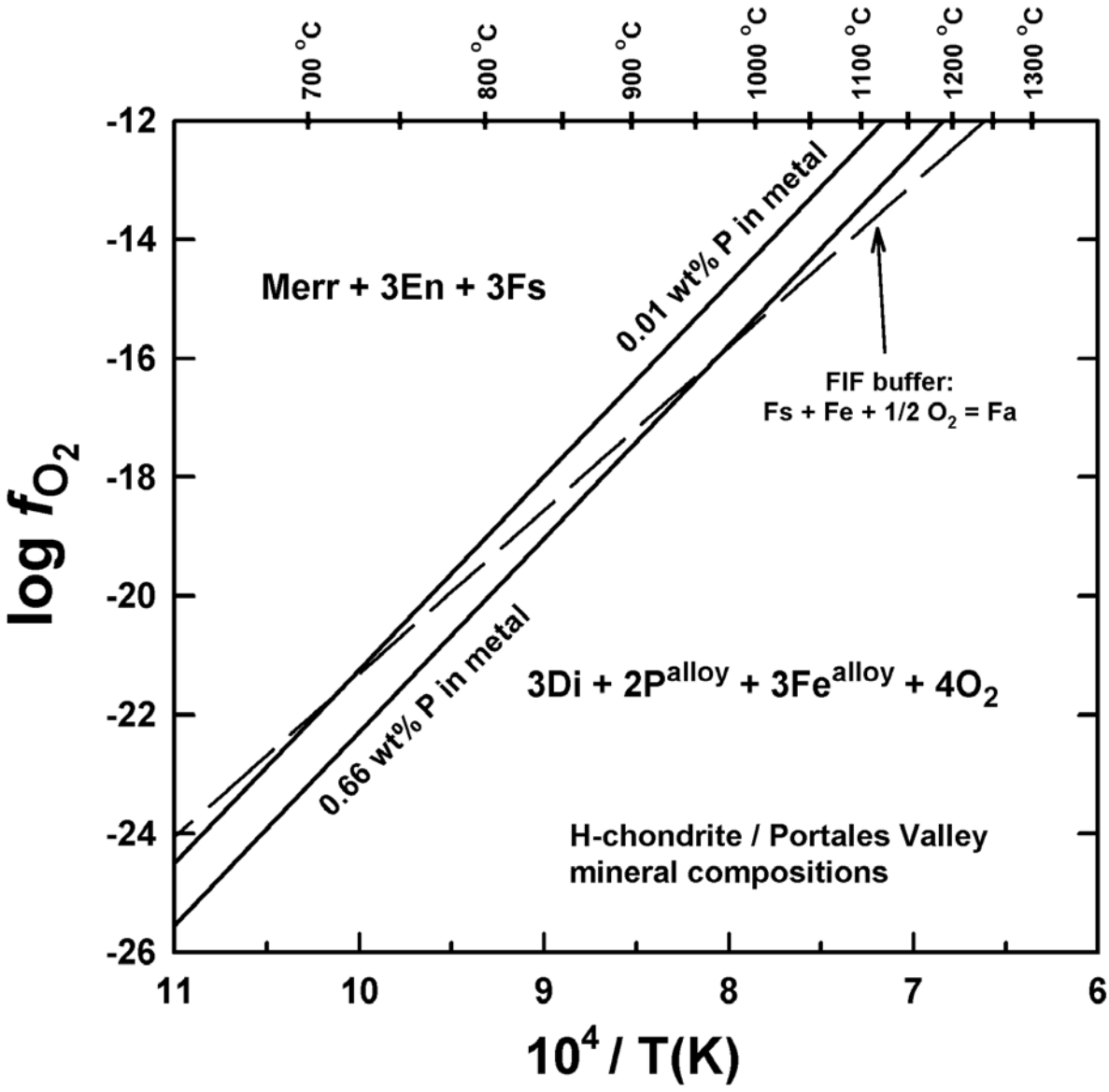

Ruzicka et al.

Fig. 19

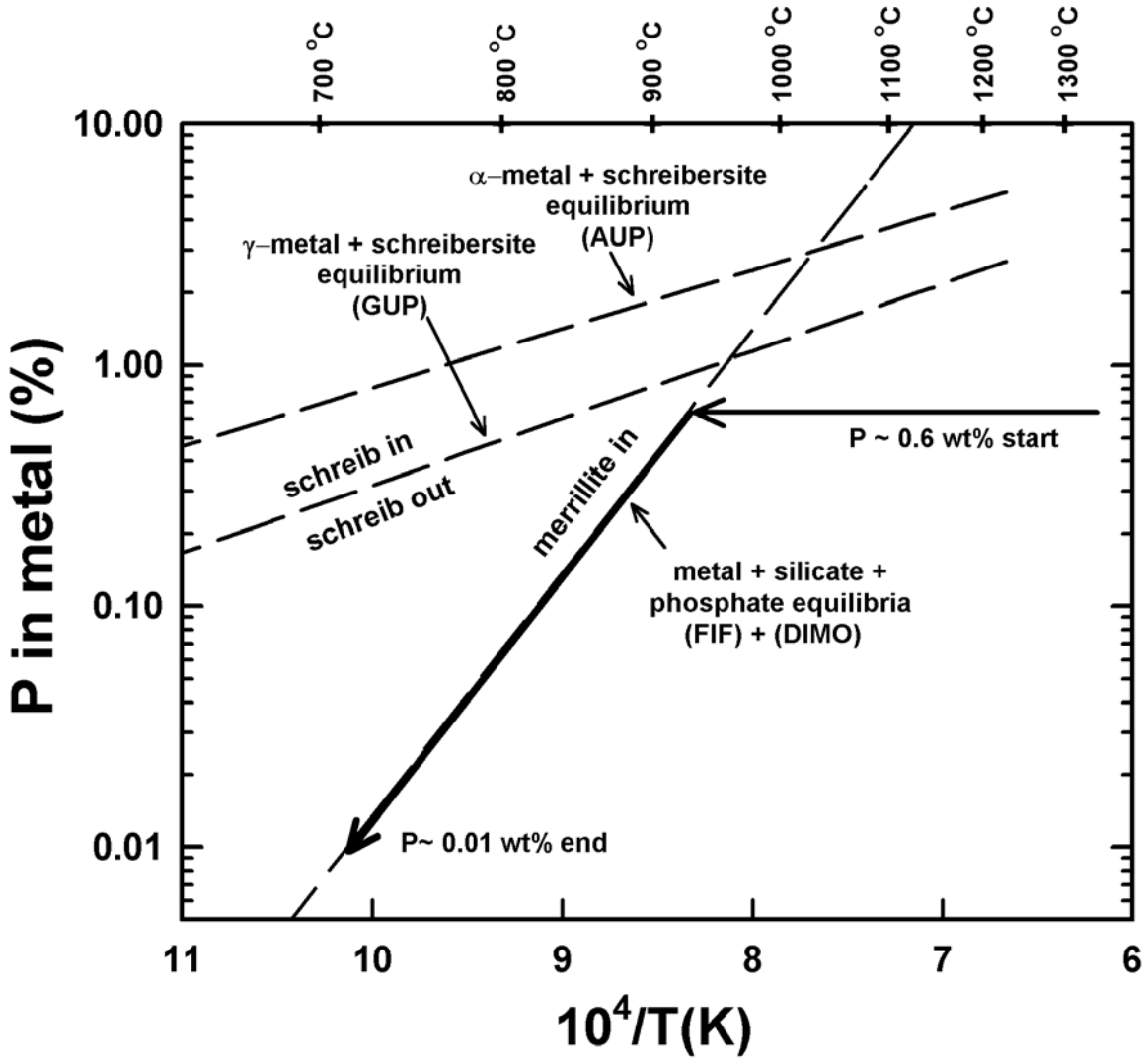

Ruzicka et al.

Fig. 20

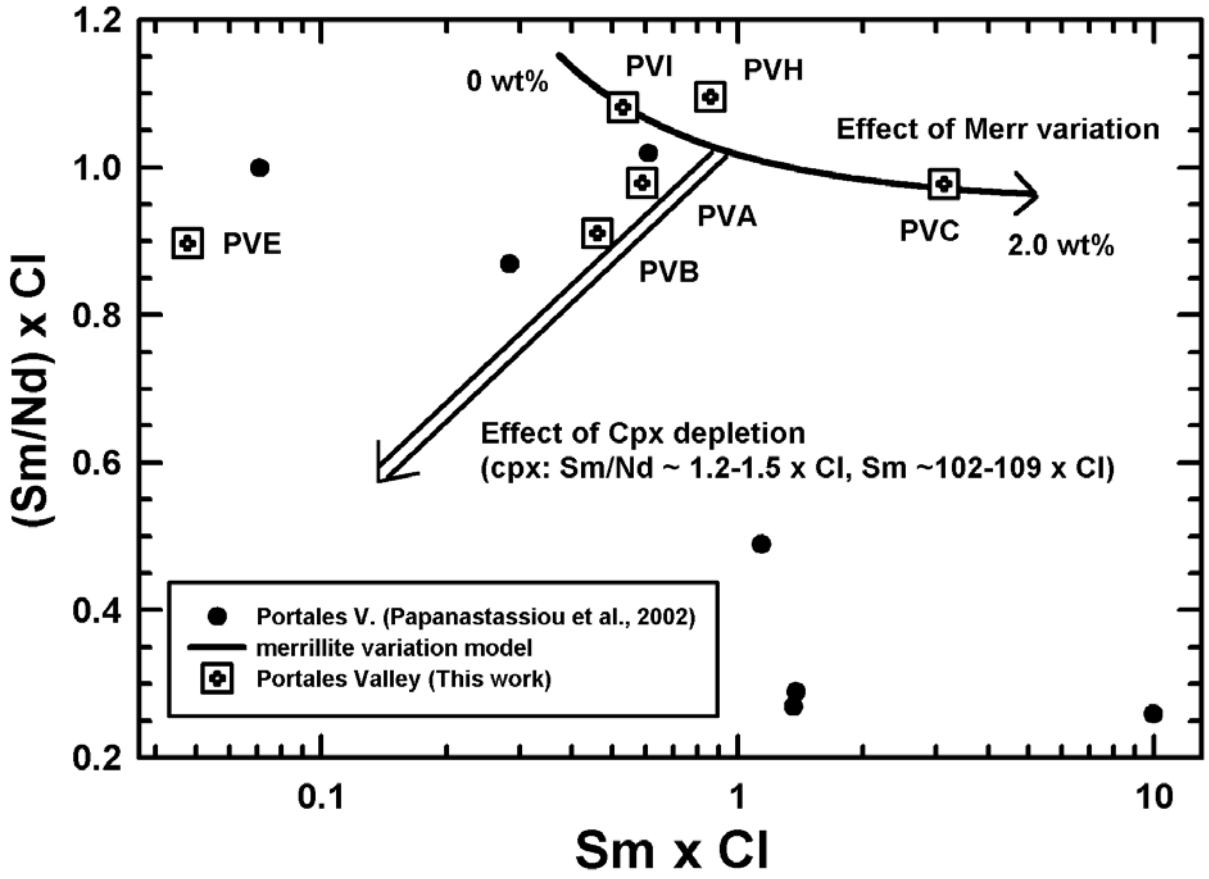

Table 1. Samples used in this study.

Sample	Mass (mg)	Source[†]	Description
Samples of Portales Valley			
4978-1	--	amnh	~1.7 cm wide, veined, polished thin-section used for petrography and x-ray mapping.
4978-2	--	amnh	~1.7 cm wide, veined, polished thin-section used for petrography, x-ray mapping, EMP & SIMS analyses.
4978-3	--	amnh	~1.7 cm wide, veined, polished section used for petrography & x-ray mapping.
4978-4	--	amnh	~1.7 cm wide, veined, polished section used for petrography & x-ray mapping.
4978-5	--	amnh	~2 cm wide, veined, polished section used for petrography, x-ray mapping, EMP & SIMS analyses.
0056-3	--	cml	~4 x 2 cm wide polished thin-section of silicate-rich portion used for petrography & EMP analyses.
M-1	–	rh	Polished section of silicate fragments, used for EMP analyses.
K-2	--	sml	~21 x 11 cm wide, veined, polished slab used for petrography & Raman analysis of graphite.
K-5	--	sml	~16 x 13 cm wide, veined, polished slab used for petrography and XRD analysis of graphite.
PVA	666	sml	Silicate-rich powder from Aliquot A*, analyzed at OSU with INAA.
PVB	866	sml	Silicate-rich powder from Aliquot A*, analyzed at OSU with INAA.
PVC	552	sml	Silicate-rich powder from Aliquot B[‡], analyzed at OSU with INAA.
PVD	166	sml	Metal fragments (Aliquot C [§]), analyzed at OSU with INAA.
PVE	212	sml	Silicate-rich powder from Aliquot A*, analyzed at WSU with ICPMS.
PVF	2017	sml	Silicate-rich powder from Aliquot A*, analyzed at WSU with XRF.
PVG	293	sml	Silicate-rich powder from Aliquot A*, analyzed at PSU with INAA.
PVH	73	rh	Silicate-rich powder of initially veined sample from Aliquot D¶, analyzed at JSC with INAA.
PVI	64	db	Silicate-rich fragment from Aliquot E i , analyzed at JSC with INAA.
Samples of El Hammami (H5) chondrite			
EH1	777	et	Powder of unweathered material, analyzed at OSU with INAA.
EH2	430	et	Powder of unweathered material, analyzed at WSU with ICPMS.

[†] Source code: amnh = American Museum of Natural History; cml = Cascadia Meteorite Laboratory, section donated by Marvin Killgore; sml = Southwest Meteorite Laboratory, Marvin Killgore; et = Edwin Thompson, sample donated by Timothy Gutschow and Dick Pugh; rh = Robert A. Haag via E.K. Gibson; db = Don Bogard. *Aliquot A = 3 fragments and dust weighing a combined 5.719 g. [‡]Aliquot B = 1.72-g fragment observed to contain ~5 x 2 mm diameter grain of phosphate. [§]Aliquot C = 2 pieces visually estimated to contain $99% metal, obtained by cutting single 1.076-g coarse-metal-rich fragment. ¶ Aliquot D = 1.1 g sample that had been handpicked to remove coarser metal and fusion crust; observed to contain a yellowish opaque mineral, probably troilite. i Aliquot E = portion of ~250 mg sample of coarsely crushed material that was prepared by D.D. Bogard for cosmogenic analyses.

Table 2. Physical dimensions of a large graphite nodule exposed in successive cut surfaces of five parallel-cut large slabs of Portales Valley.

Slab	Surface	Nodule Maximum Dimension (cm)	Nodule Perpendicular Dimension (cm)
K-1	1	not exposed	not exposed
K-1	2	0.77	0.71
K-2	3*	0.94	0.84
K-2	4	1.44	1.20
K-3	5	0.83	0.57
K-3	6	1.85	0.88
K-4	7	1.91	1.17
K-4	8	2.00	0.69
K-5	9 §	1.89	0.44
K-5	10 †	0.30, 0.18	0.18, 0.10

Thickness of slabs: K-1 = 4.4 mm, K-2 = 3.6 mm, K-3 = 3.9 mm, K-4 = 4.2 mm, K-5 = 4.0 mm. *Nodule analyzed with Raman spectroscopy. §Nodule analyzed with x-ray diffraction. †Nodule in two segments.

Table 3. Modal composition of various sections of Portales Valley AMNH 4978 determined by x-ray mapping, compared to average H-chondrite.

	4978-1 §	4978-2 §	4978-3 §	4978-4 §	4978-5 §	4978 average	avg. H-chondrite*
vol%							
olivine	13.3	26.0	26.1	20.9	35.9	24.4	38.09
low-Ca pyroxene	15.2	27.6	28.5	22.9	28.6	24.6	29.47
high-Ca pyroxene	1.13	1.76	2.29	1.18	1.44	1.56	4.76
plagioclase	6.45	11.6	11.8	9.56	13.5	10.6	13.59
Cl-apatite	3.10	0.15	0.17	0.02	5.10	1.71	--
merrillite	0.80	1.69	0.75	0.77	2.17	1.24	--
chromite	0.24	0.48	0.49	0.32	n.d.	0.31	0.57
ilmenite	n.d.	n.d.	n.d.	n.d.	n.d.	0.00	0.18
troilite	15.8	12.1	5.40	7.30	4.55	9.03	4.25
low-Ni metal	25.6	14.1	13.5	23.8	6.75	16.7	--
high-Ni metal	18.2	4.50	11.1	13.3	2.05	9.83	--
total FeNi-metal	43.8	18.6	24.6	37.1	8.80	26.5	8.21
total phosphate	3.90	1.84	0.92	0.79	7.27	2.95	0.71
area mapped (mm^2)	~210	~215	~160	~176	~220		
no. of points (x 10^6)	7.73	7.93	5.90	6.49	8.13		
classified points (%)	83.9	89.4	89.0	91.0	91.3		

§ Data normalized to 100% before rounding. n.d. = not detected. * Normative composition of average water-free, minimally weathered H-chondrite (calculated from Jarosewich, 1990).

Table 4. Mean composition of silicate minerals in Portales Valley (sections 4978-2, 4978-5, M-1), determined by electron microprobe analysis. Numbers in parentheses refer to standard deviation of the mean; N = number of analyses; n.a. = not analyzed.

	olivine	low-Ca pyroxene	high-Ca pyroxene	plagioclase
wt%				
SiO_2	39.0 (0.15)	56.0 (0.3)	53.7 (0.4)	65.3 (0.2)
TiO_2	0.01 (0.01)	0.20 (0.03)	0.42 (0.09)	n.a.
Al_2O_3	0.01 (0.01)	0.22 (0.03)	0.57 (0.09)	21.8 (0.1)
Cr_2O_3	0.01 (0.01)	0.15 (0.03)	0.71 (0.19)	n.a.
FeO	18.3 (0.3)	11.5 (0.1)	4.26 (0.09)	0.39* (0.11)
MnO	0.46 (0.02)	0.48 (0.02)	0.21 (0.01)	n.a.
MgO	42.1 (0.6)	30.5 (0.3)	17.1 (0.2)	0.01 (0.01)
CaO	0.02 (0.2)	0.87 (0.20)	22.0 (0.4)	2.69 (0.06)
NiO	0.01 (0.0)	0.01 (0.02)	0.01 (0.00)	n.a.
Na_2O	<0.01	0.02 (0.01)	0.49 (0.08)	9.42 (0.13)
K_2O	n.a.	n.a.	n.a.	1.16 (0.16)
	--------	--------	--------	--------
	99.8	99.9	99.5	100.7
mol%				
Fa	19.6 (0.5)	--	–	--
Wo	--	1.6 (0.4)	44.8 (0.4)	--
En	--	81.2 (0.3)	48.5 (0.3)	--
Fs	--	17.2 (0.2)	6.8 (0.2)	--
An	--	--	–	12.7 (0.3)
Ab	--	--	--	80.7 (0.9)
Or	--	--	--	6.6 (0.9)
N	39	41	13	28

atomic formula units

olivine: $(Mg_{1.605}Fe_{0.391}Ca_{0.001}Mn_{0.010})Si_{0.996}O_4$

low-Ca pyroxene: $(Mg_{1.612}Fe_{0.341}Ca_{0.033}Mn_{0.014}Na_{0.001}Cr_{0.004}Ti_{0.005})(Si_{1.984}Al_{0.009})O_6$

high-Ca pyroxene: $(Mg_{0.938}Fe_{0.131}Ca_{0.867}Mn_{0.007}Na_{0.035}Cr_{0.021}Ti_{0.012})(Si_{1.974}Al_{0.024})O_6$

plagioclase: $(Na_{0.802}Ca_{0.127}K_{0.065}Fe_{0.014})(Al_{1.128}Si_{2.866})O_8$

* Probable overestimate of true value, based on suspected secondary fluorescence from adjacent mafic phases.

Fa = 100 Fe/(Fe+Mg); Wo = 100 Ca/(Ca+Mg+Fe); En = 100 Mg/(Ca+Mg+Fe); Fs = 100 Fe/(Ca+Mg+Fe); An = 100 Ca/(Ca+Na+K); Ab = 100 Na/(Ca+Na+K); Or = 100 K/(Ca+Na+K).

Table 5. Mean composition of phosphate minerals in Portales Valley (sections 4978-2, 4978-5), determined by electron microprobe analysis. Numbers in parentheses refer to standard deviation of the mean; N = number of analyses.

	Cl-apatite	merrillite
wt%		
SiO_2	0.10 (0.03)	0.01 (0.01)
FeO	0.15 (0.11)	0.38 (0.08)
MnO	0.06 (0.03)	0.03 (0.02)
MgO	0.04 (0.01)	3.59 (0.05)
CaO	53.4 (0.3)	47.0 (0.2)
Na_2O	0.40 (0.05)	2.69 (0.05)
P_2O_5	40.8 (0.4)	46.0 (0.4)
Cl	5.66 (0.15)	0.01 (0.01)
	--------	--------
	100.7	99.6
N	13	18

atomic formula units

Cl-apatite: $(Ca_{4.972}Fe_{0.011}Mg_{0.005}Mn_{0.004}Na_{0.068}Si_{0.009})(PO_4)_3Cl_{0.832}(OH,F)_{0.168}$

merrillite: $(Ca_{2.586}Fe_{0.017}Mg_{0.276}Mn_{0.001}Na_{0.269})(PO_4)_2$

Table 6. Mean composition of FeNi-metal and troilite in Portales Valley, determined by electron microprobe analysis. Numbers in parentheses refer to the standard deviation of the mean; N = number of analyses; n.a. = not analyzed.

	Silicate-rich areas (0056-3, M-1)			Coarse veins with Widmanstätten texture (4978-5)				
	kamacite	taenite	troilite	kamacite	kamacite margins	zoned taenite	plessite	bulk
	1	2	3	4	5	6	7	8
wt%								
Fe	93.5 (0.8)	71.1 (4.6)	64.0 (0.1)	93.0 (0.6)	93.9 (0.6)	73.4 (7.8)	84.2 (5.4)	87.7 (6.9)
Co	0.55 (0.07)	0.19 (0.03)	<0.01	0.49 (0.04)	0.50 (0.05)	0.32 (0.10)	0.44 (0.07)	0.46 (0.08)
Ni	5.29 (0.94)	28.9 (4.8)	0.01 (0.01)	5.72 (0.38)	5.08 (0.24)	25.0 (7.3)	14.8 (5.4)	10.9 (6.9)
P	0.01 (0.01)	0.01 (0.01)	<0.01	0.01 (0.01)	0.01 (0.01)	0.01 (0.01)	0.01 (0.01)	0.01 (0.01)
Cr	0.01 (0.01)	<0.01	0.01 (0.01)	<0.01	<0.01	<0.01	<0.01	<0.01
S	0.02 (0.01)	0.02 (0.02)	36.8 (0.1)	n.a.	n.a.	n.a.	n.a.	n.a.
	99.4	100.2	100.9	99.2	99.4	98.7	99.5	99.1
wt. Co/Ni	0.10	0.0066	–	0.086	0.098	0.013	0.030	0.042
N	55	91	6	109	11	141	193	50

1, 2: Grains of metal alloy, including kamacite (3.1-6.3 wt% Ni) and taenite (23.2-49.9 wt% Ni), analyzed in thin section CML 0056-3 and polished section M-1.
3: Grains analyzed in polished section M-1.
4: Kamacite lamellae and swathing kamacite in coarse-grained alloy (5.0-6.9 wt% Ni).
5: Margins of kamacite grains (lamellae and swathing kamacite) in coarse-grained alloy (4.6-5.3 wt% Ni) adjacent to zoned taenite.
6: Zoned FeNi-metal alloy (17.0-46.4 wt% Ni) adjacent to kamacite lamellae.
7: Average composition of plessite (decomposed martensite) in coarse alloy (apparent Ni content = 4.2-34.5 wt%) within largest vein in section.
8: Estimated composition of largest vein in section, based on analyses obtained in a traverse down the vein axis.

Table 7a. Trace-element composition of phosphate in Portales Valley (4978-2, 4978-5), determined by SIMS analysis. Values are given in µg/g; those in parentheses refer to the estimated precision, based on counting statistics.

Analysis*	La	Ce	Nd	Sm	Eu	Dy	Er	Yb	Comment
Cl-apatite									
5-5-1	8.81 (0.09)	21.3 (0.2)	12.3 (0.1)	2.81 (0.05)	1.37 (0.03)	3.55 (0.07)	2.11 (0.05)	1.99 (0.05)	coarse; pair 5-5A
Merrillite									
5-5A-1	42.6 (0.2)	129.4 (0.4)	111.2 (0.4)	34.3 (0.2)	1.91 (0.04)	45.5 (0.3)	26.7 (0.2)	24.4 (0.2)	coarse; pair 5-5
5-3-1	45.7 (0.2)	134.3 (0.4)	103.2 (0.4)	30.1 (0.2)	2.42 (0.05)	36.0 (0.2)	21.1 (0.2)	22.0 (0.2)	coarse
5-1-1	50.0 (0.2)	148.8 (0.4)	127.9 (0.4)	41.5 (0.2)	2.40 (0.04)	59.5 (0.3)	34.2 (0.2)	29.4 (0.2)	coarse vein
2-1-1	55.5 (0.3)	167.6 (0.6)	141.7 (0.5)	45.0 (0.3)	2.57 (0.06)	67.1 (0.4)	40.8 (0.3)	31.4 (0.3)	coarse
2-1-2	56.2 (0.3)	166.2 (0.5)	139.2 (0.5)	43.8 (0.2)	2.40 (0.05)	66.9 (0.3)	39.7 (0.3)	31.2 (0.2)	coarse
2-6-1	54.1 (0.3)	153.7 (0.6)	123.4 (0.5)	35.5 (0.3)	1.92 (0.05)	51.9 (0.3)	31.6 (0.3)	24.8 (0.2)	matrix, finer
Mean merr.	50.7	150.0	124.4	38.4	2.27	54.5	32.3	27.2	

Table 7b. Trace-element composition of orthopyroxene in Portales Valley (4978-2), determined by SIMS analysis. Values are given in ng/g; those in parentheses refer to the estimated precision, based on counting statistics.

Analysis*	La	Ce	Nd	Sm	Eu	Dy	Er	Yb	Comment
2-6-2	14.4 (2.3)	27.1 (4.0)	28.8 (3.7)	40.0 (4.3)	106 (6)	16.0 (2.8)	33.5 (3.7)	27.4 (3.9)	all 5 cycles
2-6-2	15.9 (4.2)	27.2 (6.2)	20.1 (4.8)	27.7 (5.2)	9.3 (3.0)	19.7 (4.4)	31.0 (5.6)	24.1 (5.1)	first 2 cycles
2-1-3	116 (7)	795 (20)	44.4 (4.5)	42.3 (4.3)	3.9 (1.1)	26.7 (3.2)	33.8 (3.6)	69.8 (5.5)	all 5 cycles
2-1-3	107 (8)	592 (21)	42.6 (4.9)	43.1 (4.5)	5.1 (1.6)	27.3 (3.6)	31.5 (4.0)	74.5 (6.4)	last 4 cycles
2-1-4	10.7 (2.2)	6.4 (1.9)	21.6 (3.1)	41.8 (4.2)	5.6 (1.4)	17.0 (2.4)	29.4 (3.5)	70.0 (6.3)	
2-1-5	24.5 (4.1)	86.3 (8.9)	20.6 (2.9)	36.2 (5.0)	3.6 (1.2)	57.7 (6.4)	43.2 (5.1)	79.9 (7.9)	
2-1-6	0.6 (0.2)	9.9 (2.6)	23.5 (3.4)	33.6 (4.0)	12.2 (2.7)	23.6 (3.9)	40.5 (4.6)	54.3 (5.3)	
Mean[§]	12.9	32.4	26.0	36.3	6.9	29.0	35.6	59.6	

* Nomenclature for analyses in Tables 7a and 7b as follows: first digit indicates section number (2 = AMNH 4978-2, 5 = AMNH 4978-5), second digit indicates analysis region in section, and third digit indicates analysis number in region. [§] Uses first 2 cycles of 2-6-2 and last 4 cycles of 2-1-3; excludes high La & Ce values of analysis 2-1-3.

Table 8. Bulk composition of metal-veined (AMNH 4978) and silicate-rich (PVF) portions of Portales Valley, compared to average H-chondrite.

	AMNH 4978 †						PVF ‡	H-chondrite*
	-1	-2	-3	-4	-5	avg.		
wt%								
SiO_2	10.8	25.4	25.1	17.6	34.1	21.5	39.77	36.73
TiO_2	0.02	0.05	0.05	0.03	0.06	0.04	0.13	0.12
Al_2O_3	0.71	1.64	1.60	1.13	2.12	1.37	2.20	2.14
Cr_2O_3	0.18	0.45	0.45	0.26	0.08	0.28	0.43	0.51
FeO	2.66	6.45	6.30	4.42	9.12	5.50	[28.5]	10.55
MnO	0.08	0.20	0.20	0.14	0.28	0.17	0.33	0.31
MgO	6.43	15.6	15.2	10.7	22.1	13.3	25.13	23.31
CaO	1.44	1.30	1.05	0.66	3.85	1.56	1.61	1.74
Na_2O	0.31	0.71	0.67	0.48	0.96	0.60	0.85	0.84
K_2O	0.04	0.08	0.08	0.06	0.11	0.07	0.12	0.09
P_2O_5	0.91	0.60	0.29	0.22	2.54	0.85	0.20	0.27
Fe	62.2	38.9	40.3	54.2	20.4	45.1	–	15.43
Ni	9.12	3.68	6.64	7.67	1.98	6.16	0.15	1.71
S	5.03	4.93	2.12	2.52	2.14	3.43	n.a	1.96
Cl	0.10	0.01	0.01	0.00	0.24	0.06	n.a.	n.a.
C	n.a	n.a	n.a	n.a	n.a	n.a	n.a	0.11
	100.03	100.03	100.06	100.09	100.08	99.99	99.42	99.23
atomic								
Mg/Si	0.891	0.913	0.904	0.907	0.964	0.921	0.9418	0.9460 ± 0.0097
Al/Si	0.077	0.0759	0.0752	0.0761	0.0732	0.0754	0.0652	0.0687 ± 0.0047
Ca/Si	0.144	0.0548	0.0449	0.0403	0.121	0.0776	0.0434	0.0506 ± 0.0027
P/Si	0.072	0.020	0.010	0.011	0.063	0.033	0.0043	0.0062 ± 0.0009
Na/Si	0.056	0.054	0.052	0.053	0.055	0.054	0.041	0.044 ± 0.005
Fe^{sil}/Si §	0.206	0.212	0.210	0.211	0.224	0.214	—	0.2406 ± 0.0411
Fe^{met}/Si §	6.22	1.65	1.73	3.32	0.643	2.26	—	0.5523 ± 0.0589
Fe^{tot}/Si §	6.42	1.86	1.94	3.53	0.866	2.47	0.599	0.7929 ± 0.0462
S/Si	0.876	0.363	0.158	0.269	0.118	0.299	—	0.100 ± 0.010

† Determined by modal reconstruction. Combines modal data (Table 2) with average phase compositions (Tables 4-6) and phase densities (Gaines et al., 1997). Low-Ni and high-Ni metal in Table 2 is assumed to correspond to average kamacite and taenite, respectively.
‡ Determined by XRF analysis (Table 10). All iron as FeO. n.a. = not analyzed. * Mean water-free H-chondrite (Jarosewich, 1990), excluding weathered samples. Numbers after "±" refer to standard deviation of the mean. § Fe^{sil} = iron in silicate; Fe^{met} = iron in metal and sulfide; Fe^{tot} = total iron.

Table 9. Bulk composition of various splits of the Portales Valley meteorite and of the El Hammami Mountains H5 chondrite, analyzed by the INAA method. See Table 1 for a description of samples. Uncertainties (see Text) are given in parentheses. n.d. = not determined.

		Portales Valley							El Hammami
		PVA	PVB	PVC	PVD	PVG	PVH	PVI	EH1
Na	mg/g	6.2 (0.4)	6.1 (0.4)	6.0 (0.4)	0.1 (0.03)	6.3 (0.1)	5.86 (0.12)	6.76 (0.14)	5.9 (0.4)
K	mg/g	n.d.	n.d.	n.d.	n.d.	0.79 (0.54)	0.76 (0.09)	0.76 (0.11)	n.d.
Ca	wt%	n.d.	n.d.	n.d.	n.d.	n.d.	1.14 (0.20)	1.17 (0.14)	n.d.
Sc	µg/g	9.02 (0.27)	8.82 (0.26)	7.79 (0.23)	0.36 (0.09)	9.1 (0.09)	7.90 (0.16)	8.94 (0.18)	8.06 (0.24)
Cr	µg/g	3080 (310)	2960 (296)	4430 (440)	29 (4)	3233 (12)	4040 (800)	3830 (800)	3410 (340)
Fe	wt%	22.0 (1.1)	22.6 (1.1)	24.6 (1.2)	88.9*	25.1 (0.5)	27.8 (0.6)	22.2 (0.4)	28.1 (1.4)
Co	µg/g	328 (16)	358 (18)	175 (9)	4320 (220)	419 (8)	192 (4)	260 (5)	831 (42)
Ni	wt%	1.30 (0.16)	1.51 (0.18)	0.84 (0.06)	10.67 (0.07)	n.d.	0.57 (0.011)	1.219 (0.024)	1.93 (0.13)
Zn	µg/g	53 (8)	41 (6)	69 (10)	n.d.	56 (14)	53 (6)	53 (7)	34 (5)
Ga	µg/g	5.2 (1.3)	6.0 (1.5)	6.5 (1.6)	30.4 (7.6)	n.d.	n.d.	n.d.	8.6 (2.2)
As	µg/g	0.81 (0.10)	1.14 (0.08)	0.50 (0.09)	10.0 (0.5)	1.44 (0.33)	0.48 (0.11)	0.73 (0.15)	2.37 (0.12)
Se	µg/g	n.d.	n.d.	n.d.	n.d.	n.d.	42.5 (2.7)	22.6 (1.5)	n.d.
Sb	ng/g	n.d.	n.d.	n.d.	n.d.	n.d.	< 36	34 (15)	n.d.
La	ng/g	150 (40)	150 (30)	800 (80)	n.d.	n.d.	131 (15)	87 (14)	270 (30)
Sm	ng/g	86 (7)	68 (7)	460 (23)	n.d.	90 (10)	126 (5)	78 (7)	150 (10)
Eu	ng/g	70 (10)	73 (7)	88 (7)	n.d.	n.d.	59 (4)	64 (5)	90 (20)
Tb	ng/g	n.d.	n.d.	n.d.	n.d.	n.d.	30 (13)	< 45	n.d.
Yb	ng/g	30 (20)	200 (50)	290 (50)	n.d.	n.d.	114 (28)	139 (30)	40 (20)
Lu	ng/g	n.d.	n.d.	51 (11)	n.d.	n.d.	17 (7)	24 (4)	8 (3)
Hf	ng/g	210 (40)	190 (40)	n.d.	n.d.	n.d.	140 (50)	170 (40)	n.d.
Ir	ng/g	225 (23)	263 (26)	102 (10)	3730 (370)	n.d.	172 (5)	217 (6)	793 (79)
Au	ng/g	100 (20)	130 (20)	n.d.	1400 (200)	n.d.	58.8 (1.9)	88.0 (2.7)	240 (40)

*Calculated by difference. Apparent value (83.6 wt%) unreliable owing to large extrapolation from composition of standard.

Table 10. Bulk composition of Portales Valley splits and of the El Hammami Mountains H5 chondrite, as determined by ICPMS (samples PVE & EH2) and XRF (sample PVF) methods. See Table 1 for a description of the samples. Uncertainties (see Text) are given in parentheses. n.d. = not determined.

		Portales Valley		El Hammami
		PVE	PVF	EH2
Na	mg/g	n.d.	6.3 (0.04)	n.d.
Mg	wt%	n.d.	15.15 (0.57)	n.d.
Al	mg/g	n.d.	11.6 (0.03)	n.d.
Si	wt%	n.d.	18.59 (0.04)	n.d.
P	mg/g	n.d.	0.886 (0.005)	n.d.
K	mg/g	n.d.	0.996 (0.069)	n.d.
Ca	wt%	n.d.	1.15 (0.005)	n.d.
Sc	µg/g	8.9 (0.9)	10 (2)	8.3 (0.9)
Ti	mg/g	n.d.	0.749 (0.004)	n.d.
V	µg/g	n.d.	77 (5)	n.d.
Cr	mg/g	n.d.	2.926 (0.176)	n.d.
Mn	mg/g	n.d.	2.53 (0.04)	n.d.
Fe	wt%	n.d.	22.15 (0.18)	n.d.
Ni	mg/g	n.d.	1.524 (0.091)	n.d.
Ga	µg/g	n.d.	5 (0.5)	n.d.
Rb	µg/g	2.4 (0.3)	n.d.	2.8 (0.3)
Sr	µg/g	8 (0.4)	14 (0.05)	10 (0.5)
Y	µg/g	0.74 (0.04)	n.d.	1.89 (0.10)
Zr	µg/g	5	n.d.	5
Nb	µg/g	0.46	n.d.	0.45
Cs	ng/g	20 (5)	n.d.	10 (2)
Ba	µg/g	5.0 (0.3)	n.d.	4.0 (0.3)
La	ng/g	170 (11)	n.d.	380 (23)
Ce	ng/g	450 (18)	n.d.	730 (29)
Pr	ng/g	50 (2)	n.d.	100 (4)
Nd	ng/g	240 (12)	n.d.	500 (24)
Sm	ng/g	70 (4)	n.d.	180 (11)
Eu	ng/g	60 (4)	n.d.	80 (5)
Gd	ng/g	100 (4)	n.d.	250 (10)
Tb	ng/g	20 (1)	n.d.	50 (2)
Dy	ng/g	120 (5)	n.d.	330 (13)
Ho	ng/g	30 (1)	n.d.	70 (3)
Er	ng/g	70 (3)	n.d.	210 (9)
Tm	ng/g	10 (0.4)	n.d.	30 (1)
Yb	ng/g	80 (3)	n.d.	200 (6)
Lu	ng/g	10 (1)	n.d.	30 (2)
Hf	ng/g	140 (8)	n.d.	150 (9)
Ta	ng/g	20 (4)	n.d.	20 (4)
Pb	µg/g	2.28 (0.46)	n.d.	0.5 (0.1)
Th	ng/g	20	n.d.	30
U	ng/g	10 (3)	n.d.	10 (3)

Table 11. Model calculations for abundances of siderophile elements and S compared to observed values in Portales Valley. F_L= fraction of liquid after step. H-chondrite values used in models: 82.55 wt% Fe, 8.59 wt% S, 7.49 wt% Ni, 1.36 wt% Co, 4.22 ppm Ga, 1.04 ppm Ir, 0.348 ppm Au, 3.50 ppm As. Values in parentheses for Portales Valley reflect 1-σ measurement uncertainty (coarse vein metal) and standard deviation for multiple analyses (fine metal + sulfide in silicate-rich areas).

		H-chondrite normalized values (wt)						
model	phase	S/Ni	Ga/Ni	Fe/Ni	Ir/Ni	Au/Ni	Co/Ni	As/Ni
batch melting	liquid	6.63	0.039	1.44	0.0005	0.320	0.359	0.248
(F_L = 0.326)	solid	0	1.17	0.918	1.18	1.12	1.12	1.14
batch melting	liquid	3.66	0.199	0.925	0.023	1.50	0.593	0.904
(F_L = 0.7), then equilibrium crystallization (F_L = 0.7)	solid	0	1.41	0.854	0.380	0.740	1.22	1.44
complete melting	liquid	2.41	0.331	0.999	0.077	1.81	0.656	1.31
(F_L = 1), then fractional crystallization (F_L = 0.5)	solid	0	0.751	1.12	0.305	0.656	0.973	0.903
equilibrium melting	liquid	3.29	0.584	0.819	0.139	1.33	0.777	1.06
(F_L = 0.7), then in situ crystallization (F_L = 0.7, f = 0.5)	solid	0	4.14	0.752	2.29	0.656	1.60	1.68
equilibrium melting (F_L = 0.326)	mixture 60% solid	2.67	0.605	1.02	0.543	0.864	0.781	0.811
equilibrium melting (F_L = 0.326)	mixture 30% solid	4.66	0.379	1.28	0.354	0.559	0.585	0.493
Portales Valley	coarse metal	~0	1.74 (0.49)	0.811 (0.105)	0.878 (0.137)	0.993 (0.183)	0.781 (0.100)	0.705 (0.091)
Portales Valley	fine metal	>1	3.21 (1.09)	2.50 (1.23)	0.477 (0.150)	0.605 (0.107)	0.482 (0.089)	0.515 (0.074)

Table 12. Summary of whole-rock chronologic data for Portales Valley.

system	result	reference
Pd-Ag	No live ^{107}Pd; formation $6 Ma after IIAB, IIIAB, IVA irons	1
Re-Os	Coarse metal: H-like, formed early (age <4.56 Ga); Fine metal: Re/Os redistribution recently (0.3 ± 1.3 Ga)	1, 2, 6
U-Th-Pb	4.571 ± 0.010 Ga primary age; 94 ± 5 Ma late disturbance	2
^{40}Ar-^{39}Ar	4.477 ± 0.016 Ga, no evidence for later diffusive loss	3
Rb-Sr	T_{BABI} = 4.44 - 4.60 Ga; evidence for disturbance	2, 4
Sm-Nd	Variable Sm/Nd and Sm; no evidence for ^{142}Nd; T_{CHUR} = 1.16 - 1.85 Ga	2, 4, 5

[1] Chen et al. (1999). [2] Chen et al. (2000). [3] Garrison and Bogard (2001). [4] Papanastassiou et al. (2001). [5] Papanastassiou et al. (2002). [6] James Chen, personal communication, 2000.